



Faculty of science and technology
MASTER'S THESIS

Title of thesis:

Optimization analysis of subsea freight-glider

Guidance by:

Prof. Yihan Xing

Study program:

Marine and offshore technology

Semester:

Spring 2021

Student number:

217178

Pages:

106

Credits: 30

Name:

Tao Yu

Abstract

Pipelines can be used to transport the produced fluids in subsea oil field development from subsea wells to floating production units, and then unload them to tankers (surface ships). If CO₂ is injected into a subsea well, the flow is reversed. This CO₂ unloading process is highly dependent on weather conditions and cannot be performed under severe conditions. In addition, the cost of installation and maintenance of the submarine pipeline system can be high. In this research, a novel subsea cargo glider system is proposed as a suitable, cost-effective, and energy-saving alternative to tankers and pipelines. The proposed vehicle is automatic, with a length of 50 m and a displacement of 1500 DWT, which can carry approximately 800 tons of cargo. The underwater glider uses a variable buoyancy propulsion device instead of a traditional propeller/thruster. It uses fluid-powered wings to glide on the sea floor; this is an extremely energy-efficient way to transport large amounts of cargo over medium and long distances. Since the submarine cargo glider operates below the sea surface, it is not affected by wind and waves and can operate in any weather conditions. In addition, it is still possible to develop subsea oil fields that are not large enough to justify the reasonable installation of subsea pipelines. Even though it is recommended to use the underwater glider as a means of transportation of liquid CO₂, it can also transport various types of cargo, such as hydrocarbons, injection liquid and gas, and even use batteries to transport electricity.

1.0 Introduction	11
1.1 Subsea freight-glider	11
1.2 The focus of this article and procedure	11
2.0 Theory	13
2.1 Subsea freight-glider design	13
2.2 Concept design method	14
2.3 Structural design	15
2.4 Hydrostatic design condition	17
2.5 Longitudinal and hoop stresses	20
2.6 Deformation	22
2.6.1 Elastic deformation	22
2.6.2 Plastic deformation	24
2.7 Dynamic modeling of glider movement	26
2.8 Selection of glider parameter	31
2.9 Parameter correlation	34
3.0 Carbon fiber composite material	36
3.1 Advantages of carbon fiber	37
3.2 The strength of carbon fiber	38
3.3 Mechanical properties of deep-sea carbon fiber composite cylinder pressure shell	40
3.4 Mechanical analysis of carbon fiber cylindrical shell	43
3.4.1 Basic mechanical properties of single-layer boards	43

3.4.2 Basic mechanical properties of laminates	46
3.4.3 Carbon fiber Poisson`s ratio and modulus of elasticity	52
3.5 Ring ribbed reinforce cylinder	57
3.6 Fiber composite failure criteria	59
3.6.1 The maximum stress criterion	60
3.6.2 Tsai-Hill strength criterion	60
3.6.3 Tsai-Wu stress criteria	62
4.0 Optimization method	65
4.1 Material optimization method	65
4.2 Hull structure optimization method	66
5.0 Subsea freight-glider optimization analysis	67
5.1 Subsea freight-glider structure	68
5.2 Hull pressure and deformation analysis	72
5.2.1 Pressure and deformation of Cargo tank	75
5.2.2 Pressure and deformation of buoyancy tank	78
5.2.3 Pressure and deformation of stiffener	80
5.3 Carbon-fiber hull analysis	81
5.3.1 Cargo tank pressure and deformation analysis with Carbon fiber	83
5.3.2 Buoyancy tank pressure and deformation analysis with Carbon fiber	85
5.3.3 Carbon fiber stiffener deformation analysis	87

5.4 Integrity and reliability analysis	87
5.4.1 Weight analysis	88
5.4.2 Integrity deformation analysis	92
5.4.3 Integrity hull structure analysis	95
5.4.4 Design of experiment for measuring compression deformation	99
6.0 Summary and outlook	101
Reference	105

Figure 1 Subsea freight-glider	11
Figure 2 Subsea freight-glider working principle	13
Figure 3 Subsea freight-glider geometry presentation	16
Figure 4 Hydrostatic pressure presentation	17
Figure 5 Pressure compare sea depth description	19
Figure 6 Diagram pressure with depth	19
Figure 7 Longitudinal and hoop stresses	20
Figure 8 Stresses equation symbol	22
Figure 9 Hooke`s law, elastic deformation	24
Figure 10 Hooke`s law, plastic deformation	25
Figure 11 Deformation of reference frameworks	26
Figure 12 Freight-glider movements parameter	30
Figure 13 Definition of global glider parameter	33
Figure 14 Tensile strength	39
Figure 15 Carbon fiber tensile strength	39
Figure 16 Limiting strength	39
Figure 17 Strength value test	40
Figure 18 Tensile modulus	40
Figure 19 Theoretical tensile modulus	40
Figure 20 Hoop pressure and axial pressure	43
Figure 21 Single layer board in normal axial stress state	44
Figure 22 The off-axis stress state of single-layer plate	45

Figure 23 Carbon fiber pressure resistant cylindrical shell	47
Figure 24 Coordinate of laminated plates each single	48
Figure 25 Plane force state of the sub-laminated structure	51
Figure 26 Hoop stress and axial stress of 90 degrees layer distribution along the thickness direction	55
Figure 27 Hoop stress and axial stress of 0 degrees layer distribution along the thickness direction	56
Figure 28 Ring ribbed reinforce cylinder	58
Figure 29 Strength criterion results of 90 degrees layer	61
Figure 30 Strength criterion results of 0 degrees layer	62
Figure 31 Strength criterion results of 90 degrees layer	63
Figure 32 Strength criterion results of 0 degrees layer	64
Figure 33 China Cao Chong weight elephant	67
Figure 34 50-meter cylinder pipe face meshing	68
Figure 35 Pressure on subsea freight-glider tank	69
Figure 36 3D structure drawing freight-glider	69
Figure 37 Cargo tank cylinder	70
Figure 38 Cargo tank spherical shell	70
Figure 39 Buoyancy tank cylinder	71
Figure 40 Buoyancy tank spherical shell	71
Figure 41 3D drawing stiffener	72
Figure 42 Stable balanced path and unbalanced path	73

Figure 43 Stable balanced path and unbalanced path	73
Figure 44 Cargo tank cylinder deformation steel	76
Figure 45 Cargo tank cylinder deformation steel	76
Figure 46 Cargo tank deformation by depth steel	77
Figure 47 Cargo tank spherical shell deformation steel	77
Figure 48 Cargo tank spherical shell deformation steel	77
Figure 49 Buoyancy tank cylinder deformation steel	78
Figure 50 Buoyancy tank cylinder deformation steel	78
Figure 51 Buoyancy tank deformation by depth steel	79
Figure 52 Buoyancy tank spherical shell deformation	79
Figure 53 Buoyancy tank spherical shell deformation steel	79
Figure 54 Stiffener fixed support	80
Figure 55 Stiffener pressure direction	80
Figure 56 Stiffener deformation steel	81
Figure 57 Stiffener deformation steel	81
Figure 58 Structural steel parameter	82
Figure 59 Carbon fiber parameter	83
Figure 60 Cargo tank cylinder pressure and deformation analysis carbon fiber	83
Figure 61 Cargo tank cylinder pressure and deformation analysis carbon fiber	83
Figure 62 Cargo tank cylinder deformation steel vs carbon fiber	84

Figure 63 Cargo tank spherical shell pressure and deformation analysis carbon fiber84

Figure 64 Cargo tank spherical shell pressure and deformation analysis carbon fiber85

Figure 65 Buoyancy tank cylinder pressure and deformation analysis carbon fiber85

Figure 66 Buoyancy tank cylinder pressure and deformation analysis carbon fiber85

Figure 67 Buoyancy tank cylinder deformation steel vs carbon fiber86

Figure 68 Buoyancy tank spherical shell pressure and deformation analysis carbon fiber86

Figure 69 Stiffener carbon fiber pressure and deformation analysis87

Figure 70 Integrity stiffener91

Figure 71 Weight result compare92

Figure 72 Integrity deformation analysis steel93

Figure 73 Integrity deformation analysis carbon fiber93

Figure 74 Integrity deformation compare94

Figure 75 Stiffener structure between tanks95

Figure 76 Fluid dynamic viscosity96

Figure 77 Fluid dynamic viscosity96

Figure 78 Fluid flow on surface97

Figure 79 Flow across surface and space97

Figure 80 Fluid flow boundary layer	98
Figure 81 Design of experiment for measuring compression deformation	99
Figure 82 Optimization design final module	103
Table 1 Subsea freight-glider concept design parameter	15
Table 2 Subsea freight-glider geometry parameter	16
Table 3 Pressure changing compare seawater depth	18
Table 4 Consideration of design parameter	32
Table 5 Corresponding parameter correlation	34
Table 6 Corresponding parameter correlation	35
Table 7 Density changes with depth	89

1.0 Introduction

1.1 Subsea freight glider

This master's thesis is written under the supervision of Professor Yihan Xin, assignment write about Subsea freight glider, which is designed with system ANSYS 2020. The figure 1 below shows 3D drawing for the Subsea freight glider.

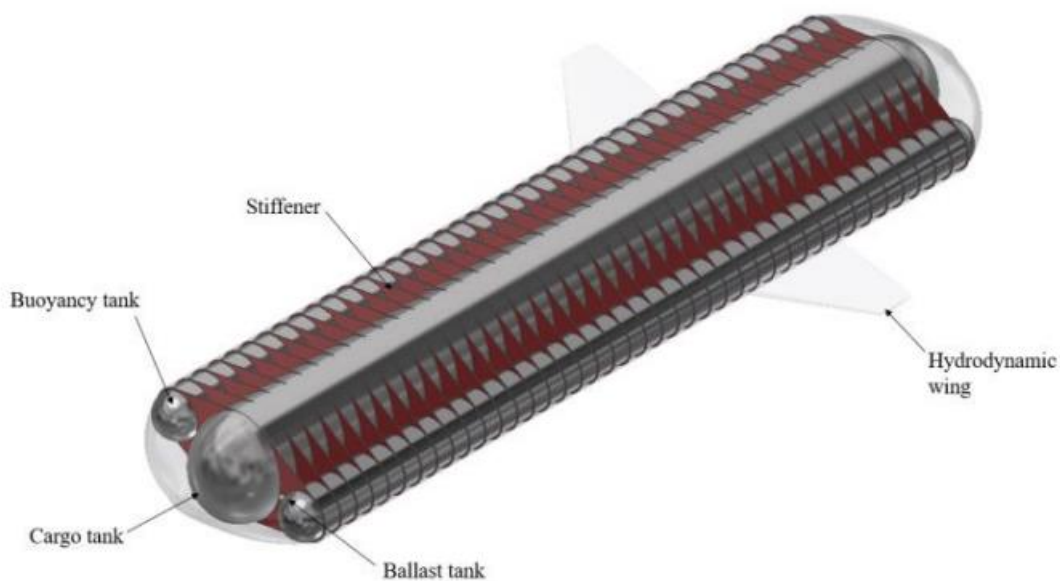


Figure 1 Freight glider

1.2 The focus of this article and procedure

This master's thesis writes about how to improve Subsea Freight Glider construction, increase construction strength, increases transport quantity. In the best possible way to reduce deformation due to ambient pressure in underwater situation. This thesis uses Ansys 2020 system with drawing collaboration with professor Yihan, Ansys drawing (3D) is first analyzed

with steel, to improve structural strength this thesis will analyze more about lightweight carbon fiber material, and analyze structure to find improving path that adapts to practical environment.

2.0 Theory

2.1 Subsea freight-glider design

The subsea freight glider is a typical autonomous underwater vehicle, which mainly adopts buoyancy drive to achieve its ascent or dive in the ocean. Its working principle is shown in Figure 2. In the initial stage of the dive, the buoyancy drive unit reduces its own drainage volume so that the gravity is greater than the buoyancy and starts to dive; after reaching the set depth, under the action of the buoyancy drive unit, the self-drainage volume is changed to make the buoyancy force greater than gravity, so as to achieve the transition from diving to floating. In the process of descending and ascending, the horizontal motion is generated by the hydrodynamic force on the fixed horizontal wing, to realize the zigzag glide motion in the longitudinal plane.

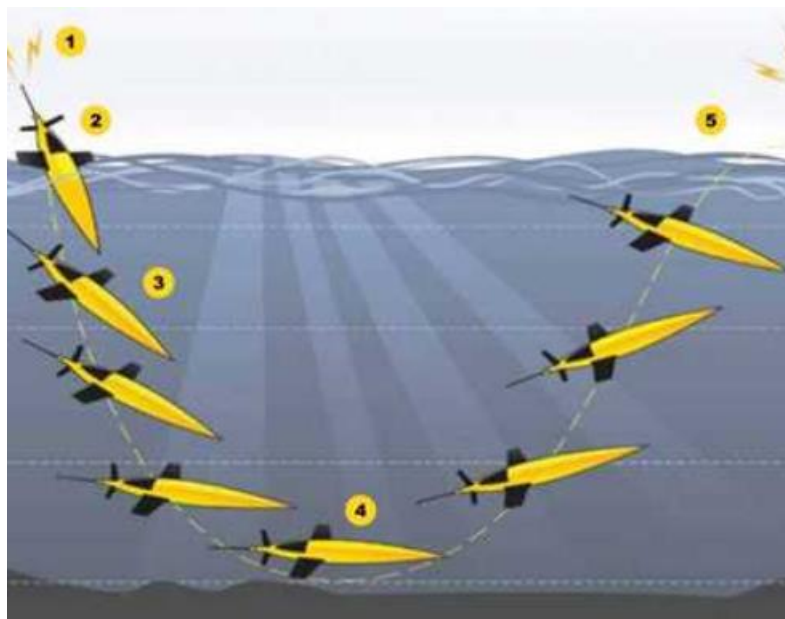





Figure 2 Working principle

As a small mobile observation platform, the subsea freight glider has the

characteristics of low energy consumption and low operating cost. It can meet the long-term and large-scale ocean three-dimensional observation requirements. It has been widely used in marine field observation, scientific research, environmental protection, and national defense security. And other fields, play an important role in the global ocean observation and detection system. Compared with traditional navigating and fixed-point submersible observation methods, underwater gliders have the advantages of flexibility, high efficiency, and low cost, which can get rid of the dependence on the launch of the mother ship and greatly reduce ocean transportation and production costs.

2.2 Concept design method

Concept in this master's thesis contains analysis of:

-  Structural design of the pressure hull.
-  hydrostatic design mode.
-  Global parameter.

The structural design, i.e., the collapse pressure capacity of the pressure hull is defined first as it drives the maximum diving depth a subsea freight-glider of a particular DWT can reach. The structural design derived must then be checked if it fulfils the hydrostatics design condition, i.e., the buoyancy force must be equal its weight. Finally, based on the maximum diving depth allowed, the global glider parameters can then be derived. Table 1 give

design parameters [4]:

Parameter	Value	Unit
Vessel length	50	m
Cargo tank diameter	5.0	m
Buoyancy tank diameter	2.2	m
Dead weight ton	1533	ton
Structural weight	470	ton
Cargo weight	785	ton
Ballast fraction	0.15	%
Diving depth	200	m
Glide path angle	38	°
Wing area	20	m ²
Volumetric drag coefficient	0.1	-
Ballast pump capacity	2000	m ³ /h
Pumping time / cycle	< 5% of half cycle	-
Horizontal speed	1	m/s
Average power	< 10	kW
Net transport economy	<0.5	-

Table 1

2.3 Structural design

The freight-glider is a large structure with a large pressure hull (cargo and buoyancy tanks) that is exposed to large amounts of external hydrostatic pressure. The design of large pressure hulls to resist external hydrostatic loads is challenging. The pressure hull will be constructed using thin steel plates. The external pressure collapse capacity of such a pressure hull is sensitive to its structural stiffness which is in turn highly dependent on the geometry. The geometry is presented in FIGURE 3 [4].

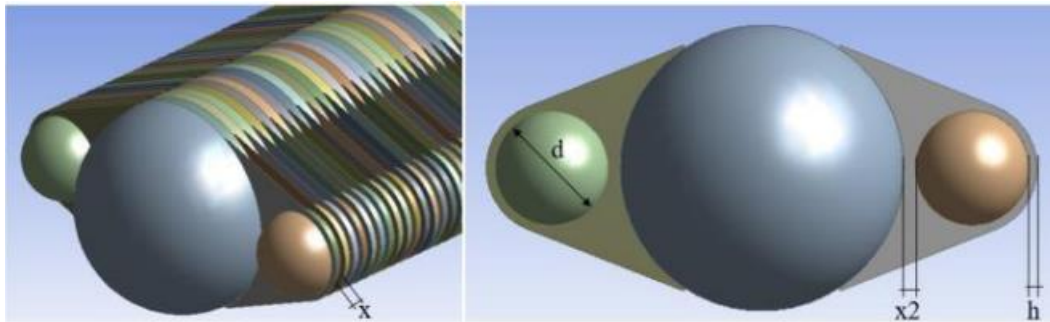


Figure 3

The geometric parameters are:

- ✧ d: diameter of the buoyancy tank
- ✧ x: distance between the stiffeners
- ✧ x2: shortest distance between the cargo tank and the buoyancy tanks
- ✧ h: height of stiffener around the buoyancy tank
- ✧ t1, t2, t3, thicknesses of the cargo tank, buoyancy tank and stiffener, respectively

d(mm)	x(mm)	x2(mm)	H(mm)	t1(mm)	t2(mm)	t3(mm)	W(kg/m)
1967	375	145	126	48.3	11.5	10.5	9395

Table 2

As shown in Figure 3 that 2 equally large buoyancy tank on both sides are used to fill with air to lift the freight-glider up from seabed to sea surface. Structure between buoyancy tank and cargo tank must be analyzed accurately, reliability and stability are central to improvement analysis. The figure shows the gaps between stiffeners will analyze more later to reduce total weight and analyze stability and reliability.

2.4 Hydrostatic design condition

The magnitude of hydrostatic pressure and water depth are inseparable. The direction of the hydrostatic pressure can be regarded as the hydrostatic pressure pointing perpendicular to the working surface. As show in Figure 4:

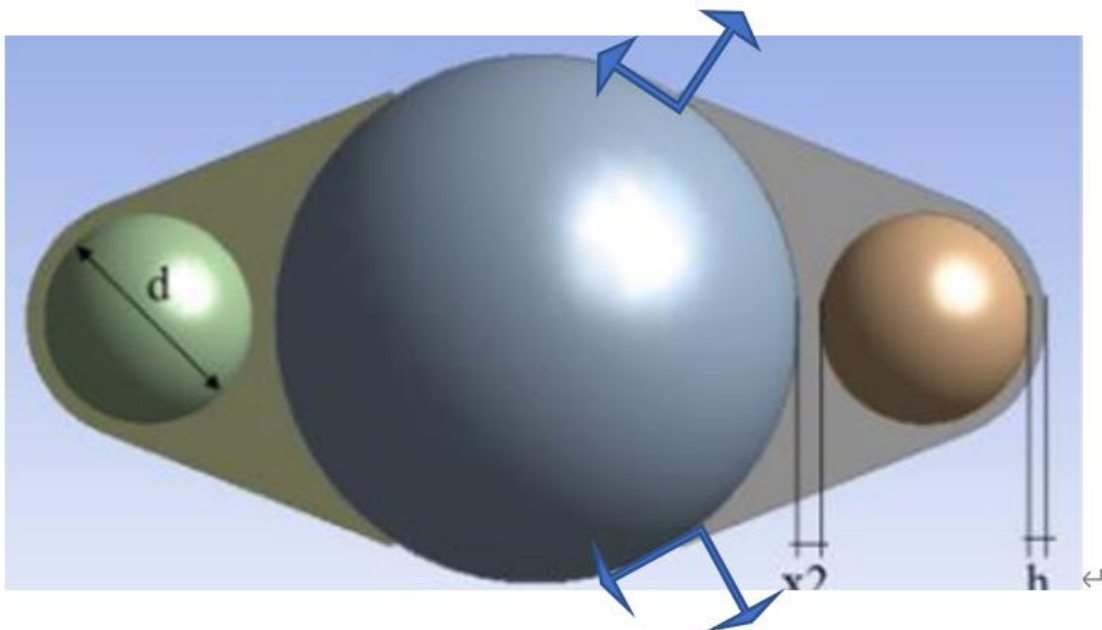


Figure 4

In this master thesis use sea water condition, ppressure equation:

$$P = \rho * g * h$$

P: Pressure

ρ : Density of fluid (1025 kg/m²)

g: Gravity (9,81)

h: Deep of fluid (from sea surface 0 to 300 meter deep)

Sea depth (meter)	Pressure (Pa)
0	0
20	201105
40	402210
60	603315
80	804420
100	1005525
120	1206630
140	1407735
160	1608840
180	1809945
200	2011050
220	2212155
240	2413260
260	2614365
280	2815470
300	3016575

Table 3

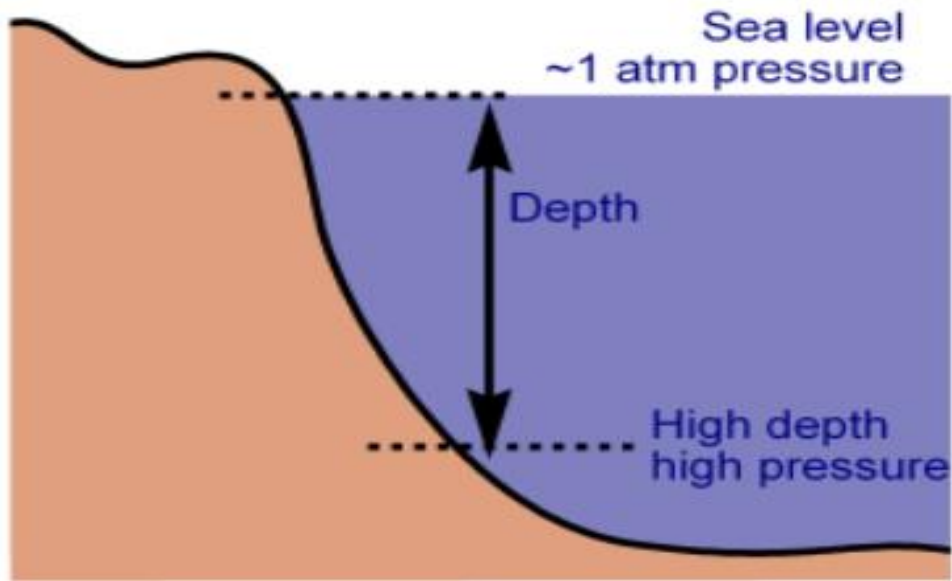


Figure 5

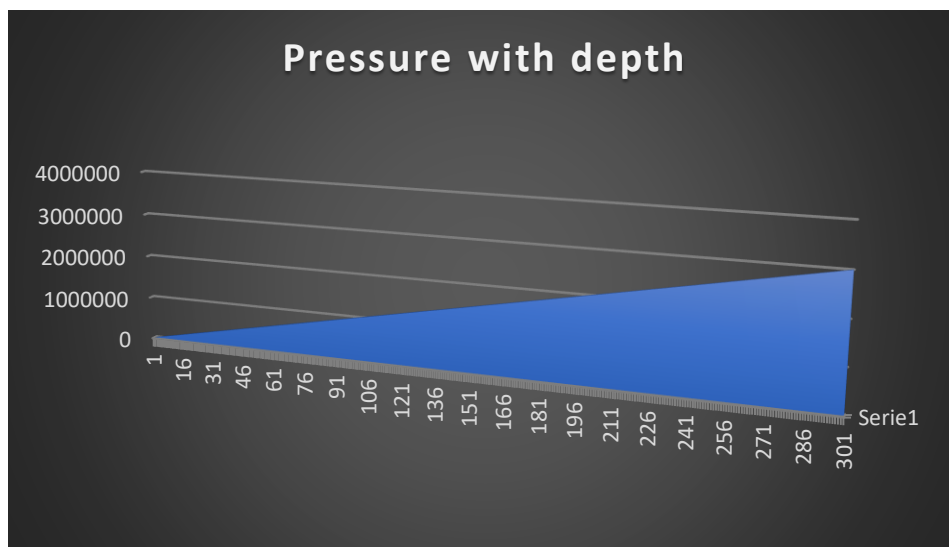


Figure 6

The subsea freight-glider must be neutrally buoyant, i.e., the buoyancy force must be equal to the weight, which is the sum of structures, cargo, machinery.

$$F_b = W_c + W_s + W_m$$

2.5 Longitudinal and hoop stresses

Longitudinal stress is defined as the stress produced when a pipe is subjected to internal pressure. The direction of the longitudinal stress in a pipe is parallel to the longitudinal axis of its centerline axis, which means that the stress acts in the direction of the pipe's length. Longitudinal stresses are classed as normal stresses and are tensile.

Closure of the ends of thin-walled pipes and the resulting build-up of internal fluid pressure induces the development of three types of mutually perpendicular stresses. In addition to longitudinal stress, circumferential or hoop stress and radial stress also occur, although the latter is minor compared to the others. Longitudinal stress has two components, the first related to pressure and second to temperature. The pressure component is positive (tensile) and temperature component is negative (compressive). The nature of resultant longitudinal stress depends on the relative magnitudes of pressure and temperature increase. Longitudinal stress is also known as axial stress.

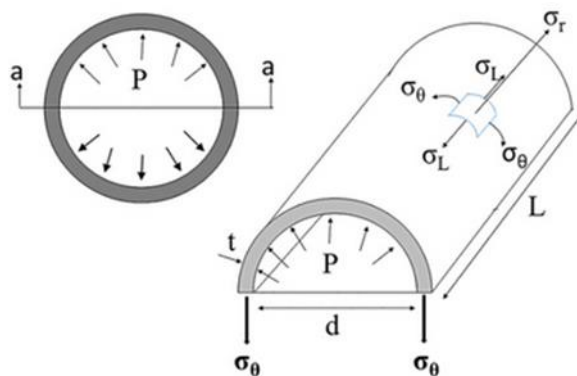


Figure 7

When evaluating longitudinal stresses, there are two main forces:

1. Bursting Force – This is the force created due to the liquid's internal pressure in a pipe, which damages the pipe through bursting.
2. Resisting Force – When the pipe is subjected to internal pressure, forces counteract the failure. This force is known as the resisting force.

$$FB \text{ (Bursting Force)} = \text{Pressure} \times \text{Area} = p \times 4 \times d^2$$

$$FR \text{ (Resisting Force)} = \text{Resisting Area} \times \text{Longitudinal Stress} = \pi dt \times \sigma_L$$

$$FB=FR \quad \rightarrow \rightarrow \quad p \times 4d^2 = \pi dt \times \sigma_L$$

$$\text{Longitudinal Stress, } \sigma_L = \frac{pd}{4t}$$

The Relationship between Longitudinal and Circumferential (Hoop) Stress
 Determination of stresses in a thin-walled pipe focuses on the two principal stresses that a pipe of this nature would be exposed to, longitudinal and circumferential. Circumferential stress acts along the pipe's circumference, with failure tending to split the pipe into two halves. The longitudinal stress in a pipe is smaller than the circumferential stress. The formula for circumferential stress demonstrates this.

$$FB \text{ (Bursting Force)} = \text{Pressure} \times \text{Area} = p \times d \times l$$

$$FR \text{ (Resisting Force)} = \text{Resisting Area} \times \text{Circumferential Stress} = 2tl \times \sigma_\theta$$

$$FB=FR \quad \rightarrow \rightarrow \quad P \times d \times L = 2tl \times \sigma_\theta$$

$$\text{Circumferential Stress, } \sigma_\theta = \frac{p \times d}{2 \times t}$$

Pressure	Length	Diameter	Thickness
P	L	d	t

Figure 8

Hoop stress σ_{θ} is statically determinate, longitudinal stress σ_L is not statically determinate and depends on whether the moves longitudinally.

2.6 Deformation

Consider the type of material, size and geometry of the object, and the forces applied, various types of deformation may result. The image to the right shows the engineering stress vs. strain diagram for a typical ductile material such as steel. Different deformation modes may occur under different conditions, as can be depicted using a deformation mechanism map. Permanent deformation is irreversible; the deformation stays even after removal of the applied forces, while the temporary deformation is recoverable as it disappears after the removal of applied forces. Temporary deformation is also called elastic deformation, while the permanent deformation is called plastic deformation.

2.6.1 Elastic deformation

Hooke's law is a law of physics that states that the force (F) needed to extend or compress a spring by some distance (x) scales linearly with respect to that distance that is,

$$F_x = k * x$$

where k is a constant factor characteristic of the spring (i.e., its stiffness), and x is small compared to the total possible deformation of the spring. Hooke's equation holds (to some extent) in many other situations where an elastic body is deformed, such as wind blowing on a tall building, and a musician plucking a string of a guitar. An elastic body or material for which this equation can be assumed is said to be linear-elastic or **Hookean**.

When a sufficient load is applied to a metal or other structural material, it will cause the material to change shape. This change in shape is called deformation. A temporary shape change that is self-reversing after the force is removed, so that the object returns to its original shape, is called elastic deformation. In other words, elastic deformation is a change in shape of a material at low stress that is recoverable after the stress is removed. This type of deformation involves stretching of the bonds, but the atoms do not slip past each other.

Linear elastic deformation is governed by Hooke's law:

$$\sigma = E * \epsilon$$

Where σ is the applied stress, E is a material constant called Young's modulus or elastic modulus, and ϵ is the resulting strain. This relationship only applies in the elastic range and indicates that the slope of the stress vs. strain curve can be used to find Young's modulus E , and E often use this

calculation in tensile tests.

Note that not all elastic materials undergo linear elastic deformation; some, such as concrete, gray cast iron, and many polymers, respond in a nonlinear fashion. For these materials Hooke's law is inapplicable.

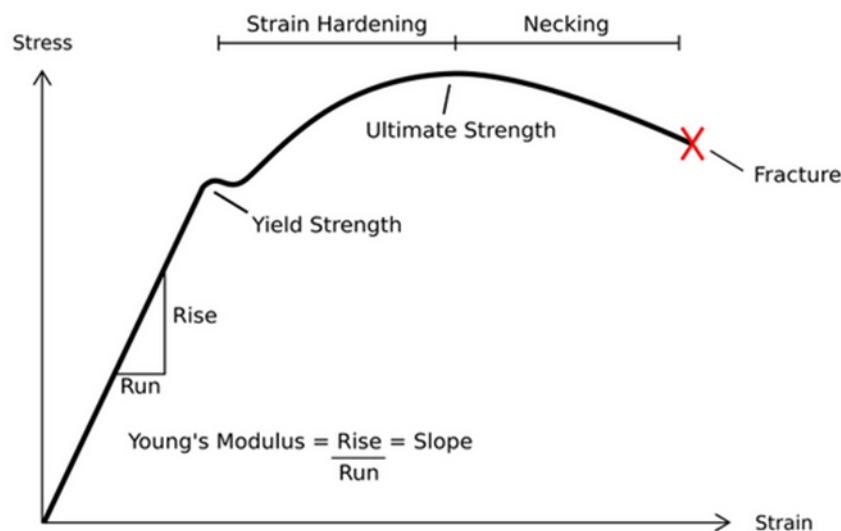


Figure 9

2.6.2 Plastic deformation

Plastic deformation is not undone simply by removing the applied force. An object in the plastic deformation range, however, will first have undergone elastic deformation, which is undone simply by removing the applied force, so the object will return part way to its original shape. Soft thermoplastics have a rather large plastic deformation range as do ductile metals such as copper, silver, and gold. Steel does, too, but not cast iron. Hard thermosetting plastics, rubber, crystals, and ceramics have minimal plastic deformation ranges. An example of a material with a large plastic deformation range is

wet chewing gum, which can be stretched to dozens of times its original length. Under tensile stress, plastic deformation is characterized by a strain hardening region and a necking region and finally, fracture (also called rupture). During strain hardening the material becomes stronger through the movement of atomic dislocations. The necking phase is indicated by a reduction in cross-sectional area of the specimen. Necking begins after the ultimate strength is reached. During necking, the material can no longer withstand the maximum stress and the strain in the specimen rapidly increases. Plastic deformation ends with the fracture of the material.

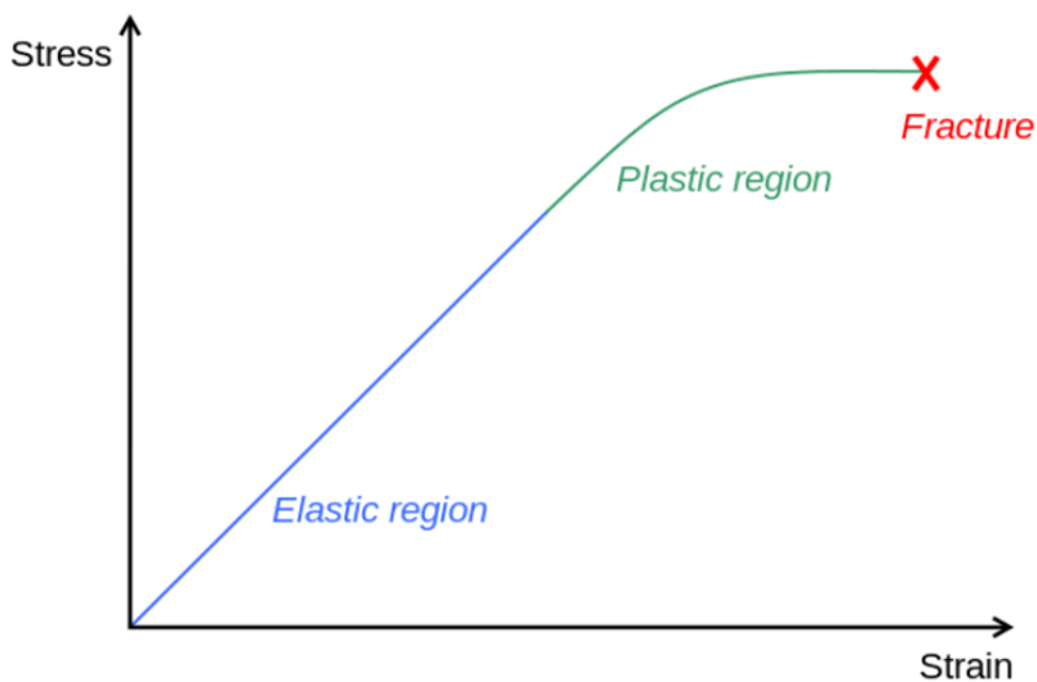


Figure 10

2.7 Dynamic modeling of glider movement

For underwater vessels, it is difficult to separate the static and dynamic aspects, because most of the two effects always coexist. The static stability of the underwater glider in the lateral and longitudinal directions (rotation of the longitudinal and lateral axes) requires the center of gravity to be located below the center of buoyancy. The motion of an object in the fluid includes motion along the longitudinal, lateral, and vertical axes, which are called surge, sway, and heave, respectively, and also includes rotational motion around these three axes, which are called roll, pitch, or Yaw (Figure 11). Since this model is only studied on the XZ plane, only the balance in this area is checked. Therefore, the center of mass and the center of buoyancy are on the X axis, and only the center of mass on this axis will be displaced to study its influence on the motion of the glider. Various complex and non-linear forces, such as hydrodynamic drag, damping, lift, Coriolis and centrifugal force, gravity, and buoyancy, as well as propulsion and environmental interference, will affect the motion of the underwater glider, and ultimately make its motion difficult to control. Therefore, the kinematics and dynamics modeling of the glider has a great influence on the control of underwater motion.

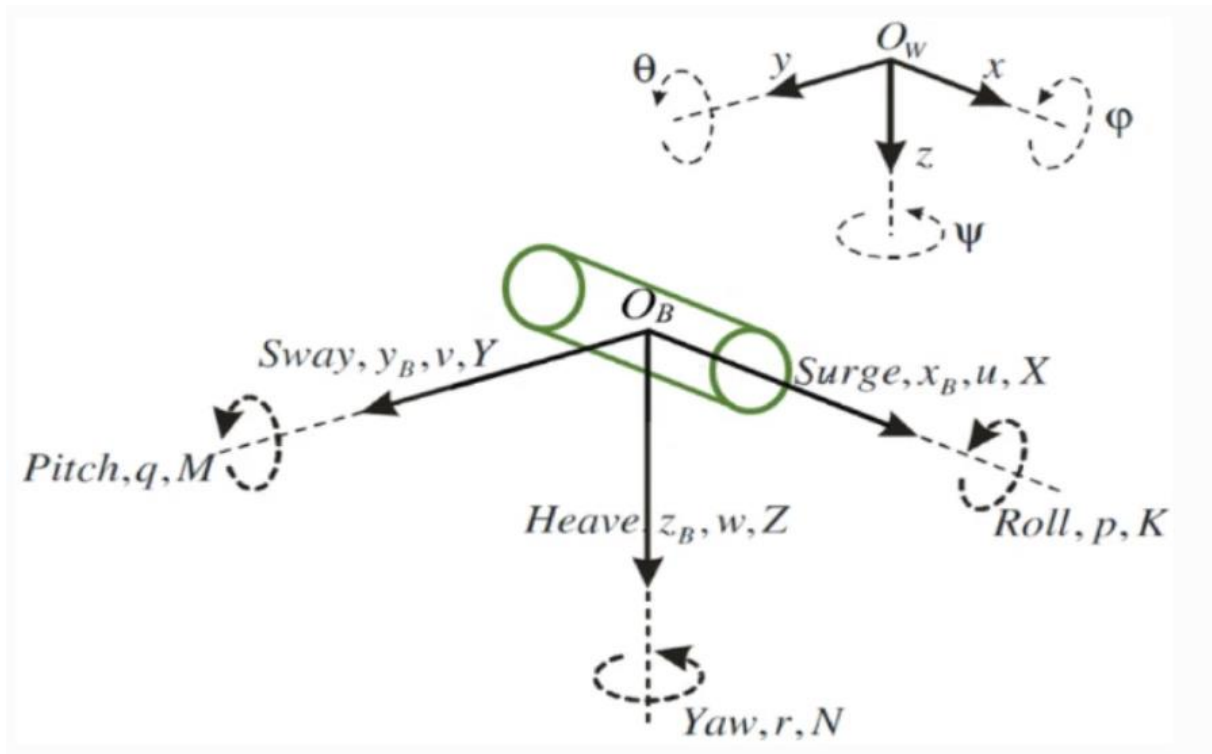


Figure 11 Definition of reference frameworks, along with all degrees of freedom

To derive the 6 degrees of freedom equations, two reference coordinates are provided for the glider; one is the global fixed reference framework (W) and the other is the fixed reference framework (B) on body. The direction of the axes in both (W) and (B) frames are shown in Figure. 5. Euler relations are used to transfer each coordinate to the other O [1].

To obtain the 6 degrees of freedom equations, it is assumed that the coordinate system B is located on the center of the glider buoyancy, so that in this case the inertia tensor will be in diagonal form.

$$I_B = \begin{bmatrix} I_{xx} & 0 & 0 \\ 0 & I_{yy} & 0 \\ 0 & 0 & I_{zz} \end{bmatrix}$$

Newton and Euler equation, the six degrees of freedom equation of the glider are [1]:

$$m[\dot{u} - vr + wg - xG(q^2 + r^2) + yG(pq - \dot{r}) + zG(pr + \dot{q})] = \sum X_i$$

$$m[\dot{v} - wp + ur - yG(r^2 + p^2) + zG(qr - \dot{p}) + xG(qp + \dot{r})] = \sum Y_i$$

$$m[\dot{w} - uq + vp - zG(z^2 + q^2) + xG(rq - \dot{q}) + yG(rq + \dot{p})] = \sum Z_i$$

$$I_x \dot{p} + (I_z - I_y)qr + m[y_g(\dot{w} - uq + vp) - z_g(\dot{v} - wp + ur)] = \sum K_i$$

$$I_y \dot{q} + (I_x - I_z)rp + m[z_g(\dot{u} - vr + wq) - x_g(\dot{w} - uq + vp)] = \sum M_i$$

$$I_z \dot{r} + (I_y - I_x)pq + m[x_g(\dot{v} - wp + ur) - y_g(\dot{u} - vr + wq)] = \sum N_i$$

Considering the Newton-Euler equation with respect to the motion of a rigid object in fluids, the dynamic model of the glider motion can be considered as follow 0(1)

$$M\dot{v} + C(v)v + D(v)v + g(\eta) = \tau$$

M is the inertial matrix of the rigid body and the added mass, C(v) is the Coriolis matrix and the centrifuge of the rigid body and the added mass. D(v) is Damping matrix, $g(\eta)$ is gravity and buoyancy matrix, and τ is the force/torque vector, however, τ is the considered zero in the glider. It is worth noting that in equation:

$$D(v) = D_q(v) + D_L(v)$$

Matrix mass and inertia rigid body mass:

$$M = M_{RB} + M_A$$

The body mass term is written as:

$$M_{RB}\dot{v} = \begin{bmatrix} m \dot{v}_B + m \dot{w}_B \times r_G \\ I_B \dot{w}_B + m r_G \times \dot{v}_B \end{bmatrix}$$

r_G is the position of the center of gravity of the glider in the coordinate system on the body [1].

$$r_G = [x_G \ y_G \ z_G]^T$$

$$M_{RB} = \begin{bmatrix} m & 0 & 0 & 0 & m_{zG} & -m_{yG} \\ 0 & m & 0 & -m_{zG} & 0 & m_{xG} \\ 0 & 0 & m & m_{yG} & -m_{yG} & 0 \\ 0 & -m_{zG} & m_{yG} & I_{xx} & -I_{xy} & -I_{xz} \\ m_{zG} & 0 & -m_{xG} & -I_{yx} & I_{yy} & -I_{yz} \\ -m_{yG} & m_{xG} & 0 & -I_{zx} & -I_{zy} & I_{zz} \end{bmatrix}$$

The glider is symmetric on the XZ and XY planes, and with good approximation one can assume that it has symmetry on the YZ plane as well. This will dramatically reduce the computation. The mass of the rigid body is obtained as follows:

$$M_{RB} = \begin{bmatrix} m & 0 & 0 & 0 & m_{zG} & -m_{yG} \\ 0 & m & 0 & -m_{zG} & 0 & m_{xG} \\ 0 & 0 & m & m_{yG} & -m_{xG} & 0 \\ 0 & -m_{zG} & m_{yG} & I_{xx} & 0 & 0 \\ m_{zG} & 0 & -m_{xG} & 0 & I_{yy} & 0 \\ -m_{yG} & m_{xG} & 0 & 0 & 0 & I_{zz} \end{bmatrix}$$

Hydrodynamic added mass is defined as [2]

$$M_A = \begin{bmatrix} x_{\dot{u}} & x_{\dot{v}} & x_{\dot{w}} & x_{\dot{p}} & x_{\dot{q}} & x_{\dot{r}} \\ y_{\dot{u}} & y_{\dot{v}} & y_{\dot{w}} & y_{\dot{p}} & y_{\dot{q}} & y_{\dot{r}} \\ z_{\dot{u}} & z_{\dot{v}} & z_{\dot{w}} & z_{\dot{p}} & z_{\dot{q}} & z_{\dot{r}} \\ k_{\dot{u}} & k_{\dot{v}} & k_{\dot{w}} & k_{\dot{p}} & k_{\dot{q}} & k_{\dot{r}} \\ m_{\dot{u}} & m_{\dot{v}} & m_{\dot{w}} & m_{\dot{p}} & m_{\dot{q}} & m_{\dot{r}} \\ n_{\dot{u}} & n_{\dot{v}} & n_{\dot{w}} & n_{\dot{p}} & n_{\dot{q}} & n_{\dot{r}} \end{bmatrix}$$

$$X_{\dot{u}} = \frac{\partial X}{\partial \dot{u}}$$

Hydrodynamic in sea water involves drag and lift forces.

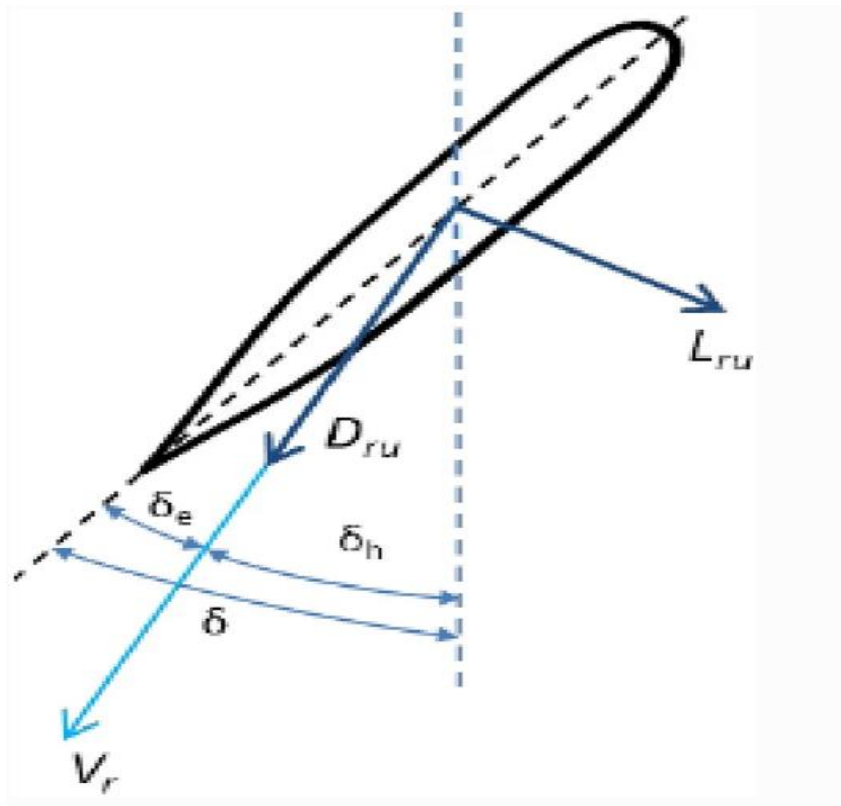


Figure 12

$$F_x = -D_{RU} \cos \delta_h - L_{RU} \sin \delta_h$$

$$F_y = L_{RU} \cos \delta_h - D_{RU} \sin \delta_h$$

$$\tau = x \times (F_x, F_y, 0)$$

These components are transformed into longitudinal and lateral forces and momentum in the Yaw direction.

The drag force caused by the hull on the XZ plane is[3]:

$$D_x = -\frac{\rho}{2}A_f C_{d-hull}(u^2 + w^2) \cos \alpha \cong -\frac{\rho}{2}A_f C_{d-hull}(u^2 + w^2)\left(1 - \frac{\alpha^2}{2}\right)$$

$$D_z = -\frac{\rho}{2}A_f C_{d-hull}(u^2 + w^2) \sin \alpha \cong -\frac{\rho}{2}A_f C_{d-hull}(u^2 + w^2)\alpha$$

The gravitational and buoyancy vector is [2]:

$$g(\eta) = \begin{bmatrix} -(W - B)\sin(\theta) \\ (W - B)\cos(\theta)\sin(\phi) \\ (W - B)\cos(\theta)\cos(\phi) \\ y_g W \cos(\theta)\cos(\phi) - z_g W \cos(\theta)\sin(\phi) \\ -z_g W \sin(\theta) - x_g \cos(\theta)\cos(\phi) \\ x_g W \cos(\theta)\sin(\phi) + y_g W \sin(\theta) \end{bmatrix}$$

All the above equation is for six degrees of freedom motion. In this master thesis consider linear motion model on the XZ plane.

2.8 Selection of glider parameter

The vessel class (which is DWT1500) and the structural design constraints (basically the diving depth) are used as the inputs. Based on these inputs, the glide path angle and ballast fraction are to be defined. The glide path angle and ballast fraction will drive the other global glider parameters that includes the glider velocities, lift force, drag force, and net buoyancy. Finally, the lift to drag ratio, reference wing area and ballast volumetric pump rate can be determined. These last three parameters should be within the range of values determined in the design considerations presented in TABLE 4 below [4].

Key design parameter	Consideration
Diving depth	Minimize to avoid overly heavy structural weight
Glider path angel	This is a parameter to be chosen such that the constraints defined on the other key design parameter can be achieved
Lift/drag ratio	Minimize to avoid large wing areas and aspect ratios(wingspan)
Horizontal speed	100-year design current of 1m/s
Pump capacity	Should be less than 1000 to 1000 m ³ /h to avoid overly large pumps
Ballast fraction	Minimize to avoid overly large pumps
% weight allocated to machinery and miscellaneous items	At least 3 to 5% of DWT

Table 4

Definition of the global glider parameter shows in figure 13 below and the equations used in the calculations are presented inequation below.

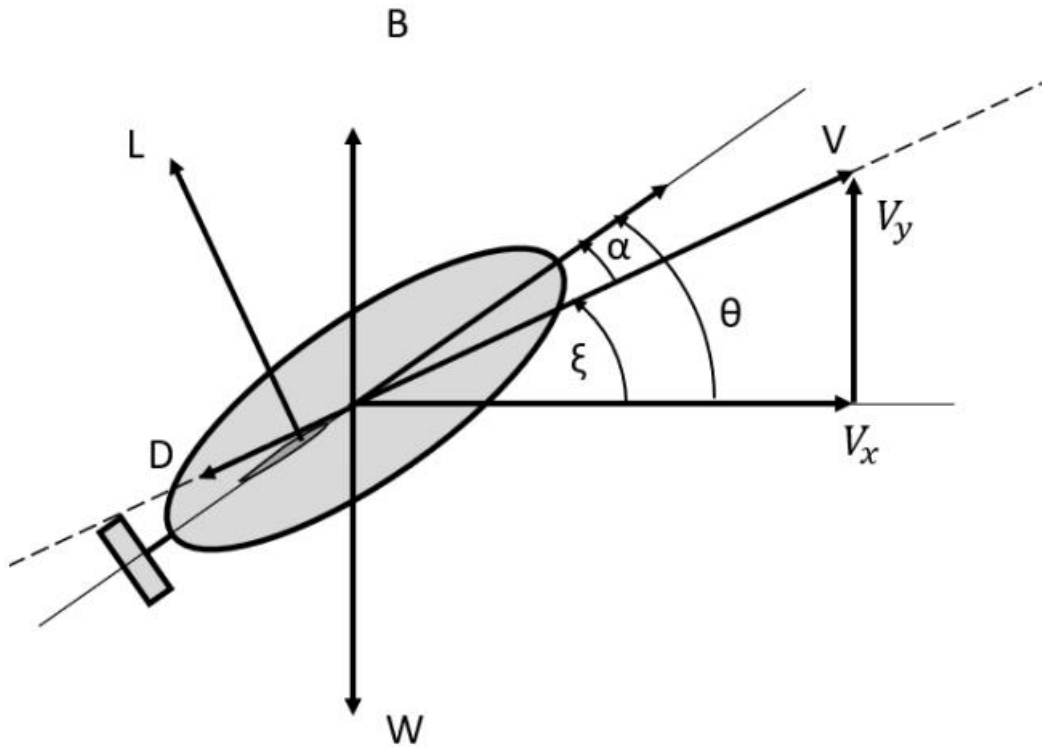


Figure 13 Definition of global glider parameter

$$Frac_{ballast} = \frac{m_0}{DWT * 1000}$$

$$V = \left(\frac{m_0 g \sin \xi}{\frac{1}{2} C_{D,Vol} Vol^{2/3}} \right)^{\frac{1}{2}}$$

$$V_x = V \cos \xi$$

$$D = \frac{1}{2} \rho C_{D,Vol} Vol^{2/3} V^2$$

$$L = \frac{D}{\tan \xi}$$

$$A_{ref} = \frac{L}{\frac{1}{2} \rho C_L V^2}$$

$$Q = \frac{\frac{m_0}{\rho}}{Frac_{pump-time} \frac{T}{2}}$$

The design optimization procedure is employed to determine the most optimal $\text{Frac}_{\text{ballast}}$ and ξ based on constraints set on the following parameters:

- ✧ $V_x = 1 \text{ m/s}$
- ✧ $L/D < 1,5$
- ✧ $A_{\text{ref}} < 20 \text{ m}^2$
- ✧ $Q < 2000 \text{ m}^3/\text{h}$

2.9 Parameter correlation

The parameter for the freight-glider in this master thesis are assumed to be normally distribution with a coefficient of variation (COV) of 5% applied for $C_{D,\text{Vol}}$ and ξ , A COV of 1% is applied for $\text{Frac}_{\text{ballast}}$ and H . The corresponding parameter correlation matrix is presented below:

$\text{Frac}_{\text{ballast}}$ (%)	0,12
C_{D_col}	0,1
C_L	2,1926
ξ (°)	37,5
H (m)	200
A_{ref} (m²)	7,7
V_x (m/s)	1,0
Q (m³/h)	950
NTE	0,02

Table 5

	$\text{Frac}_{\text{ballast}}$	$C_{D,\text{vol}}$	ξ	H	A_{ref}	V_x	Q
$\text{Frac}_{\text{ballast}}$	1	-0,04	-0,07	-0,08	0,03	0,26	0,19
$C_{D,\text{vol}}$		1	0,04	-0,06	0,54	-0,96	-0,30
ξ			1	0,03	-0,81	-0,19	0,90
H				1	-0,05	0,03	-0,12
A_{ref}					1	-0,41	-0,93
V_x						1	0,21
Q							1

Table 6

The following observations are made from the parametric correlation study and the following parameters have strong correlation:

- $C_{D,\text{vol}}$ is strongly correlated to A_{ref} and V_x
- ξ is strongly correlated to A_{ref} and Q
- A_{ref} is strongly correlated to Q

The subsea freight-sliding global design parameters have wide range in probability analysis. in this master thesis I will not go deep into probabilistic analysis, thesis places most emphasis on improvement process and result. In the improvement process in the assignment will come more about probability analysis result.

3.0 Carbon fiber composite material

With the development of science and technology today, the requirements for materials are getting higher and higher, and materials composed of a single substance can no longer meet people's requirements. Therefore, composite materials composed of two or more substances have gradually become people's attention today. The focus of the company and has shown immeasurable development prospects in various industries. Today, when intelligent and environmental protection are vigorously promoted, the development of high-performance, high-value-added composite materials has become an inevitable trend in the development of composite materials. Carbon fiber composite materials are an advanced composite material and their research cannot be ignored.

Carbon fiber composite material is a new type of material formed by the compound of two or more different elements, different shapes, and different properties. Various substances can complement each other in properties and functions, enhance the functions and effects of the substances, make the overall functions and properties of carbon fiber composite materials superior to the constituent substances, and can meet the requirements of various occasions and places. Carbon fiber composite materials also have many applications in the civil field, such as aircraft shell components, EMU brake systems, automotive composite material structures, automotive high-

performance carbon fiber bearings, fishing poles, skis, rackets, etc. Due to the gradual decline in the production cost of carbon fiber and the expansion of production scale, its application will also be rapidly expanded, such as new electrode materials, reinforced concrete, new heating devices and even daily necessities. At the same time, its quality and performance requirements will also increase.

3.1 Advantages of carbon fiber

The composite material composed of carbon fiber and epoxy resin has become an advanced aerospace material due to its small specific gravity, good rigidity, and high strength. Because the weight of the spacecraft is reduced by 1 kilogram, the launch vehicle can be reduced by 500 kilograms. Therefore, in the aerospace industry, there is a rush to adopt advanced composite materials. There is a vertical take-off and landing fighter, which uses carbon fiber composite materials that account for 1/4 of the weight of the aircraft and 1/3 of the weight of the wings. According to reports, the key components of the three rocket thrusters on the US space shuttle and the advanced MX missile launch tube are all made of advanced carbon fiber composite materials. The main advantages of carbon fiber are:

- High strength (5 times that of steel)
- Excellent heat resistance (can withstand high temperatures above 2000°C)

- Excellent thermal shock resistance
- Low thermal expansion coefficient (small deformation)
- Small heat capacity (energy saving)
- Small specific gravity (1/5 of steel)
- Excellent anti-corrosion and radiation performance

3.2 The strength of carbon fiber

Polyacrylonitrile (PAN) polymer was the precursor material from which currently high strength carbon fibers can be processed. carbon filaments were first used in light bulbs in late nineteenth century, PAN based carbon fiber (T1100G) with a tensile strength of 6.6 GPa and tensile modulus of 324 GPa. The tensile strength of high strength PAN based carbon fibers is still less than 10% of the theoretical strength of the carbon–carbon bond, and the modulus is about 30% of the theoretical modulus. On the other hand, continuous pitch-based carbon fibers can be manufactured with modulus as high as 965 GPa. However, these high modulus pitch-based carbon fibers have relatively low tensile strength (3.1 GPa), resulting from large graphitic grain boundaries and relatively low inter-planar shear modulus. Although it is possible to process PAN based carbon fibers with tensile modulus approaching 600 GPa via high temperature carbonization, this high tensile modulus is achieved at the expense of tensile strength (Figure 14) [5]:

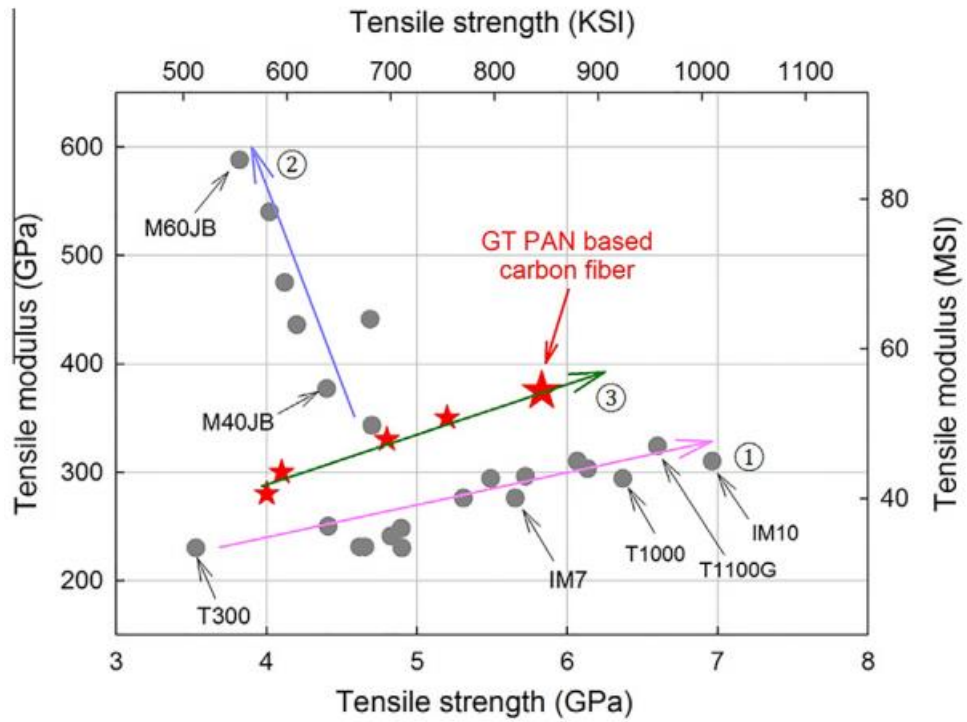


Figure 14

Tensile strength of the GT PAN based carbon fibers at different gauge lengths; defect size calculated by Griffith's equation [22,23] for various carbon fibers based at:

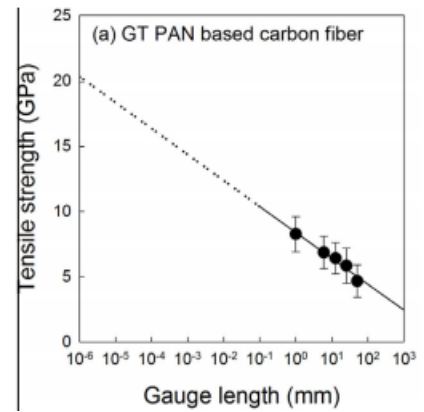


Figure 15

Limiting strength values obtained by extrapolation to 1 nm gauge length.

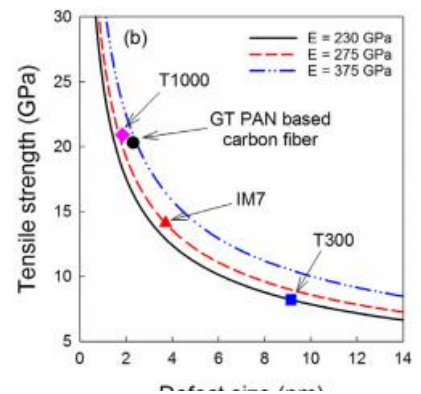


Figure 16

Strength values tested at 25.4 mm gauge length.

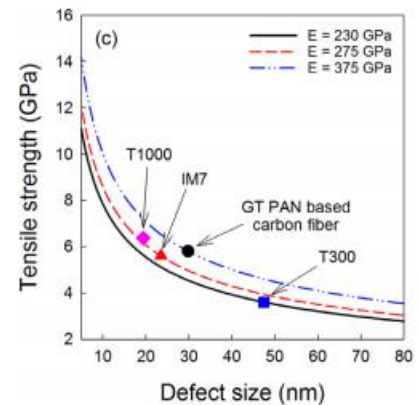


Figure 17

Tensile modulus of the GT PAN based carbon fiber as a function of inverse gauge length to obtain the compliance corrected tensile modulus.

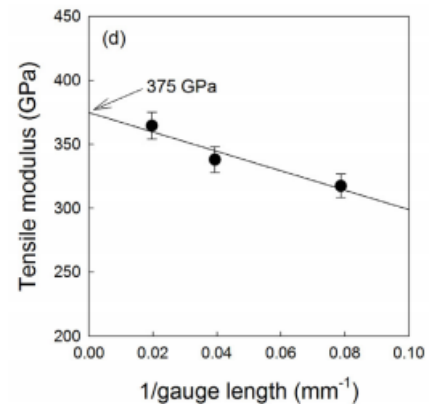


Figure 18

Theoretical tensile modulus [10,25] as a function of full width at half maximum (FWHM) of the (0 02) azimuthal scans for various inter-planar shear modulus (G_{12}) values. Data points for the selected carbon fibers are also shown.

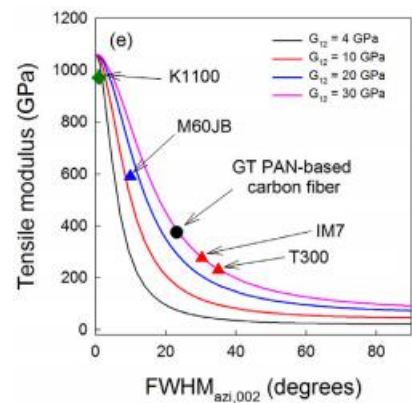


Figure 19

3.3 Mechanical properties of deep-sea carbon fiber composite cylindrical pressure shell

The design of the structural characteristics of the fiber reinforced resin

composite cylindrical pressure shell mainly covers two aspects of micro-fiber interweaving and macro-structural morphology, both of which not only affect the mass-to-volume ratio of the composite pressure shell, but also determine its strength and stability[6].

At present, at the meso level, the fiber reinforced resin composite cylindrical pressure shell mainly includes winding and lamination. The critical buckling load and ultimate buckling load of cylindrical composite laminates such as winding angle, layup angle, and layup type depend on the material type, geometry, boundary conditions and laminate specifications of the composite laminate. The dynamic characteristics and buckling response of thin shell structures change significantly with the changes in thickness, length ratio and stacking sequence between layers. Mon et al. prepared a relatively thick-walled composite cylinder (thickness to radius ratio $t/R=1/18.8$) using filament winding technology, using spiral winding and stirrups ($[\pm 30/90]$ FW, $[\pm 45/90]$ FW and $[\pm 60/90]$ FW) with different parameters, the buckling and post-buckling behaviors and failure modes of medium-thick wall composite cylindrical shells with different winding angles under external static pressure are studied. The layer type, fiber angle and number of layers of carbon fiber/epoxy resin, boron fiber/epoxy resin and glass fiber/epoxy resin composite materials have been optimized. The design pressure of composite materials has a certain restrictive effect. In order to overcome the delamination and shortcomings of the performance of laminated composite

pressure vessels, the braiding process was applied to the design of composite pressure vessels, the effect of braiding angle on elastic constants was studied, and the elastic constants of different volume fractions were studied. prediction. For the structural design and optimization of pressure vessels, the use of woven composite materials instead of fiber winding is of great significance to the structural design and optimization of pressure vessels. However, physical weaving and related tests have not been carried out, and the braided composite pressure vessel is still in the stage of simulation research. Regarding winding, layup and braided composite pressure shells, the existing research lacks standardized design schemes, and does not provide optimal values and design basis for related parameters such as layup method, winding angle, and layup type. No general conclusion has been formed yet. In recent years, with the increase in ocean depth and additional functional requirements, a new type of sandwich/sandwich cylindrical pressure shell has emerged. By rationally selecting the core material and setting the geometric parameters of the cylindrical shell, the sandwich composite cylindrical shell can withstand a pressure of more than 1000m in water depth, which can provide reference for the design and research of the sandwich cylindrical shell of various structures such as deep-sea submersibles and marine pipelines[6].

In the deep-sea environment, composite cylindrical shells are required to withstand huge external pressure, mainly uniform hoop pressure and axial

pressure (as shown in Figure 20). Among them, the hoop pressure presses from the outside to the inside of the cylindrical shell in the

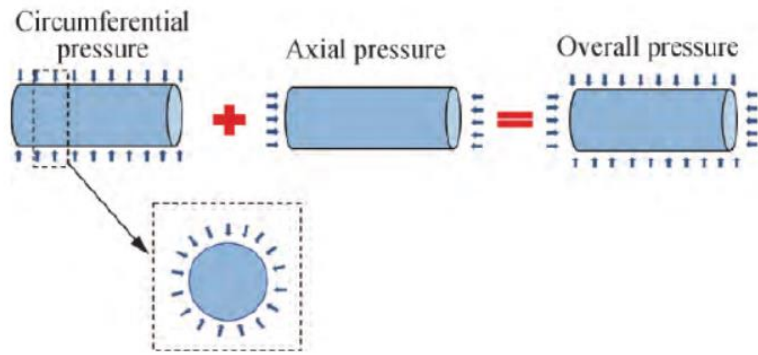


Figure 20

hoop direction, and the axial pressure acts evenly on the end of the cylindrical shell to press from outside to inside.

3.4 Mechanical Analysis of Carbon Fiber Cylindrical Shell

3.4.1 Basic mechanical properties of single-layer boards

A single ply is called a single-layer board, which is the basic unit of the carbon fiber layer and structure. First, discuss the properties of single-layer boards under complex stress states, and then discuss the mechanical properties of composite layers and structures on this basis. 1. The normal axis stress-strain relationship of a single-layer plate under plane stress The single-layer board is used as the basic unit of laminated materials, and its thickness is usually small compared to other dimensions (generally the thickness of a single layer of carbon fiber wound is only 0.2mm), so it can be approximated as:

$$\sigma_z = 0, \tau_{yz} = \tau_{zx} = 0$$

That is, the single-layer material is in a plane stress state. When the

component of the normal stress coincides with the main axis direction of the single-layer board, the single-layer board is in the normal axial stress state, as shown in Figure 21. The normal axial stress-strain behavior of the single-layer plate still conforms to the generalized Hooke's law. Unlike the isotropic material, the orthotropic single-layer plate has five elastic constants, namely:

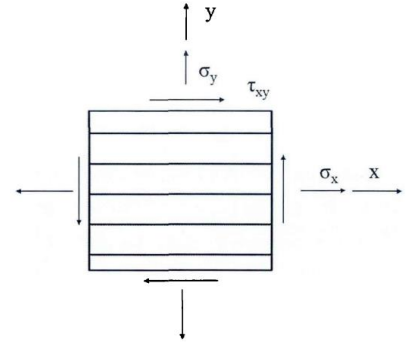


Figure 21

$$E_x, E_y, V_{xy}, V_{yx}, G_{xy}$$

And:

$$\frac{V_{xy}}{V_{yx}} = \frac{E_x}{E_y}$$

The strain-stress relationship in the plane stress state is:

$$\begin{cases} \epsilon_x = \frac{1}{E_x} \sigma_x - \frac{V_{yx}}{E_y} \sigma_y \\ \epsilon_y = -\frac{V_{xy}}{E_x} \sigma_x + \frac{1}{E_y} \sigma_y \\ r_{xy} = \frac{1}{G_{xy}} \tau_{xy} \end{cases}$$

And $E_x, E_y, V_{xy}, V_{yx}, G_{xy}$ is the elastic modulus and Poisson's ratio in the two main directions of the unidirectional plate.

The stress-strain matrix form is:

$$\begin{pmatrix} \sigma_x \\ \sigma_y \\ \tau_{xy} \end{pmatrix} = \begin{pmatrix} Q_{xx} & Q_{xy} & 0 \\ Q_{yx} & Q_{yy} & 0 \\ 0 & 0 & Q_{ss} \end{pmatrix} \begin{pmatrix} \epsilon_x \\ \epsilon_y \\ r_{xy} \end{pmatrix}$$

$$Q_{xx} = \frac{E_x}{1 - V_{xy}V_{yx}}, Q_{yy} = \frac{E_y}{1 - V_{xy}V_{yx}}, Q_{ss} = G_{xy}, Q_{xy} = \frac{E_x V_{yx}}{1 - V_{xy}V_{yx}},$$

$$Q_{yx} = \frac{E_y V_{xy}}{1 - V_{xy}V_{yx}}$$

The off-axis stress state of the single-layer plate is shown in Figure 22.

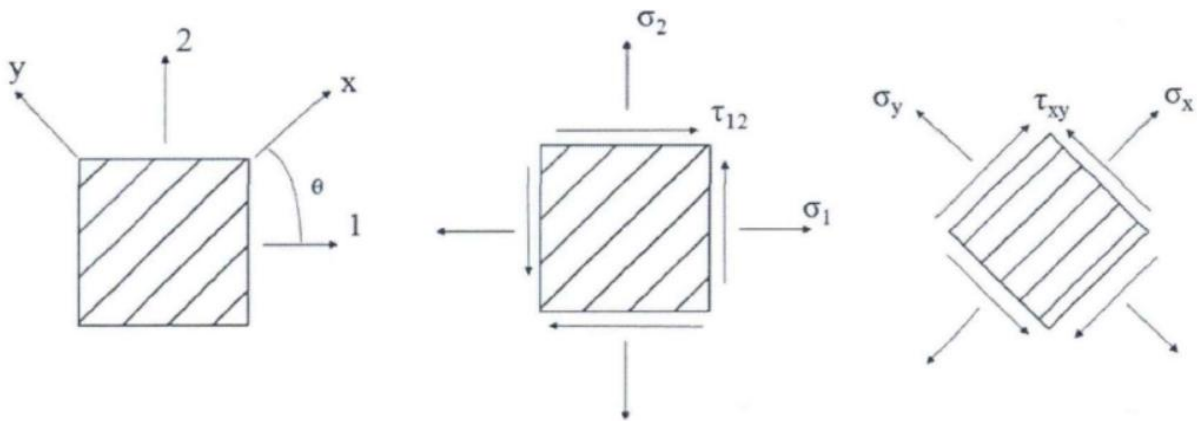


Figure 22

The stiffness characteristics of the single-layer plate in the direction of the material axis still follow the generalized Hooke's law. However, the in-plane stiffness of the single-layer plate changes with the layering angle. This characteristic is the basis of the complex mechanical behavior of laminates. The change of the stiffness of the single-layer board with the layering angle is closely related to the law of the change of stress and strain with the coordinate, and the conversion relationship between stress and strain in different coordinate systems is adopted. It can be obtained that the relationship of the single-layer plate in the off-axis stress-strain state can be expressed as

$$\begin{Bmatrix} \sigma_1 \\ \sigma_2 \\ \tau_{12} \end{Bmatrix} = \begin{Bmatrix} \overline{Q_{xx}} & \overline{Q_{xy}} & \overline{Q_{xs}} \\ \overline{Q_{yx}} & \overline{Q_{yy}} & \overline{Q_{ys}} \\ \overline{Q_{sx}} & \overline{Q_{sy}} & \overline{Q_{ss}} \end{Bmatrix} \begin{Bmatrix} \varepsilon_1 \\ \varepsilon_2 \\ r_{12} \end{Bmatrix}$$

$$\overline{Q_{xx}} = Q_{xx} \cos^4 \theta + 2(Q_{xy} + 2Q_{ss}) \sin^2 \theta \cos^2 \theta + Q_{yy} \sin^4 \theta$$

$$\overline{Q_{xy}} = (Q_{xx} + Q_{yy} - 4Q_{ss}) \sin^2 \theta \cos^2 \theta + Q_{xy} (\sin^4 \theta + \cos^4 \theta)$$

$$\overline{Q_{yy}} = Q_{xx} \sin^4 \theta + 2(Q_{xy} + 2Q_{ss}) \sin^2 \theta \cos^2 \theta + Q_{yy} \cos^4 \theta$$

$$\overline{Q_{xs}} = (Q_{xx} - Q_{xy} - 2Q_{ss}) \sin \theta \cos^3 \theta + (Q_{xy} - Q_{yy} + 2Q_{ss}) \sin^3 \theta \cos \theta$$

$$\overline{Q_{ys}} = (Q_{xx} - Q_{xy} - 2Q_{ss}) \sin^3 \theta \cos \theta + (Q_{xy} - Q_{yy} + 2Q_{ss}) \sin \theta \cos^3 \theta$$

$$\overline{Q_{ss}} = (Q_{xx} + Q_{yy} - 2Q_{xy} - 2Q_{ss}) \sin^2 \theta \cos^2 \theta + Q_{ss} (\sin^4 \theta + \cos^4 \theta)$$

It can be seen from the above that the main difference between the off-axis stress-strain and the normal-axis stress-strain of the single-layer plate is that the off-axis elastic modulus matrix increases the shear coupling component of the normal stress and the shear stress $\overline{Q_{xs}}$ and $\overline{Q_{ys}}$. In other words, a unidirectional laminate that is off axis can cause shear strain under the action of normal stress, and it can also cause normal strain under the action of shear stress. This is called the tension (compression) shear coupling effect of the single-layer plate. This coupling effect is not available in isotropic materials.

3.4.2 Basic mechanical properties of laminates

Laminates are usually composed of multiple single-layer boards glued together to form a whole. The mechanical properties of the layers and boards are related to the mechanical properties of the individual single-layer boards and are related to the order and direction of each layer of single-layer boards.

related. If the main directions of the materials of each single-layer board are laid in different directions and in different orders, laminated structures with different properties can be obtained. Understanding the mechanical properties of layers and plates plays a vital role in the analysis of carbon fiber pressure-resistant cylindrical shells. As show in figure 23 [11]:

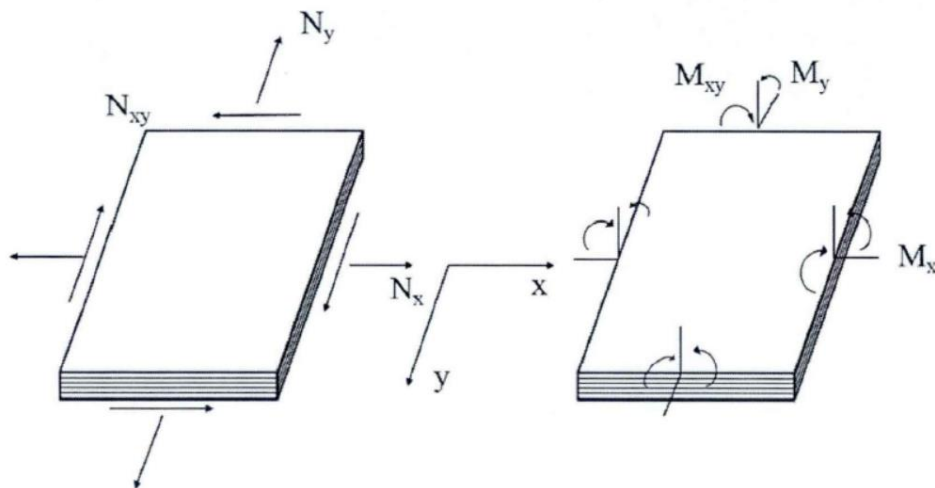
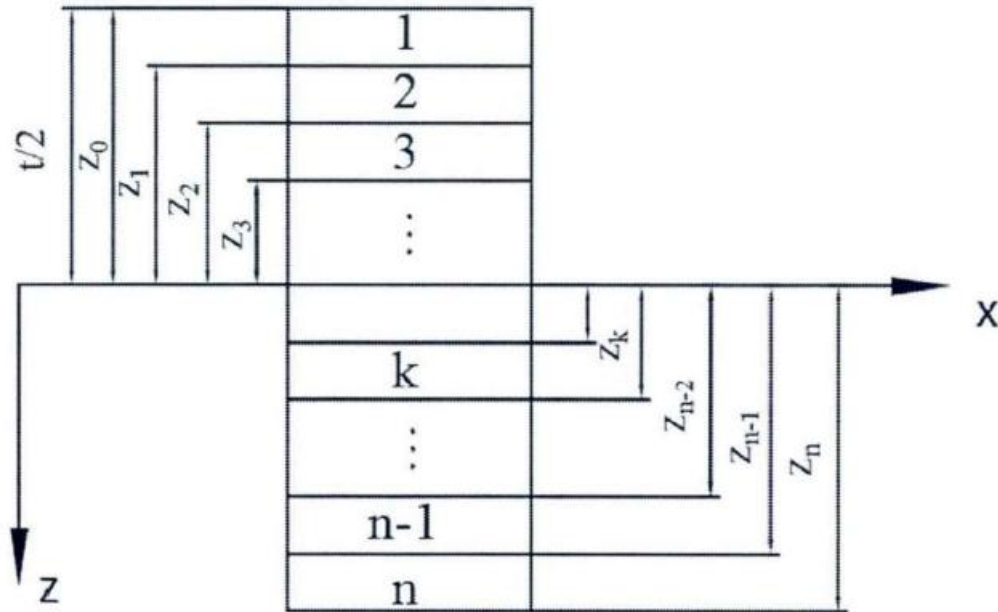


Figure 23

N_x, N_y, N_{xy} is the internal force (tension, pressure or shear force) of the laminate cross section per unit width and M_x, M_y, M_{xy} Is the internal moment of the laminate cross-section per unit width. Coordinate of laminated plates each single show in figure 24 below:


Figure 24

The internal force and internal moment can be obtained by integrating the stress of each layer of the single-layer board along the thickness direction of the laminated board. Assuming that the thickness of the laminated board is “ t ”, then:

$$\begin{Bmatrix} N_x \\ N_y \\ N_{xy} \end{Bmatrix} = \int_{-t/2}^{t/2} \begin{Bmatrix} \sigma_x \\ \sigma_y \\ \tau_{xy} \end{Bmatrix} dz, \quad \begin{Bmatrix} M_x \\ M_y \\ M_{xy} \end{Bmatrix} = \int_{-t/2}^{t/2} \begin{Bmatrix} \sigma_x \\ \sigma_y \\ \tau_{xy} \end{Bmatrix} Z dz$$

Due to the discontinuity of the stress distribution of the laminate, the internal force and internal moment can only be obtained by layered integration, which can be written in the following form:

$$\begin{Bmatrix} N_x \\ N_y \\ N_{xy} \end{Bmatrix} = \sum_{k=1}^n \int_{z_{k-1}}^{z_k} \begin{Bmatrix} \sigma_x \\ \sigma_y \\ \tau_{xy} \end{Bmatrix}_k dz, \quad \begin{Bmatrix} M_x \\ M_y \\ M_{xy} \end{Bmatrix} = \sum_{k=1}^n \int_{z_{k-1}}^{z_k} \begin{Bmatrix} \sigma_x \\ \sigma_y \\ \tau_{xy} \end{Bmatrix}_k Z dz$$

The stress-strain relationship of the “ k ” layer is:

$$\begin{Bmatrix} \sigma_x \\ \sigma_y \\ \tau_{xy} \end{Bmatrix}_k = \begin{Bmatrix} \overline{Q_{xx}} & \overline{Q_{xy}} & \overline{Q_{xs}} \\ \overline{Q_{yx}} & \overline{Q_{yy}} & \overline{Q_{ys}} \\ \overline{Q_{sx}} & \overline{Q_{sy}} & \overline{Q_{ss}} \end{Bmatrix}_k \begin{Bmatrix} \left\{ \begin{matrix} \varepsilon_1^0 \\ \varepsilon_2^0 \\ r_{12}^0 \end{matrix} \right\} + z \left\{ \begin{matrix} k_x \\ k_y \\ k_{xy} \end{matrix} \right\} \end{Bmatrix}$$

K_x, K_y is the bending deflection rate of the single-layer board with respect to the mid-plane of the laminated board, and K_{xy} is a single-layer board with respect to the torsion rate of the mid-plane of the laminated board. So, relation of internal force-strain with laminate layer is:

$$\begin{Bmatrix} \left\{ \begin{matrix} N_x \\ N_y \\ N_{xy} \end{matrix} \right\} \\ \left\{ \begin{matrix} M_x \\ M_y \\ M_{xy} \end{matrix} \right\} \end{Bmatrix} = \begin{Bmatrix} A_{xx} & A_{xy} & A_{xs} \\ A_{yx} & A_{yy} & A_{ys} \\ A_{sx} & A_{sy} & A_{ss} \end{Bmatrix} \begin{Bmatrix} \varepsilon_x^0 \\ \varepsilon_y^0 \\ r_{xy}^0 \end{Bmatrix} + \begin{Bmatrix} B_{xx} & B_{xy} & B_{xs} \\ B_{yx} & B_{yy} & B_{ys} \\ B_{sx} & B_{sy} & B_{ss} \end{Bmatrix} \begin{Bmatrix} k_x \\ k_y \\ k_{xy} \end{Bmatrix}$$

$$\begin{Bmatrix} \left\{ \begin{matrix} M_x \\ M_y \\ M_{xy} \end{matrix} \right\} \\ \left\{ \begin{matrix} M_x \\ M_y \\ M_{xy} \end{matrix} \right\} \end{Bmatrix} = \begin{Bmatrix} B_{xx} & B_{xy} & B_{xs} \\ B_{yx} & B_{yy} & B_{ys} \\ B_{sx} & B_{sy} & B_{ss} \end{Bmatrix} \begin{Bmatrix} \varepsilon_x^0 \\ \varepsilon_y^0 \\ r_{xy}^0 \end{Bmatrix} + \begin{Bmatrix} D_{xx} & D_{xy} & D_{xs} \\ D_{yx} & D_{yy} & D_{ys} \\ D_{sx} & D_{sy} & D_{ss} \end{Bmatrix} \begin{Bmatrix} k_x \\ k_y \\ k_{xy} \end{Bmatrix}$$

$$\text{and} \begin{cases} A_{ij} = \sum_{k=1}^n \overline{(Q_{ij})}_k (Z_k - Z_{k-1}) \\ B_{ij} = \frac{1}{2} \sum_{k=1}^n \overline{(Q_{ij})}_k (Z_k^2 - Z_{k-1}^2) \\ D_{ij} = \frac{1}{3} \sum_{k=1}^n \overline{(Q_{ij})}_k (Z_k^3 - Z_{k-1}^3) \end{cases}$$

A_{ij} is just the stiffness coefficient related to the internal force and the mid-surface strain, which is the tensile (compression) stiffness. D_{ij} is the stiffness coefficient related to the internal torque and the curvature and torsion rate, which is called the bending stiffness. And B_{ij} is represents the coupling relationship between bending and tension (compression), which is called coupling stiffness. Due to the existence of the coupling stiffness, the inward force will not only cause the bending and torsional deformation of the midplane strain at the same time; similarly, the internal torque will not only

cause the torsion deformation, but also the midplane strain. To avoid this tension (compression coupling) effect, even if the B_{ij} coupling stiffness matrix is 0, the laminate can be designed to be a mirror-symmetric ply with respect to the midplane, then:

$$\overline{(Q_{ij})}_{\frac{n}{2}-i} = \overline{(Q_{ij})}_{\frac{n}{2}+i}$$

Coupling stiffness matrix is:

$$B_{ij} = \frac{1}{2} \sum_{k=1}^n \overline{(Q_{ij})}_k (Z_k^2 - Z_{k-1}^2)$$

The basic mechanics equations of composite materials are used for mechanical analysis of carbon fiber cylindrical shells. According to the criteria for distinguishing between thin-walled cylindrical pressure vessels and thick-walled cylindrical pressure vessels, when the ratio of outer diameter to inner diameter is greater than 1.2, the pressure vessel is a thick-walled pressure vessel. The isotropic stress of a thick-walled pressure vessel of isotropic material is [10]:

$$\sigma_{\theta} = A + \frac{B}{r^2}, \sigma_r = A - \frac{B}{r^2}, \sigma_z = \frac{P_i R_i^2 - P_o R_o^2}{R_o^2 - R_i^2}$$

Where

$$A = \frac{P_i R_i^2 - P_o R_o^2}{R_o^2 - R_i^2}, B = \frac{(P_i - P_o) R_i^2 R_o^2}{R_o^2 - R_i^2}$$

Because the hoop stress of the thick-walled cylindrical barrel is distributed in the direction of the wall thickness, and the anisotropy of the composite material increases the complexity of the mechanical analysis of the carbon

fiber cylindrical shell, in order to simplify the mechanical model of the carbon fiber cylindrical shell, the cylindrical shell designed above is The structure of is $[90/90/0]_{25}$, evenly wound, the 150-layer laminated structure is divided into 50 $[90/90/0]$ sub-laminated structures, first consider the plane force state of the sub-laminated structure such as shown in Figure 25.

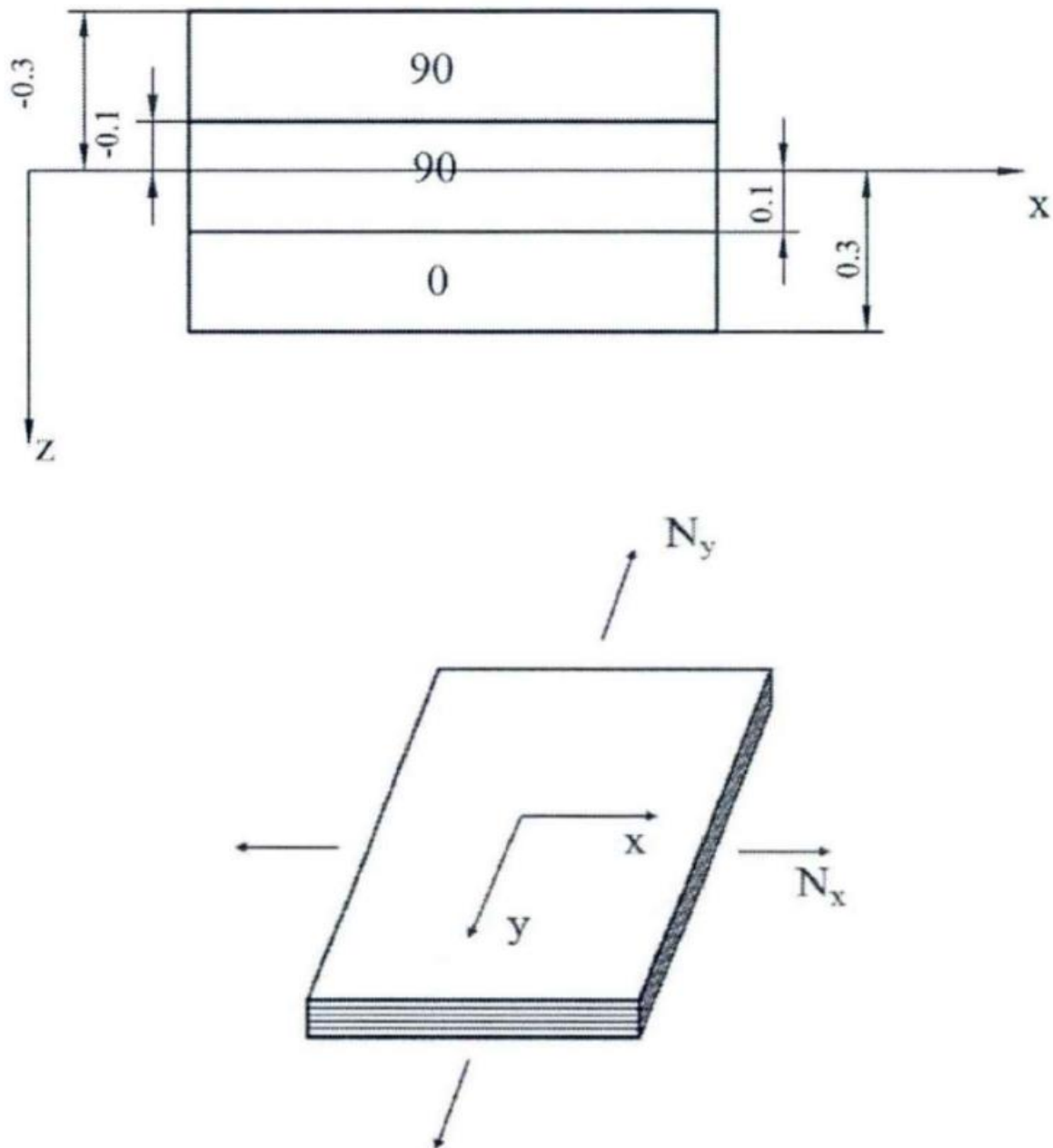


Figure 25

Since the number of layers of the sub-laminated structure is very small and the thickness is very small, it can be considered that the strain of the sub-laminated board is the same, and the internal force-strain relationship of the laminate can be simplified as [10]:

$$\begin{pmatrix} N_x \\ N_y \\ N_{xy} \end{pmatrix} = \begin{pmatrix} A_{xx} & A_{xy} & A_{xs} \\ A_{yx} & A_{yy} & A_{ys} \\ A_{xs} & A_{ys} & A_{ss} \end{pmatrix} \begin{pmatrix} \varepsilon_x^0 \\ \varepsilon_y^0 \\ r_{xy}^0 \end{pmatrix}$$

3.4.3 Carbon fiber Poisson's ratio and modulus of elasticity

Carbon fiber has the two major characteristics of carbon material's strong tensile strength and fiber softness and processability. It is a new material with excellent mechanical properties. The tensile strength of carbon fiber is about 2 to 7 GPa, and the tensile modulus is about 200 to 700 GPa. The density is about 1.5 to 2.0 grams per cubic centimeter, which is mainly determined by the temperature of the carbonization process in addition to the structure of the original silk. Generally, after high temperature 3000°C graphitization treatment, the density can reach 2.0 grams per cubic centimeter. In addition, its weight is very light, its specific gravity is lighter than aluminum, less than 1/4 of steel, and its specific strength is 20 times that of iron. The thermal expansion coefficient of carbon fiber is different from other fibers, and it has the characteristics of anisotropy. The specific heat capacity of carbon fiber is generally 7.12. The thermal conductivity decreases with increasing temperature and is negative (0.72 to 0.90) parallel

to the fiber direction, and positive (32 to 22) perpendicular to the fiber direction.

T700 Carbon fiber is a new type of fiber material with high strength and high modulus fiber with a carbon content of more than 95%. The T number of carbon fiber refers to the grade of carbon material. In the industry, it specifically refers to a certain type of carbon material produced by Japan's Toray Company. Outside the industry, it refers to ultra-high-precision carbon materials. How much T refers to the tonnage of tensile force that this type of carbon fiber with a cross-sectional area of 1 square centimeter can withstand. Therefore, in general, the higher the T number, the higher the carbon fiber grade and the better the quality[12]. The parameters of carbon fiber T700-12K are as follows:

- ✚ Monofilament diameter: 0-8 μ
- ✚ Poisson's ratio 0.307
- ✚ Elastic modulus (MPa) $\geq 2.1 \times 10^5$
- ✚ Tensile strength (MPa) ≥ 3500
- ✚ Fiber density: 1.74-1.79G/cm³
- ✚ Elongation (%) ≥ 1.5
- ✚ Carbon content: $\geq 95\%$

From 3.4.2 equation about laying angle of sub-laminate find the stiffness matrix:

$$\begin{Bmatrix} A_{xx} & A_{xy} & A_{xs} \\ A_{yx} & A_{yy} & A_{ys} \\ A_{xs} & A_{ys} & A_{ss} \end{Bmatrix} = \begin{Bmatrix} 28 & 1,68 & 0 \\ 1,68 & 50,3 & 0 \\ 0 & 0 & 2,88 \end{Bmatrix}$$

With reference to the stress distribution of the thick-walled cylindrical shell of isotropic materials, it can be seen that the sub-laminated plate on the inner wall of the carbon fiber cylindrical shell is subjected to the largest stress, because the thickness of the single layer is 0.3%. 2mm, the thickness of the sub-laminated structure is 0.6mm, which is very thin. It can be approximated that the binomial stress of the sub-laminated structure keeps changing along its thickness direction. Then the internal force of the sub-laminate on the inner wall is:

$$\begin{Bmatrix} N_x \\ N_y \\ N_{xy} \end{Bmatrix} = \begin{Bmatrix} \sigma_z^t \\ \sigma_\theta^t \\ 0 \end{Bmatrix}$$

Strain of the middle layer of the sub-laminate is:

$$\begin{Bmatrix} \varepsilon_x^0 \\ \varepsilon_y^0 \\ r_{xy}^0 \end{Bmatrix} = \begin{Bmatrix} A_{xx} & A_{xy} & A_{xs} \\ A_{yx} & A_{yy} & A_{ys} \\ A_{xs} & A_{ys} & A_{ss} \end{Bmatrix}^{-1} \begin{Bmatrix} N_x \\ N_y \\ 0 \end{Bmatrix}$$

The plane stress of the 90-degree layer in the sub-laminate is as follows:

$$\begin{Bmatrix} \sigma_x \\ \sigma_y \\ \tau_{xy} \end{Bmatrix}_{90} = \begin{Bmatrix} \overline{Q_{xx}} & \overline{Q_{xy}} & \overline{Q_{xs}} \\ \overline{Q_{yx}} & \overline{Q_{yy}} & \overline{Q_{ys}} \\ \overline{Q_{sx}} & \overline{Q_{sy}} & \overline{Q_{ss}} \end{Bmatrix}_{90-degree} \begin{Bmatrix} \varepsilon_1^0 \\ \varepsilon_2^0 \\ 0 \end{Bmatrix}$$

The 0-degree layer stress in the sub-laminated board is as follows

$$\begin{Bmatrix} \sigma_x \\ \sigma_y \\ \tau_{xy} \end{Bmatrix}_0 = \begin{Bmatrix} \overline{Q_{xx}} & \overline{Q_{xy}} & \overline{Q_{xs}} \\ \overline{Q_{yx}} & \overline{Q_{yy}} & \overline{Q_{ys}} \\ \overline{Q_{sx}} & \overline{Q_{sy}} & \overline{Q_{ss}} \end{Bmatrix}_{0\text{-degree}} \begin{Bmatrix} \varepsilon_1^0 \\ \varepsilon_2^0 \\ r_{xy}^0 \end{Bmatrix}$$

From this, the stresses of all 90-degree layers and 0-degree layers in different directions can be obtained, and the 90-degree layer stress results in figure 26 and figure 27 below:

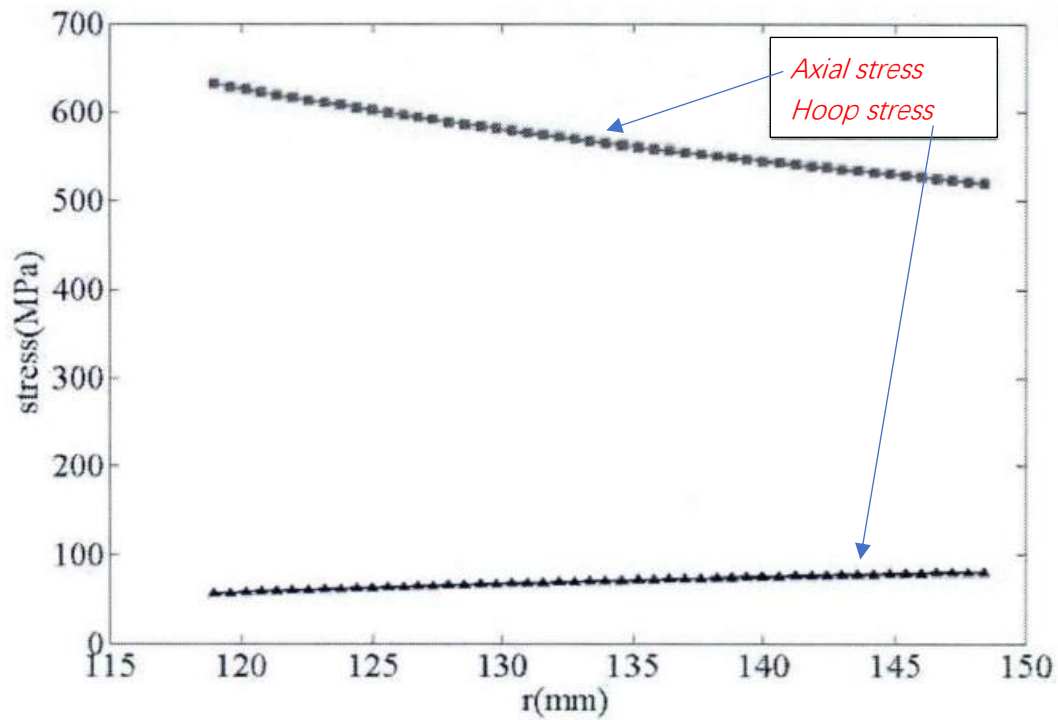


Figure 26 Hoop stress and axial stress of 90 degrees layer distribution along the thickness direction

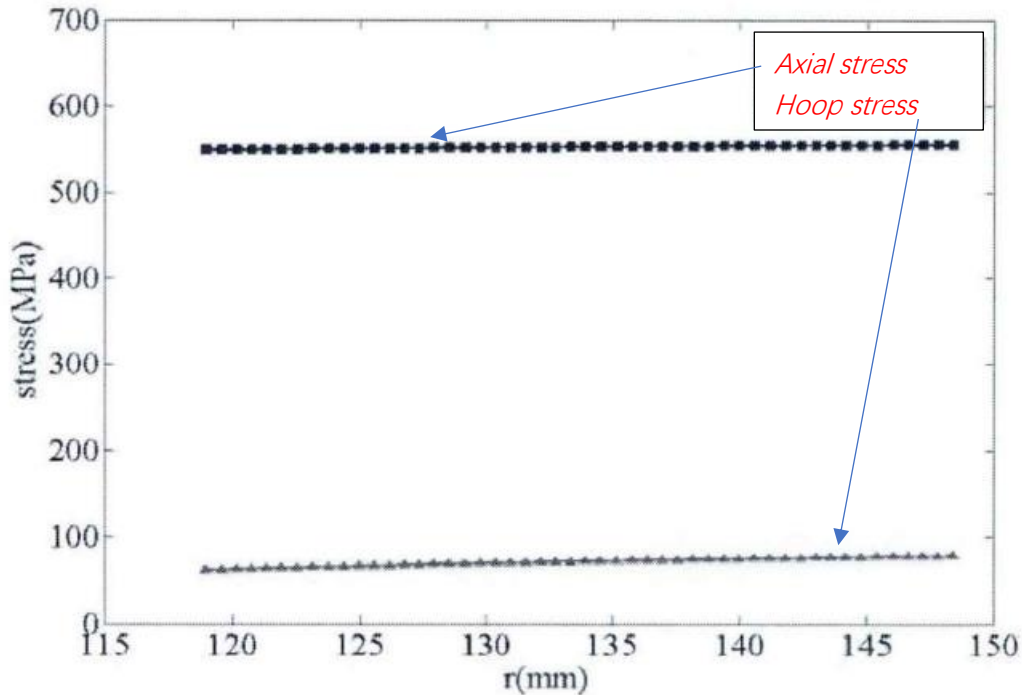


Figure 27 Hoop stress and axial stress of 0 degrees layer distribution along the thickness direction

The maximum axial stress of the 90-degree layer is 80 MPa and the minimum is 56 MPa. The maximum circumferential stress is 631 MPa and the minimum is 543 MPa. The maximum circumferential stress occurs in the thickness direction of the cylinder. The innermost wall. The result of 0-degree layer stress is shown in Figure 15. Shown. The maximum axial stress of the 0-degree layer is 556 MPa, and the minimum stress of 549 MPa remains basically unchanged. The maximum axial stress occurs on the outermost side of the cylinder wall. The maximum circumferential stress is 78.2MPa and the minimum is 61MPa. It is distributed along the wall thickness in a gradient. The maximum circumferential stress occurs on the innermost side of the cylinder wall. This result is different from the equal-

strength design theory in the quasi-grid design, which is mainly caused by the neglect of the rigidity and bearing capacity of the matrix in the grid design.

3.5 Ring ribbed reinforce cylinder

The ring-fin reinforced cylindrical shell is the main pressure-resistant structure of the submarine, which can effectively improve the structural stability of the cylindrical shell. It mainly includes two forms of ring-shaped rib reinforcement and shape reinforcement [8].

- ✚ The stiffened ribs can greatly improve the efficiency of the pressure shell structure, and the buckling load of the stiffened structure is little affected by the initial defects.
- ✚ The mesh stiffening can effectively reduce or eliminate the local buckling response near the opening area. It can increase the critical load of the shell more effectively. The grid-reinforced shell (especially the grid column) is still a common structural form of the deep-sea pressure shell.
- ✚ Ribbed and ribbed cylindrical pressure shell. The initial buckling and post-buckling resistance of the axial compression have been significantly improved. In the elastic deformation stage of the axial compression process, the influence of the stiffened ribs on the structural rigidity plays a leading role.

- ✚ The cylindrical shell with layered stiffened ribs has Higher specific strength, but the overall instability and local buckling are restricted by the layered stiffened ribs.
- ✚ In the ring-ribbed sandwich cylindrical shell structure, when the support stiffness of the ring ribs increases to a certain value, the long cabin The buckling mode will change from overall buckling to a multi-segment single-segment buckling mode limited by the boundary of the ring ribs. The height of the ring ribs is called the critical ring rib height for effective support of the ring ribs. When the height of the ring ribs is greater than the critical height of the ring ribs, the segmented buckling load of the structure has little to do with the properties of the ring ribs, which is mainly related to the size and material properties of the sandwich cylindrical shell itself.
- ✚ The number of ribs can affect the criticality of the cylindrical shell For pressure, when the thickness-radius ratio is constant, the critical pressure of a cylindrical shell increases with the increase of the number of ribs, and the increase of the critical pressure increases with the increase of the number of ribs. Figure 28 shows the manufacturing process of a layered orthogonally stiffened column of carbon fiber reinforced resin composite materials.

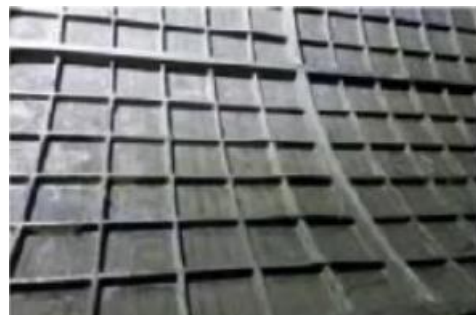


Figure 28

The existing researches mainly focus on the design of shallow water composite cylindrical pressure shells. The research on thin shells is relatively mature, while the research on medium thick shells (thickness to radius ratio $t/R > 1/10$ [38-41]) Research is relatively small. In fact, the fiber-reinforced structure used for composite materials has a rich design, and can also include three-dimensional weaving, three-dimensional weaving, fine-knitting puncture, stitching puncture, three-dimensional stitching, or coupling forms of several structures. However, only winding, and laminated structures are currently used, which greatly limits the application and development of fiber-reinforced resin composite pressure shells. Therefore, with the increase of deep diving depth, how to realize the effective design of meso and macro structure, and then meet the pressure and weight requirements of the pressure hull is the development focus.

3.6 Fiber composite failure criteria

The fiber composite laminate is composed of a single-layer board as the basic unit. To study and judge the damage of the laminate structure, it is necessary to first understand the basis for the failure of the single-layer board. The single-layer thin sheet of fiber-reinforced composite material can be regarded as an orthotropic sheet under plane stress. The strength theory of orthotropic materials can predict the strength failure value of composite materials under various loads. The final failure strength value of the material

is a basic index to ensure safety in engineering design. Therefore, it is necessary to study the destruction criterion.

3.6.1 The maximum stress criterion

The maximum stress criterion for unidirectional composite materials believes that when the material enters failure from the linear elastic state under complex stress transitions, it is because a certain stress component has reached the corresponding basic strength of the material, that is, the direction of the main axis of the material is obtained through coordinate conversion σ_x , σ_y , σ_{xy} Should satisfy the following conditions:

$$\begin{cases} |\sigma_x| < X_t(X_c) \\ |\sigma_y| < Y_t(Y_c) \\ |\tau_{xy}| < S \end{cases}$$

$X_t(X_c)$ Is the tensile (compressive) strength in the fiber direction. $Y_t(Y_c)$ is the tensile (compressive) strength perpendicular to the fiber direction. S is the in-plane shear strength. The three inequalities are independent of each other, and only one of the above inequalities If it is not satisfied, it is considered that the material has been damaged. In this theory, the interaction between various failure modes is not considered.

3.6.2 Tsai-Hill Strength criterion

The Tsai-Hill strength criterion is based on Tsai Weylin's in 1965 in R. Hill's anisotropic material is proposed based on plasticity. The criterion considers

the mutual influence between various stresses, and the condition for the material not to fail is [9]:

$$F. I = \left(\frac{\sigma_x}{X}\right)^2 + \left(\frac{\sigma_y}{Y}\right)^2 + \left(\frac{\tau_{xy}}{S}\right)^2 - \left(\frac{\sigma_x \sigma_y}{X^2}\right) < 1$$

X is the tensile (compressive) strength in the fiber direction, Y is the tensile and compressive strength perpendicular to the fiber direction, S is the in-plane shear strength. When σ_x is tensile stress, $X=X_t$, on the contrary $X=X_c$. when σ_y is tensile stress, $Y=Y_t$, contrary $Y=Y_c$. F.I is failure criteria. When $F. I=1$ indicates a critical state. When $F. I < 1$, the farther the distance 1 is, the farther away from the destruction. From section 3.4.3 Interaction between stresses in all directions considered in Tsai-Hill theory Therefore, each layer should be checked one by one. The Strength criterion results of the check are shown in Figure 29 and 30.

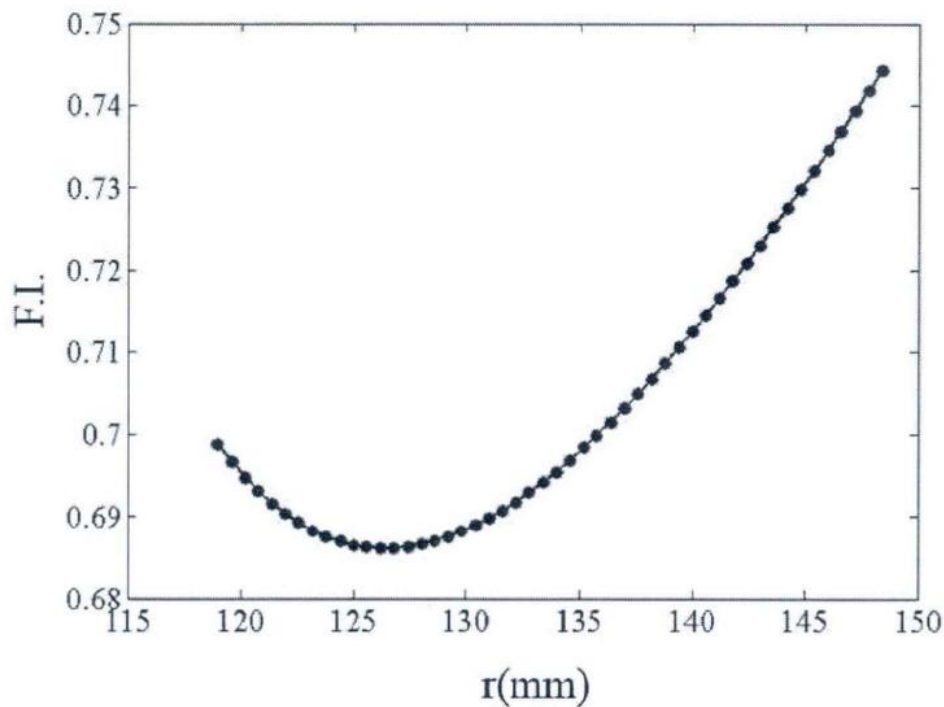


Figure 29 Strength criterion results of 90 degrees layer

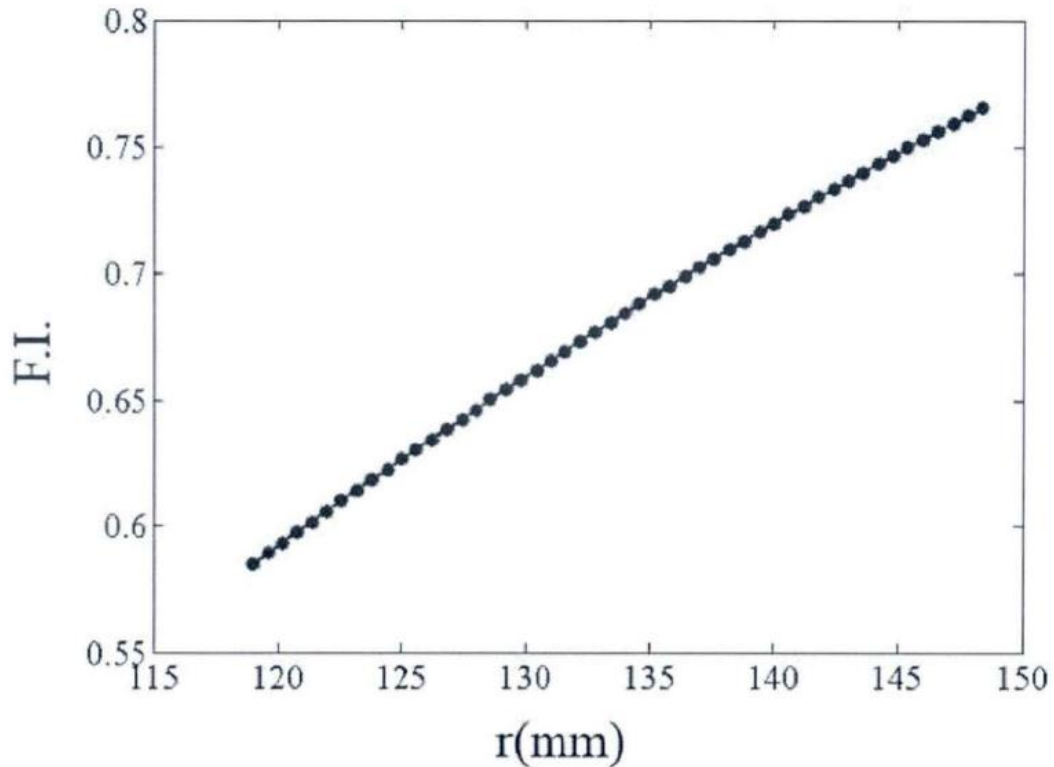


Figure 30 Strength criterion results of 0 degrees layer

3.6.3 Tsai-Wu stress criteria

Since the Tsai-Hill criterion does not consider composite materials with different tensile and compressive properties, the Tsai-Wu strength criterion is further improved based on the previous criterion for the orthotropic single-layer plate in the plane stress state. The condition that the material does not break under the strength criterion is:

$$F.I. = F_x \sigma_x + F_y \sigma_y + F_{xx} \sigma_x^2 + F_{yy} \sigma_y^2 + F_{xy} \sigma_x \sigma_y < 1$$

Where

$$F_x = \frac{1}{X_t} - \frac{1}{X_c}, F_y = \frac{1}{Y_t} - \frac{1}{Y_c}, F_{xx} = \frac{1}{X_t X_c}$$

$$F_{yy} = \frac{1}{Y_t Y_c}, F_{ss} = \frac{1}{S^2}, F_{xy} = -\frac{1}{2\sqrt{X_t X_c Y_t Y_c}}$$

Different from the maximum strength criterion, the Tsai-Wu strength criterion considers the interaction between the stresses, as long as the failure factor ($F.I < 1$) When it is considered that the strength of the ply meets the condition. Here

$$F.I = F_x \sigma_x + F_y \sigma_y + F_{xx} \sigma_x^2 + F_{yy} \sigma_y^2 + F_{ss} \sigma_s^2 + 2F_{xy} \sigma_x \sigma_y < 1$$

Therefore, the layer with the greatest stress should not be taken for a separate check, and all layers should be checked one by one. Pay attention to the positive and negative of the stress when checking, where the tensile stress is positive, and the compressive stress is negative. Figures 31 and 32 show the results of the Tsai-Wu verification for the 90-degree and 0-degree layers.

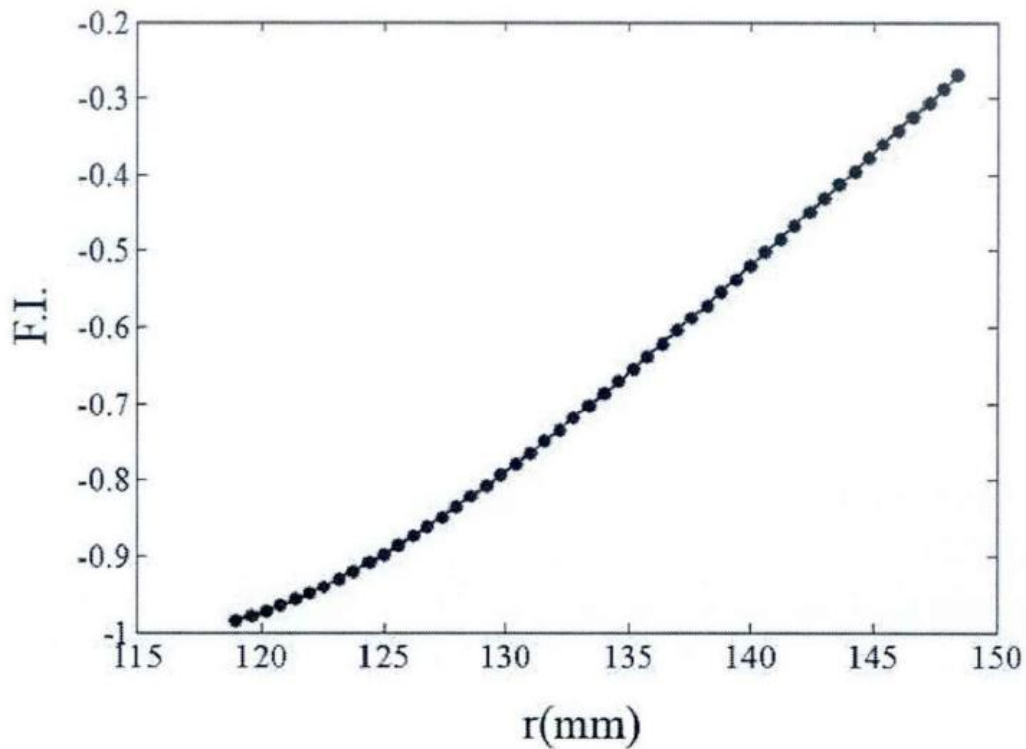


Figure 31 Strength criterion results of 90 degrees layer

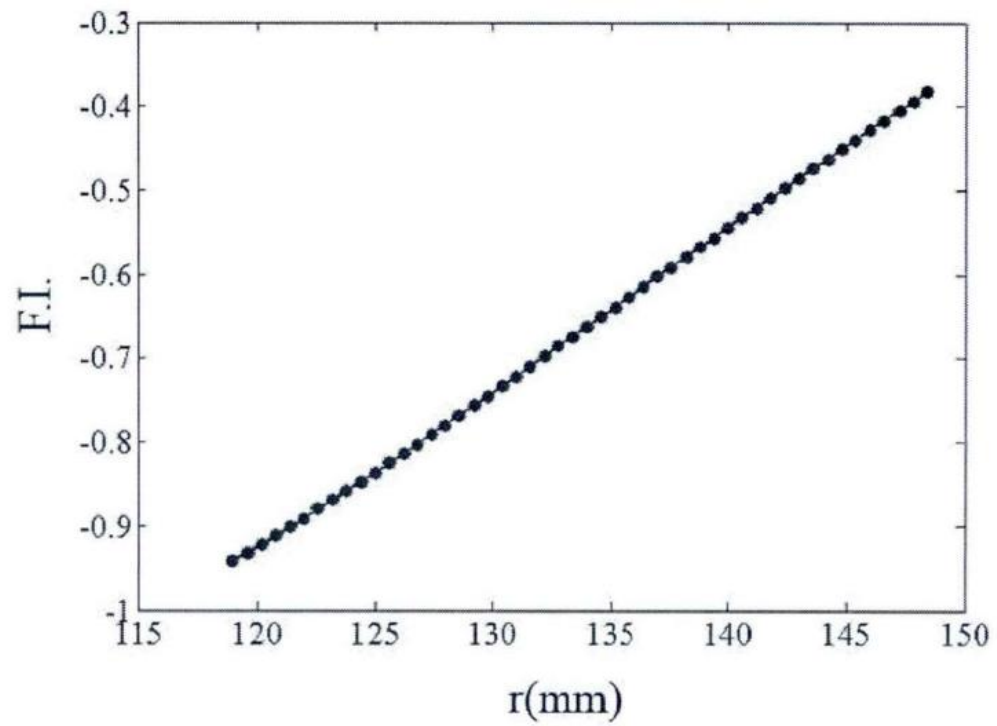


Figure 32 Strength criterion results of 0 degrees layer

4.0 Optimization method

In the previous section, an assignment was written about whether the optimization process will take place in both material and cabin body construction.

4.1 Material optimization method

This section will analyze the use of carbon fiber composite as a material to replace steel in subsea freight gliders. analysis will include analysis of partial or total compensation. Analysis considers changes in weight, pressure, deformation, economic reason, and reliability. Carbon fiber has a lower density than steel, but at the same time with a greater tolerance for pressure and deformation. deformation to analyze simultaneously with hydrostatic pressure, subsea pressure from both outside and pressure from inside with oil and gas that has less density than seawater. Analysis with 3D drawing using ANSYS system to analyze deformation in different subsea depths. task has analyzed pressure change at different depths from section 2.1 and this will be used for deformation change in the whole freight glider throughout the analysis. at the same time, the optimization process will also try to find the maximum diving depth after new material change. Consider reliability will task analyze also about new material replacement possibility, this argument consider and the floating stability of the dive angle and the maximum lift during, and the changes in the hull when internal and external

pressures are applied at the same time. From section 2.3 figure 3 shows the freight-glider body including cylinder shape, ring shape, plate shape and hemispherical shape. form difference performs different degree of deformation, task will use ANSYS to find the safest reliability for practical possible.

4.2 Hull structure optimization method

In section 3.4, the task name has a difference in structure building. analysis of structure is combined with material. The 2 analyzes must be analyzed simultaneously to find the best optimization. analysis takes place a layer plates and laminar plate in relation to pressure and deformation. For reliability, holes will include multiple layers, i.e. laminar structure. Analyzing pressure tolerance for laminar layer and deformation takes place through ANSYS which shows later in the thesis. In section 3.1 has described density for weight for Carbon fiber, it may lead to structure optimization which has the potential to reduce the number of Stiffeners as the name in section 2.2. In the event of material change leading to a reduced total weight for the Freight glider, it will be possible to enlarge the Cargo tank by the same size as the Buoyancy tank. Analysis will be using ANSYS program to analyze opportunity and discuss reliability.

5.0 Subsea freight-glider optimization analysis

Finite element analysis (FEM) uses simple problems to replace complex problems before solving. It decomposes the original complex model into many finite and simple sub-domains, assumes a more appropriate approximate solution for each sub-domain, and then derives the total solution of the entire domain to obtain the solution of the complex problem. The solution obtained by finite element is not an accurate solution, but a result of myopia. As most practical engineering problems are difficult to obtain accurate solutions, and finite element not only has high calculation accuracy, but also has good adaptability, so it has become a very effective practical engineering analysis method. The idea of the finite element method can be traced back to the ancients' practice of "turning the whole into parts" and "turning the circle into straightness". Such as China's "Cao Chong weight elephant" allusions. Figure 33.

These reflect the idea of discrete approximation, that is, many simple small objects are used to "fill" large complex objects. Figure 34 below show the ANSYS

analysis face meshing for a cylinder pipe with 50-meter length.



Figure 33

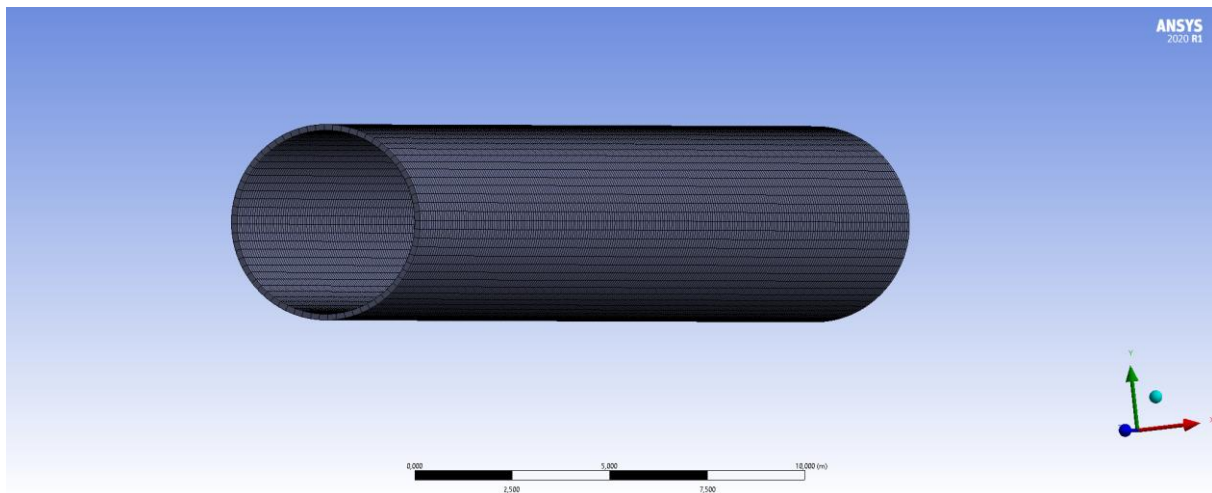


Figure 34

The Ansys finite element software simulates the layering direction of the fiber composite material and the thickness of each layer through the lamination unit to model the fiber composite material. It can accurately analyze the failure and damage of the fiber composite material and the interlayer Effect and so on. This chapter uses Ansys finite element software to analyze the strength and stability of the metal parts of the carbon fiber cylindrical shell and the spherical shell. Based on the Ansys analysis, the problem of stress concentration at the contact between the spherical shell and the cylinder is improved. Finally, a quantitative analysis of the volumetric compression of the entire pressure cabin during the dive of the glider is carried out.

5.1 Subsea freight-glider structure

In Sections 1.1 and 2.3 show the task design subsea freight-glider built of Cargo tank, Buoyancy / ballast tank and stiffener. Hydrodynamic wing is not

considered in this pressure analysis process.

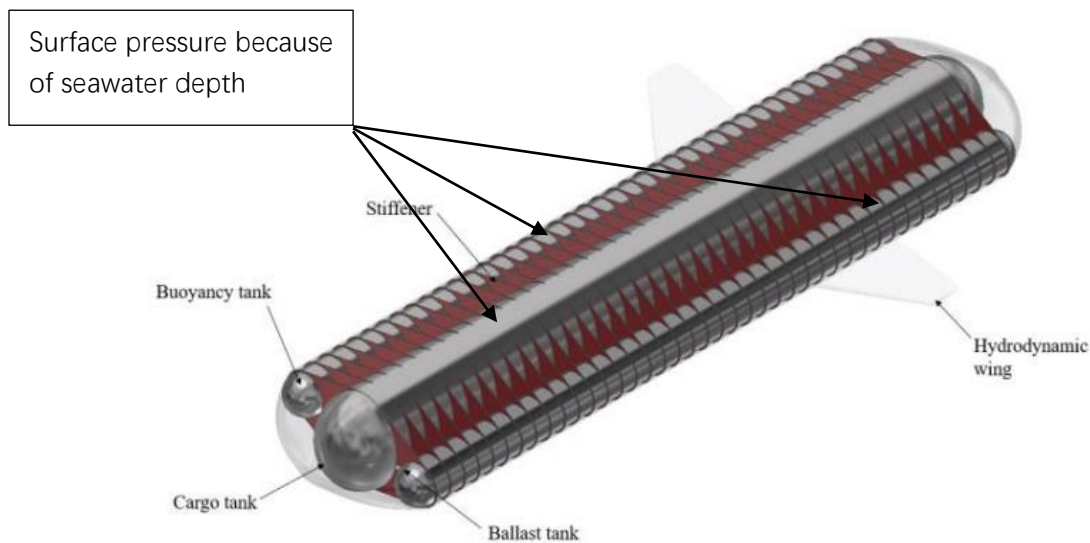


Figure 35

And drawing 3D structure with ANSYS in figure 36 below

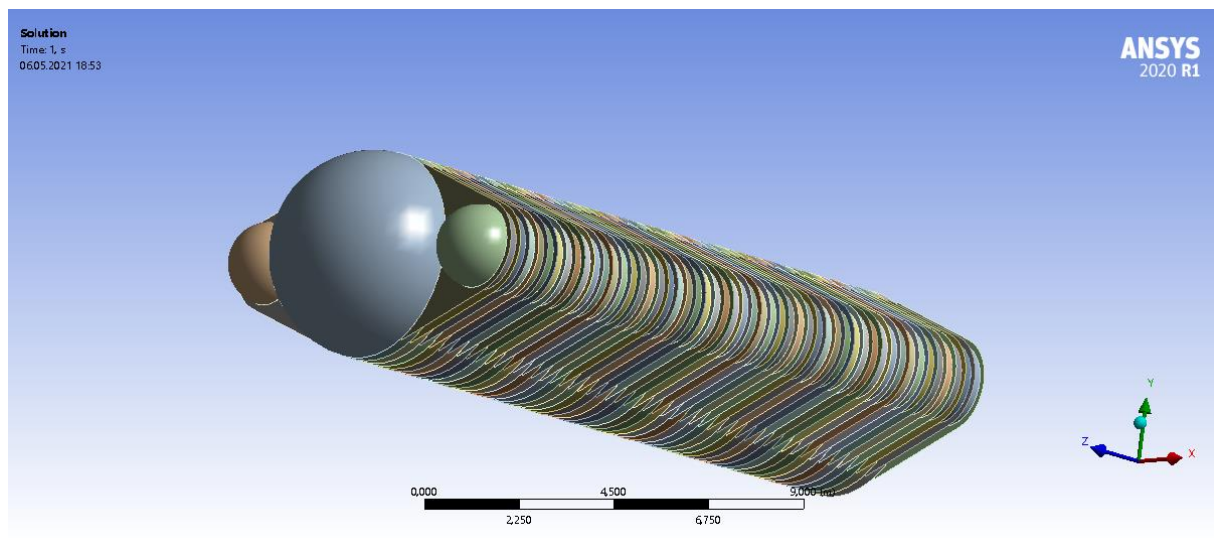


Figure 36

In section 2.3, the subsea freight-glider parameter for vessel length has a total of 50 meters and a cargo tank with an outer diameter of 5 meters and a cargo tank weighing 785 tons. Steel has density with 7850 kg/m^3 , and so equation below show cargo tank inner diameter with 4.7 meter. And the Spherical shell used the same outer/inner diameter.

$$W = (r_{outer}^2 - r_{inner}^2) * \pi * h * \rho$$

Used ANSYS 2020 R1 3 D drawing show the cargo tank below in figure 37 and figure 38.

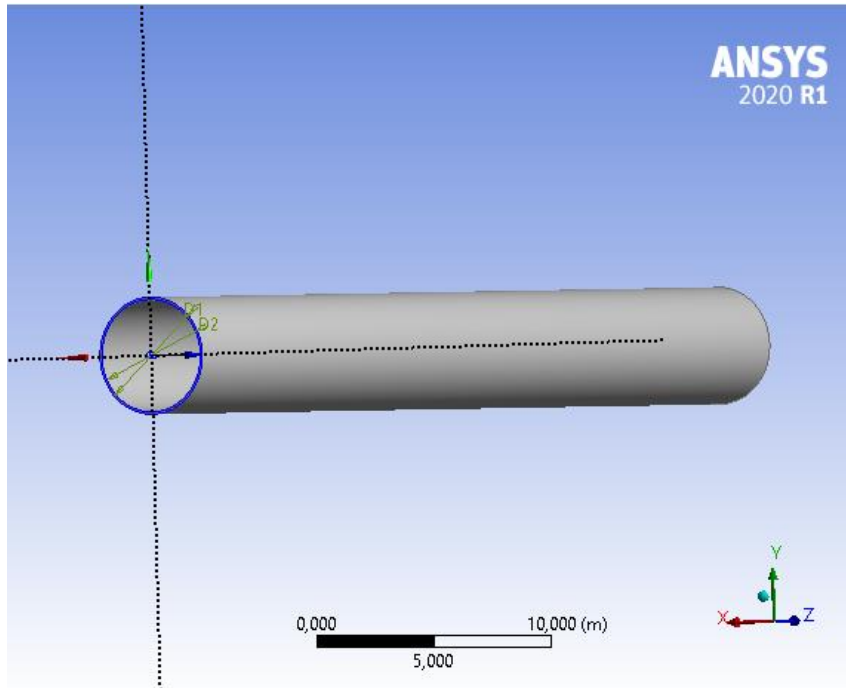


Figure 37

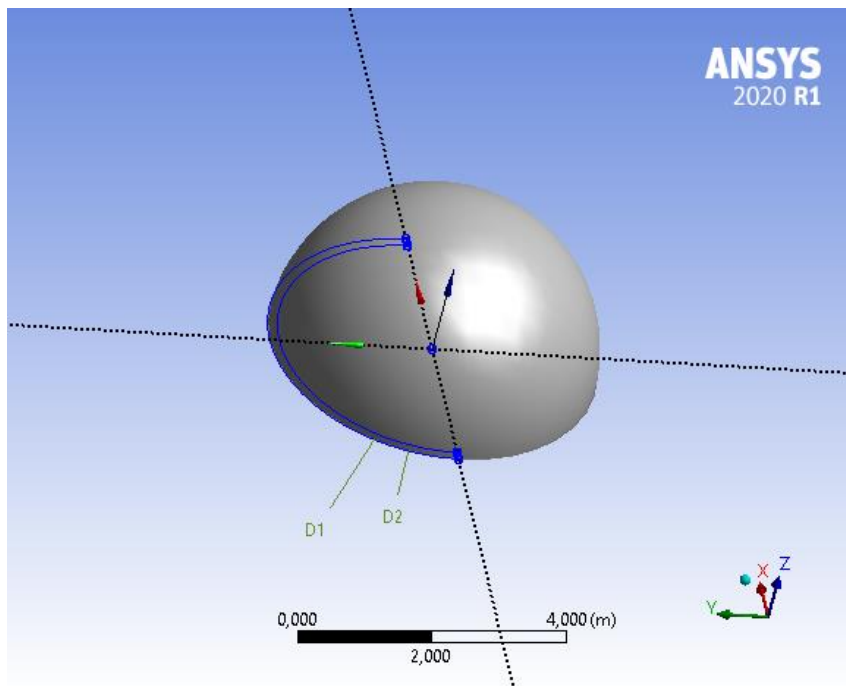


Figure 38

Buoyancy tank used same principle with the same diameter and 3D drawing shows below in figure 39 and figure 40:

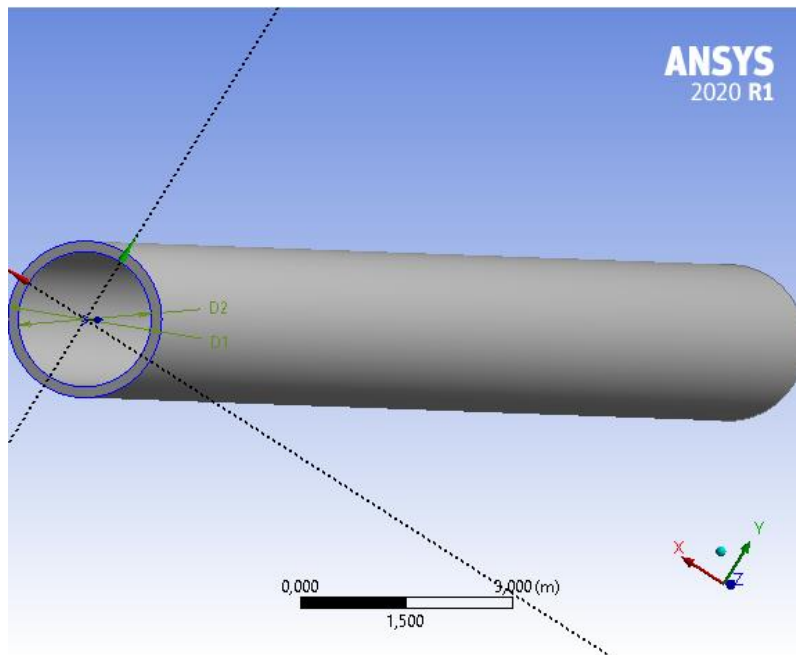


Figure 39

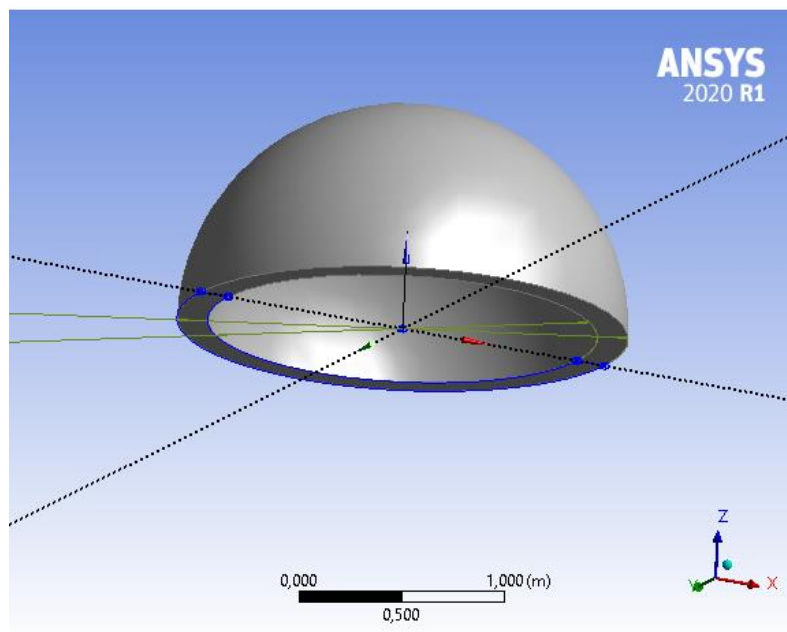


Figure 40

Freight-glider built by cargo and buoyancy tank, between dem built by stiffener as show in figure 35. Used the same principle with ANSYS 3 D

drawing in figure 41 below:

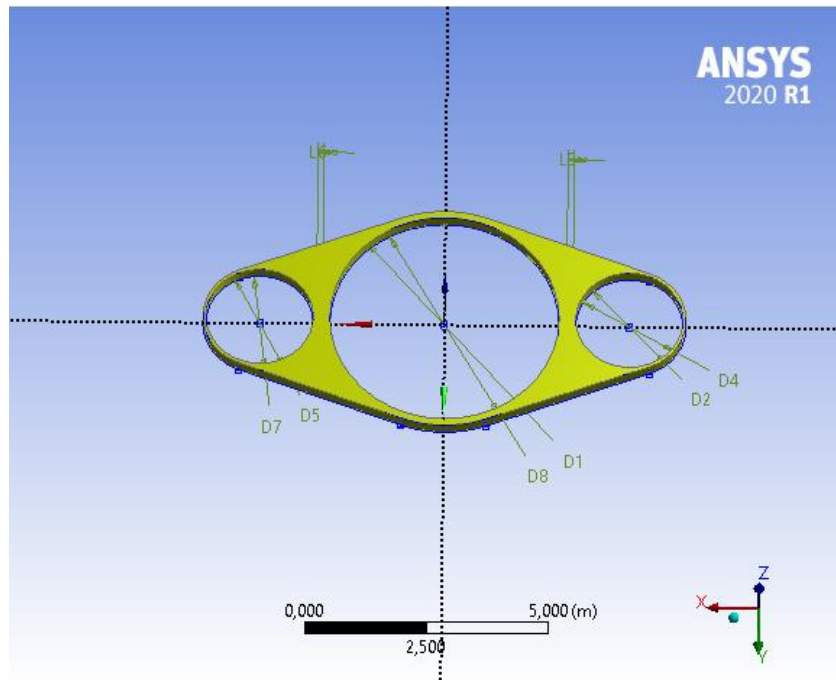


Figure 41

In the later analysis section, the task will analyze pressure for both simple building parts and the whole hull.

5.2 Hull pressure and deformation analysis

Buckling is an important element for pressure and deformation analysis. Buckling refers to the sudden loss of the original geometric shape and folds or folds when the load carried by the pressure chamber exceeds a certain critical value. Buckling is another main failure form of pressure cabin. The purpose of buckling analysis is to obtain the critical load and buckling mode when the pressure cabin buckles. The buckling of the structure generally has two forms, namely bifurcation point buckling and ultimate buckling. The

corresponding load critical points can be divided into bifurcation critical

points and extreme value

critical points. In figure 42 and

figure 43 below shows the

stable balanced path and

unbalanced path. The solid

line in the figure represents a

stable balanced path, and the

dashed line represents an

unbalanced path. P_{cr} is the

critical load. For the case of bifurcation buckling (as shown in Figure 42),

when the load reaches the

critical point, the curve will

divide two or more equilibrium

paths, and the path along the

initial path that changes the

shape of the displacement is

called the basic path , The

structure is unbalanced on this

path, and branching may occur at any time, and other balanced paths are

called branch paths. On the branch path, if the load is in the form of rising,

it is called stable branch buckling; The fruit load is in a declining form,

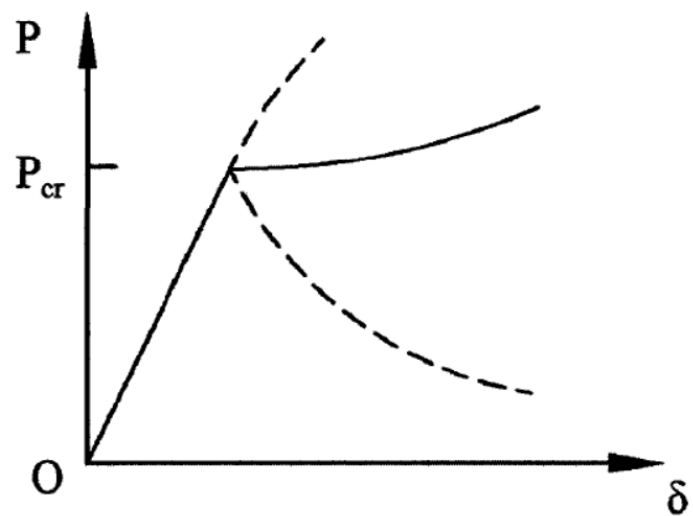


Figure 42

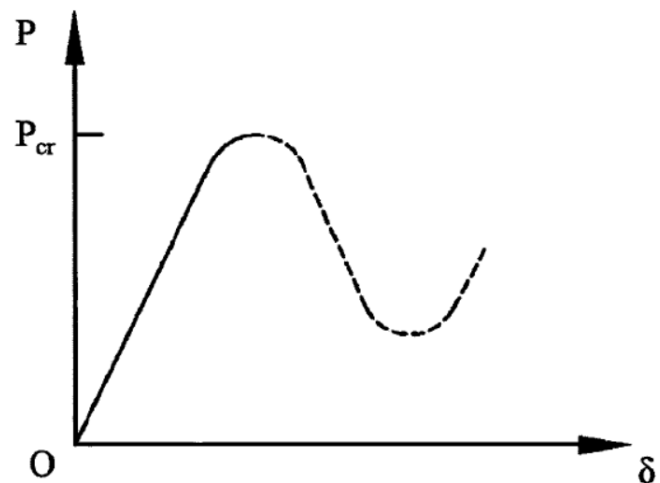


Figure 43

which is called unstable branch buckling. In the case of limit buckling (see Figure 43), there is only one equilibrium path after the critical point. The curve of this path is descending, and the balance of the structure is unstable. When the curve drops to the lowest point, it may rise again, that is, enter a state of equilibrium, and the structure will again Possesses load-bearing capacity, this change is sometimes referred to as sudden spring buckling. Linear buckling is also called eigenvalue buckling analysis. It is based on the theory of small deformation. The analysis does not consider the change of the structure configuration during the load process, that is, at each stage of external force application, it is always at the initial stage of the structure. Establish a balance equation on the configuration. When the load reaches a certain critical value, the structure suddenly jumps to another casual equilibrium state. Before discussing the principle of linear buckling, we first introduce the "stress stiffening and weakening effect" of the component. Stress stiffening refers to the stiffness change of the component in the unstressed transition state and the stressed state. When the component is subjected to tensile stress, the stiffness of the component the stiffness in a certain direction will increase significantly. For example, when no axial tension is applied to the wire rope, its transverse rigidity the degree is almost zero. However, when subjected to a large tensile force, its lateral stiffness increases significantly, which is the stress stiffening effect. On the contrary, when the component is under pressure, its stiffness matrix will be weakened,

which is the "stress weakening effect". We know that the stress stiffness matrix can strengthen or weaken the stiffness of the structure, which depends on whether the stiffness stress is tensile or compressive. For compression, when F increases, the weakening effect increases. When a certain load is reached, the weakening effect exceeds the inherent stiffness of the structure has no net stiffness at this time, the displacement increases wirelessly, and the structure buckles. In section 2.4 has described pressure duration below sea level. The deeper the Subsea freight-glider down, the more pressure affected on the surface, this will lead to deformation of the entire freight-glider building. In section 2.6, the name of deformation has a formal and different definition of deformation. In this analysis section, ANSYS is used to analyze the duration of deformation in relation to pressure affected on the surface of the entire freight-glider body. Deformation analysis takes place on both simple hull parts and the entire pre-assembled module. Max pressure in this example analysis be $1, e+005$ Pa(ramped)

5.2.1 Pressure and deformation of Cargo tank

Cargo tank including 2 parts, 5 meters diameter Cylinder with steel and wall thickness of 0.3 meters as shown in figure 44 and spherical shell with the same outer and inner diameter as shown in figure 45. deformation analyze with ANSYS program with steel as material. max pressure on hull surface as described in section 5.2. Figure 44 shows the change in cargo tank

cylinder deformation with 1×10^5 Pa and in figure 45 shows the deformation with pressure by 200 meters deeps under sea surface. Pressure value shows in section 2,3. Both deformation analysis has fixed support by end of the subject.

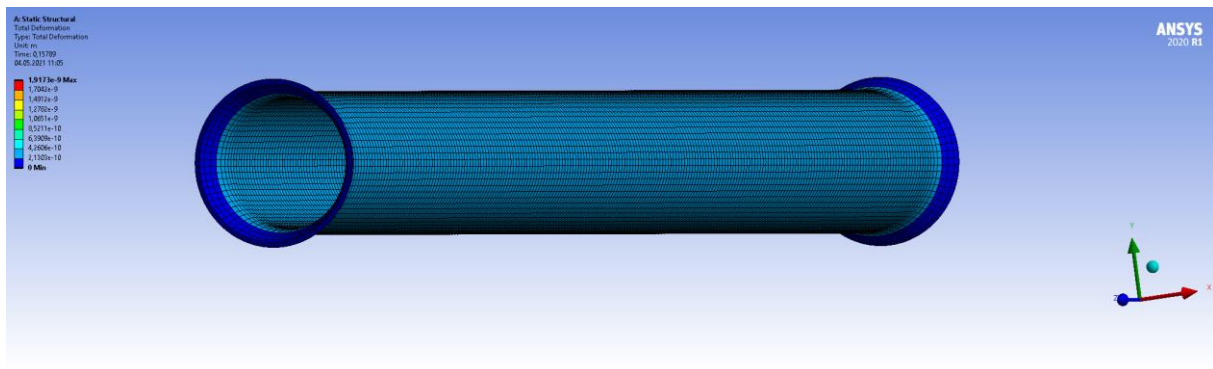


Figure 44

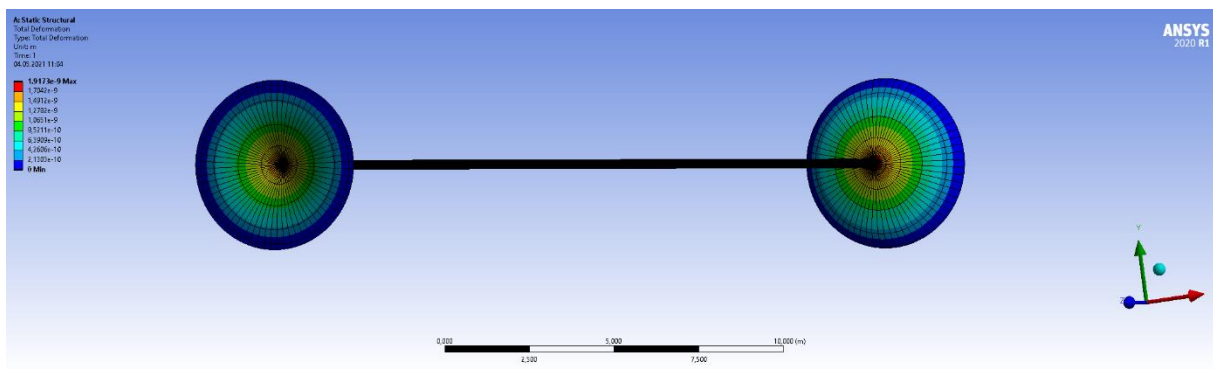


Figure 45

Diagram below figure 46 shows the deformation change by sea depth.



Figure 46

Figure 47 and figure 48 show the deformation change for cargo tank spherical shell by $1e+005$ Pa. The red area in figure 48 is the max deformation area. Fixed support with the connect area to cargo tank cylinder.

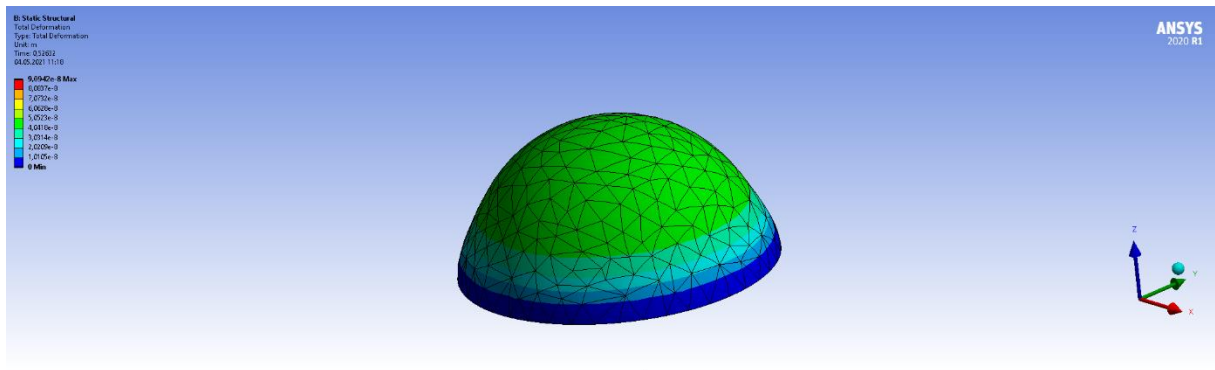


Figure 47

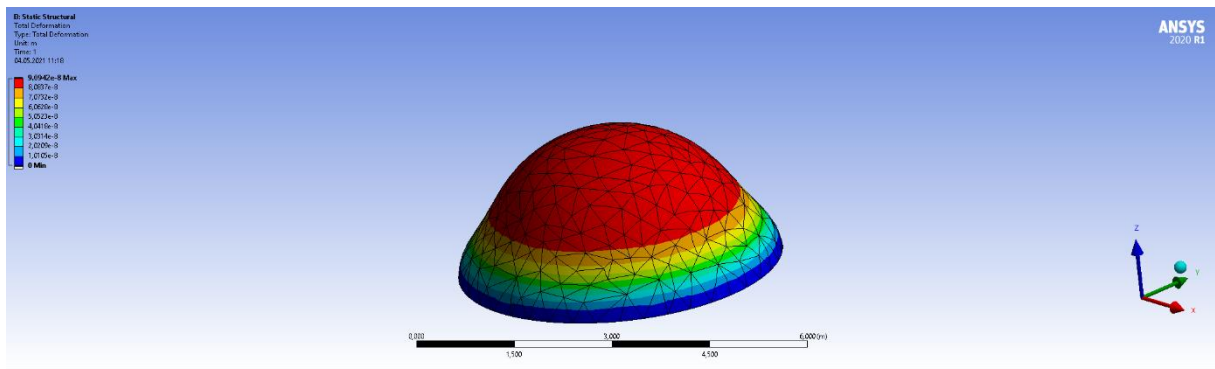


Figure 48

5.2.2 Pressure and deformation of buoyancy tank

Buoyancy tank also included 2 parts, same as Cargo tank with smaller dimension. a 2.2-meter outer diameter cylinder and a spherical shell part the same as the cargo tank. In Figure 49 and Figure 50, 3D drawing for buoyancy tank cylinders shows the duration of deformation at $1e+005$ Pa.

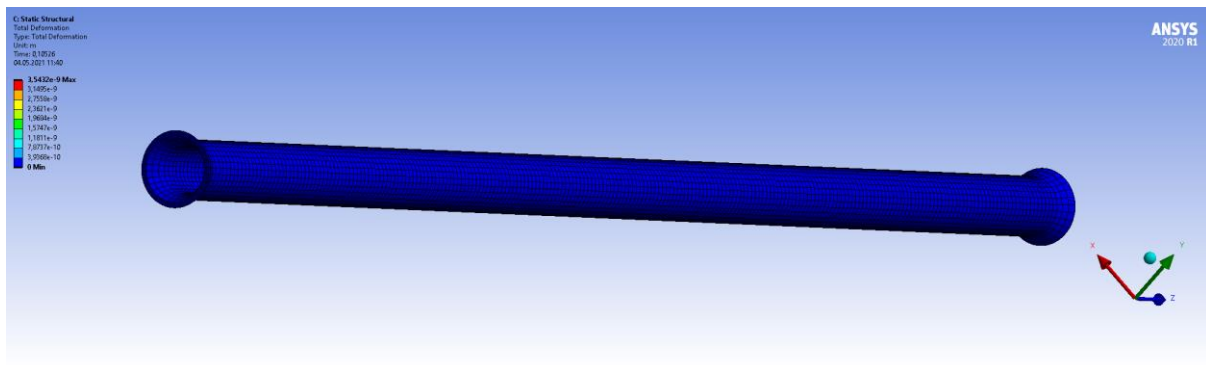


Figure 49

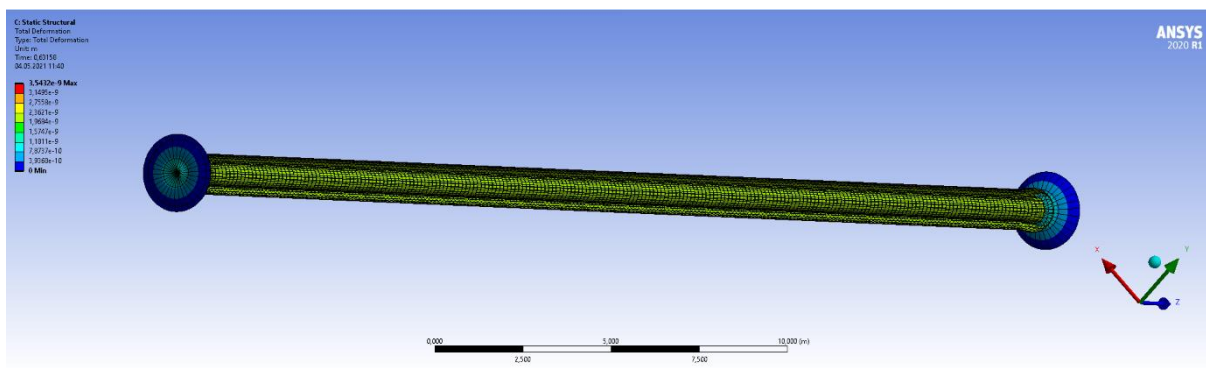


Figure 50

Figure 51 below shows buoyancy tank cylinder deformation change by depth from sea surface.

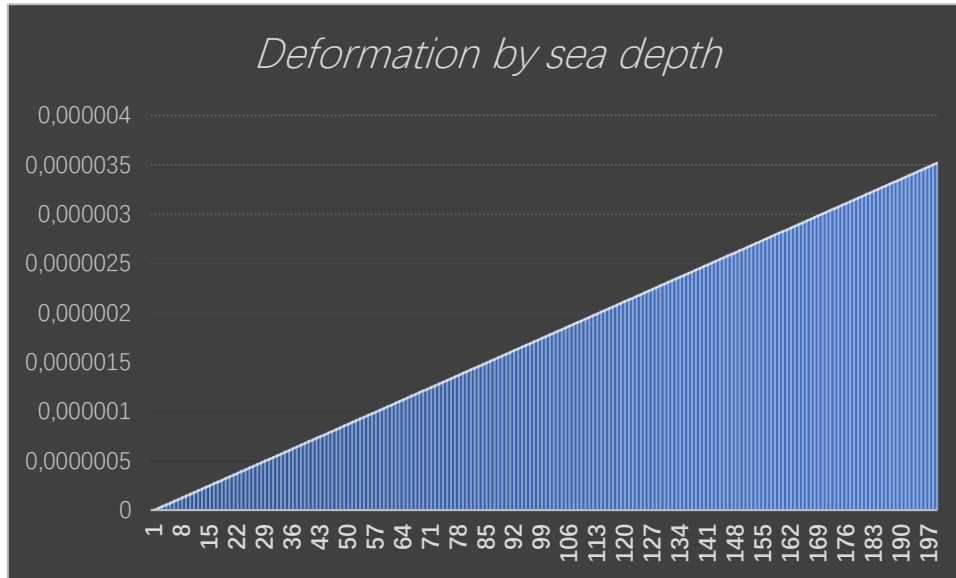


Figure 51

Figure 52 and 53 shows the deformation change for buoyancy tank spherical shell. The red area is the max deformation area by fixed support with connect area to buoyancy tank cylinder.

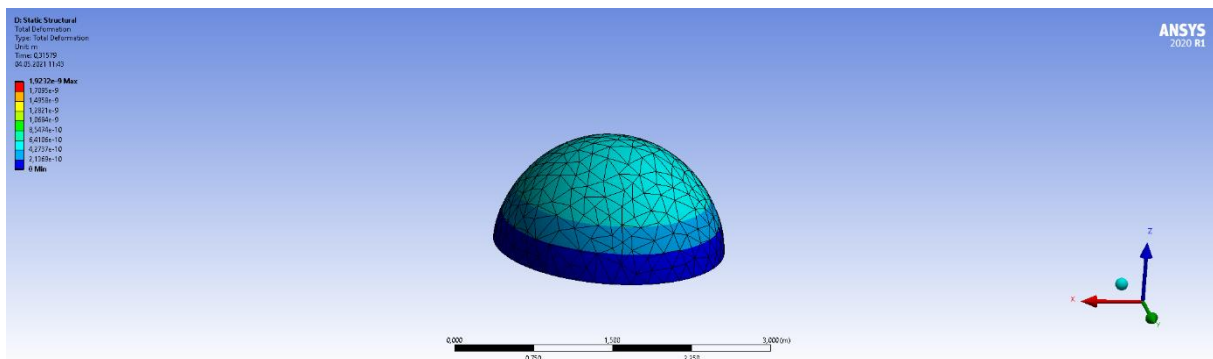


Figure 52

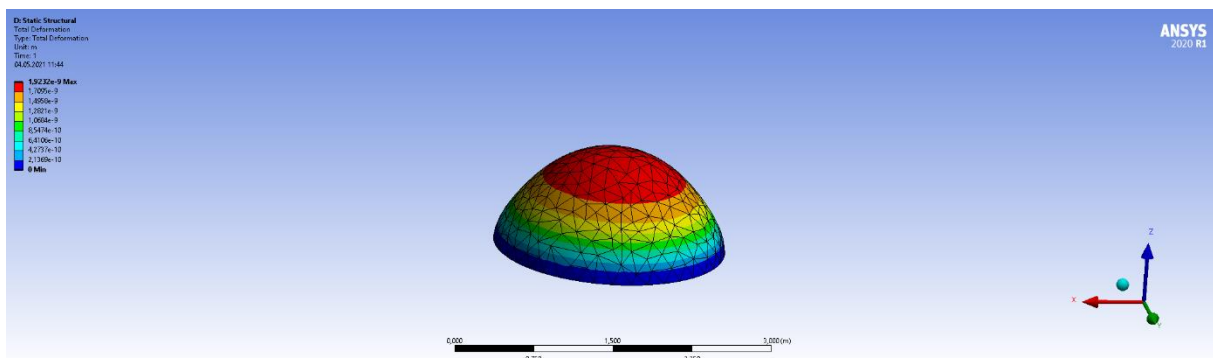


Figure 53

5.2.3 Pressure and deformation of stiffener

Stiffener is an important part of the entire Freight-glider building. functional has both reinforced cargo tank, buoyancy tank and reduce deformation due to increasing pressure from the outside of the tank. In this section, analysis has used the same method as Cargo tank and buoyancy tank, deformation duration analyzes with ANSYS drawing and with Fixed support inside of Stiffener who has contact with the tanks. Figure 54 shows the Fixed Support area and Figure 55 shows pressure direction from outside.

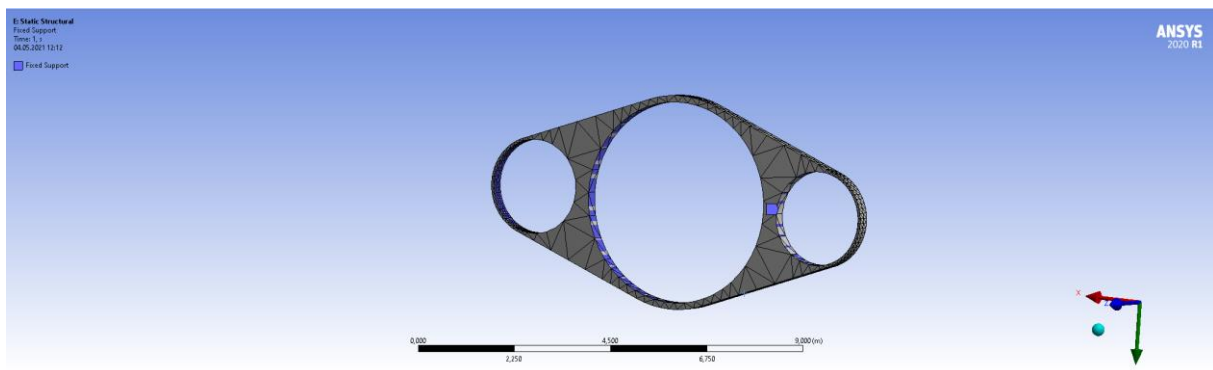


Figure 54

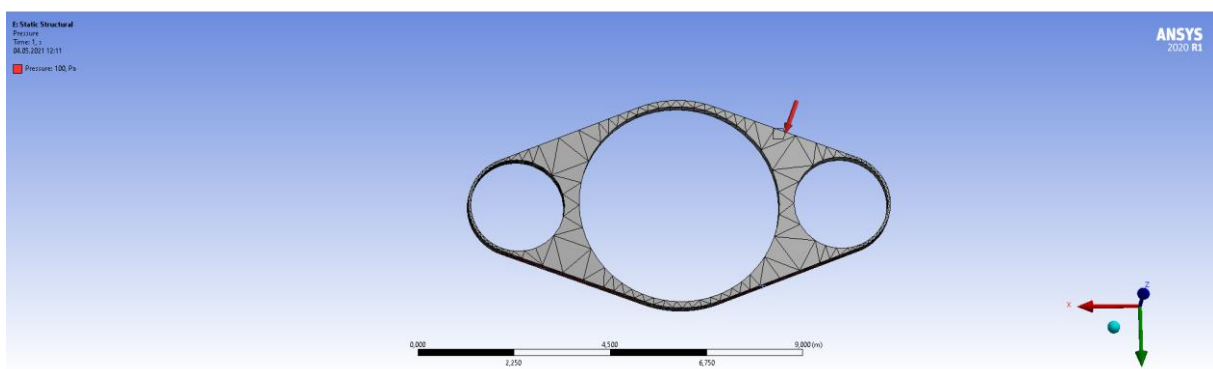


Figure 55

Figures 56 and 57 below show deformation of Stiffener with material by steel. Analysis with $1e + 005$ Pa as the same principle in section 5.2.2 The 2 figures clearly show the duration of deformation in relation to increasing

external pressures that simulate pressure increase around the hull.

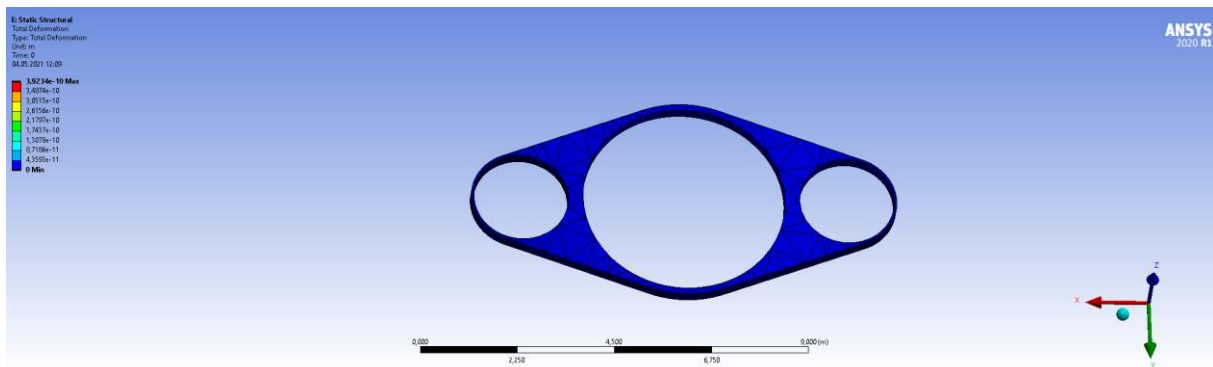


Figure 56

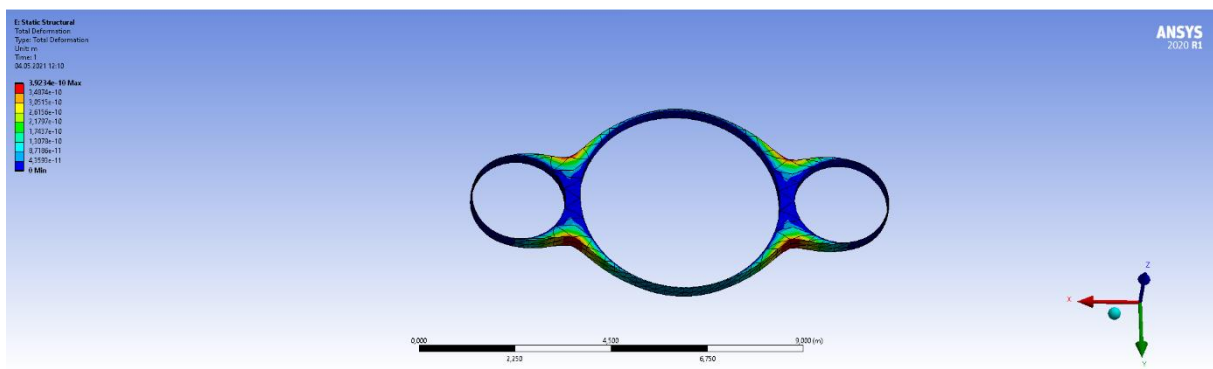


Figure 57

5.3 Carbon-fiber hull analysis

Carbon fiber cabin body is different from isotropic metal parts, carbon fiber cabin body has obvious anisotropy, so the stress in different directions of each layer of carbon fiber cabin body should be analyzed and checked. At the same time, due to the influence of the spherical shell and the middle section of the link, the stress distribution of the carbon fiber cabin between the middle part of the cylinder and the two ends of the cylinder is quite different, so the two parts of the cabin are compared and analyzed. Analysis for pressure and deformation in Carbon fiber material uses the same value

as in section 5.2. in this section will compare the result with previous analysis result from 5.2.1 to 5.2.3, Press with the same value of $1e + 005$ Pa deformation analysis by ANSYS program. Figure 57 and figure 58 show the parameter to steel and carbon fiber

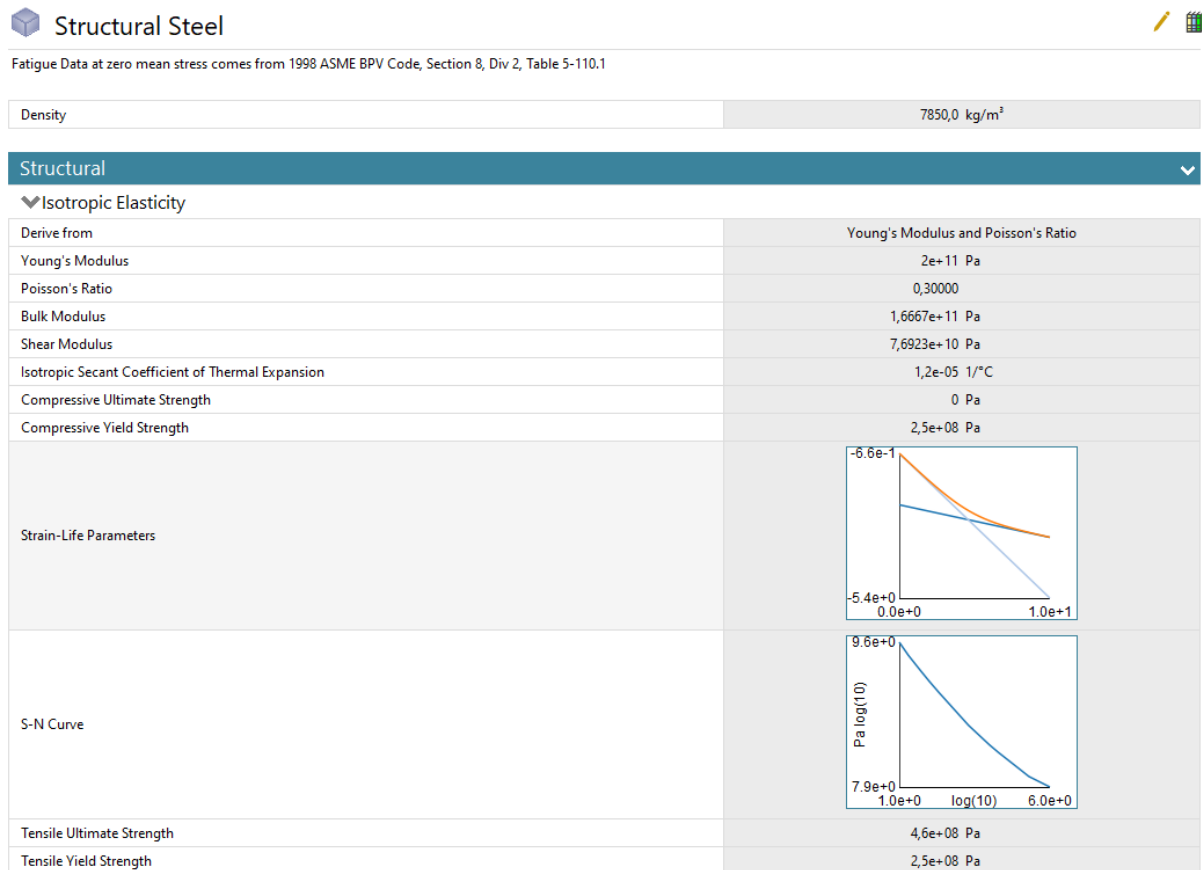


Figure 58

Carbon Fiber (395 GPa)	
Fibers only	
Density	1800,0 kg/m ³
Structural	
▼ Orthotropic Elasticity	
Young's Modulus X direction	3,95e+11 Pa
Young's Modulus Y direction	6e+09 Pa
Young's Modulus Z direction	6e+09 Pa
Poisson's Ratio XY	0,20000
Poisson's Ratio YZ	0,40000
Poisson's Ratio XZ	0,20000
Shear Modulus XY	8e+09 Pa
Shear Modulus YZ	2,1429e+09 Pa
Shear Modulus XZ	8e+09 Pa

Figure 59

5.3.1 Cargo tank pressure and deformation analysis with Carbon fiber

In figure 60 and figure 61 below show the deformation changing to Cargo tank cylinder with 1e+005 Pa simulate pressure under sea surface.

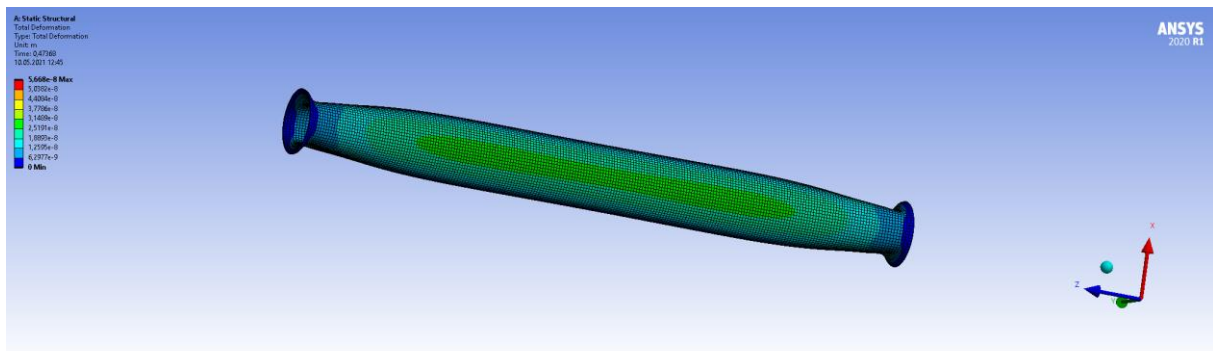


Figure 60

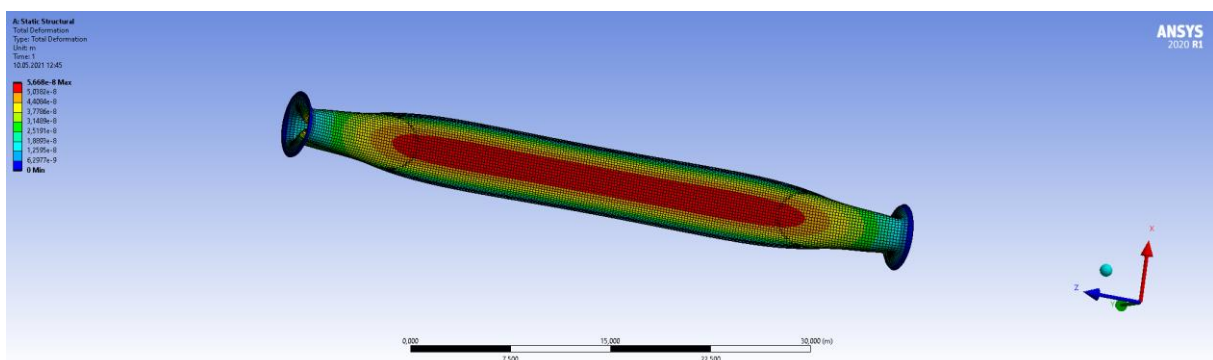


Figure 61

Diagram below figure 62 show the deformation changing comparison, Serie 1 Carbon fiber value from figure 61 and Serie 2 Steel, value from figure 45.

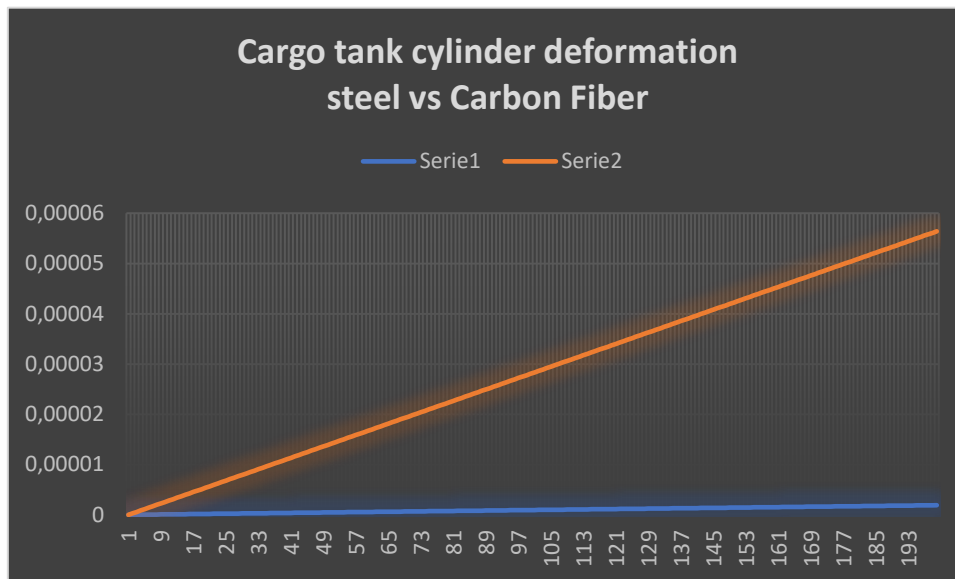


Figure 62

Figure 63 and figure 64 below show the deformation changing to Cargo tank spherical shell with fixed area by connect to cylinder, the same as I section 5.2.1 The red area in figure 64 is the max deformation area. Picture show clearly with less area than figure 48.

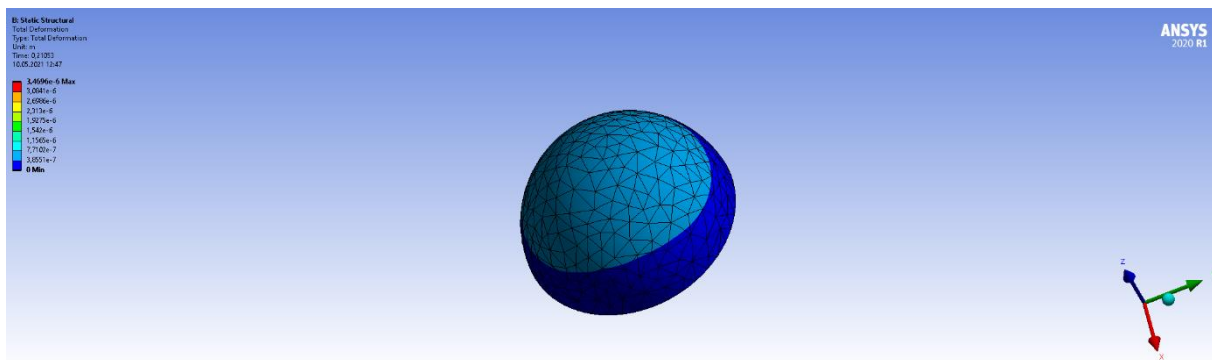


Figure 63

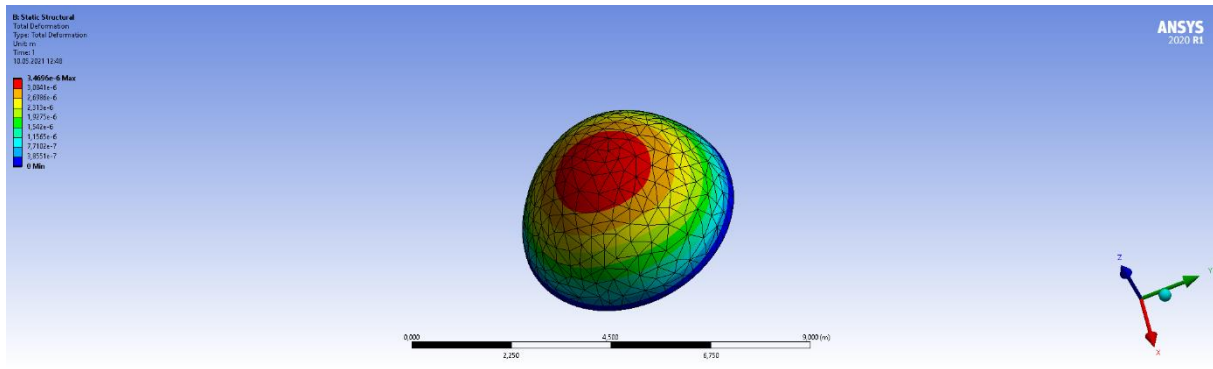


Figure 64

5.3.2 Buoyancy tank pressure and deformation analysis with Carbon fiber

Figure 65 and figure 66 show the deformation changing to Buoyancy tank cylinder with 1×10^5 Pa. ANSYS analysis shows it unless deformation area relative to figure 51.

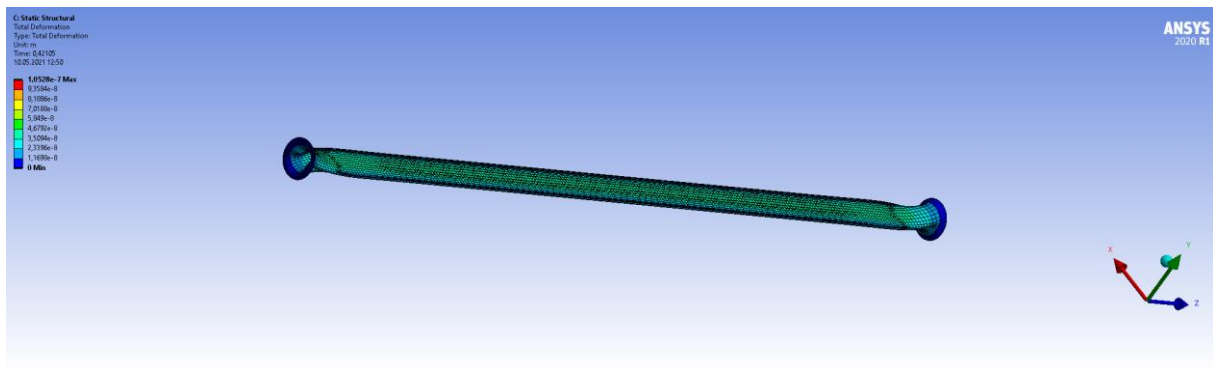


Figure 65

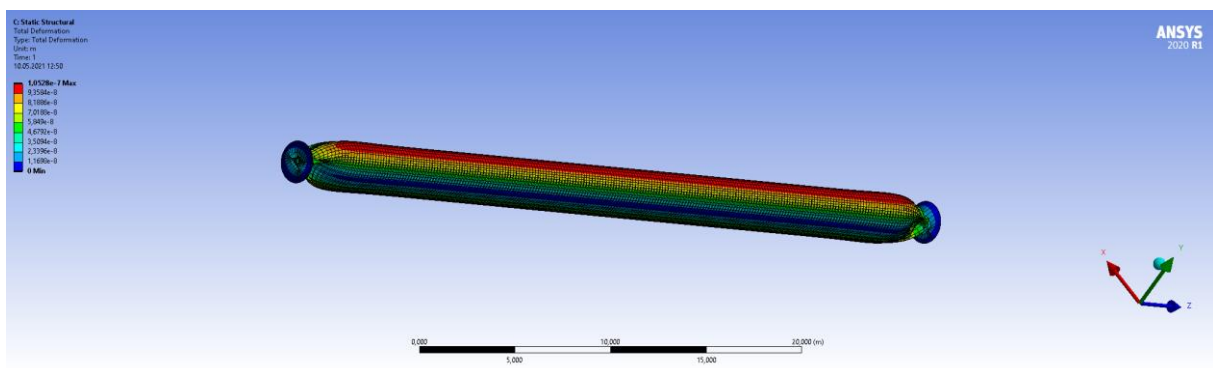


Figure 66

Figure 67 describes deformation between steel and carbon fiber for Buoyancy tank cylinder. Blue area represents Carbon fiber deformation and orange area represents deformation value for steel. the value is compared with section 5.2.2

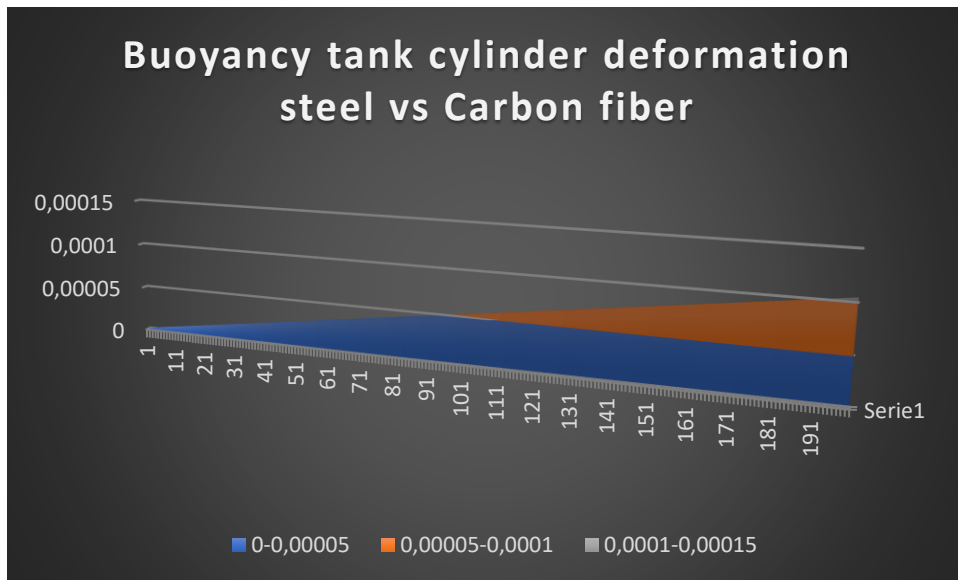


Figure 67

Figure 68 below is Buoyancy tank Spherical shell compared image for steel and carbon fiber deformation with same pressure value, left side is steel and right side is Carbon fiber. The red area at the top of the spherical shell is the max deformation area. Comparative images clearly show that Carbon fiber has less deformation with the same external condition.

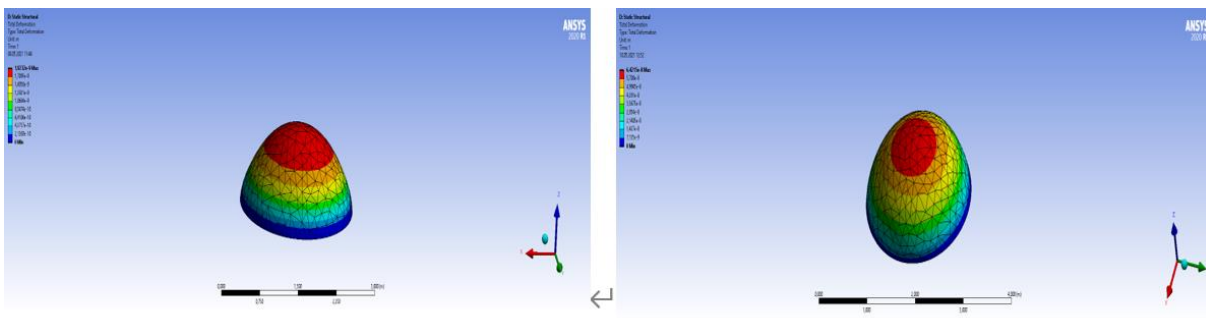


Figure 68

5.3.3 Carbon fiber stiffener deformation analysis

Through analysis of ANSYS for stiffeners deformation with external pressure with $1e + 005$ Pa gets the answer for max deformation for steel is $3.9234e-10$ meters, while stiffeners with carbon fiber material have a max deformation value for $8.7681e-9$ meters. Figure 69 show the ANSYS analysis deformation. Clearly Carbon fiber material by less deformation value.

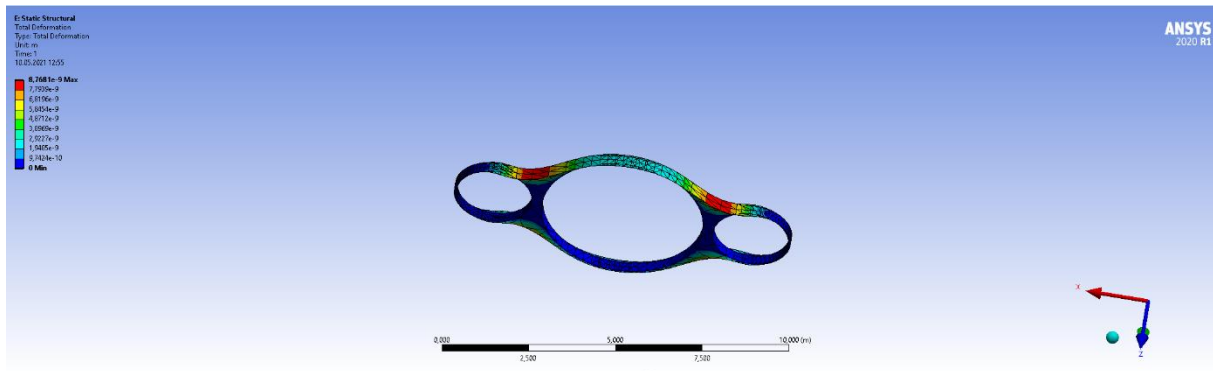


Figure 69

5.4 Integrity and reliability analysis

based on practical wholeness and reliability, analysis will benefit in weight, structure, pressure and deformation and reliability analysis in this section. The subsea freight-glider works in a deep-sea high-pressure environment, and its floating and diving movements are achieved by changing the drainage volume to change its net buoyancy. In addition to actively adjusting the buoyancy of a glider, its net buoyancy is also affected by the external environment. As the working depth span of the underwater glider is very large, the density of the seawater in the vertical direction changes more

obviously. As the density of the seawater during the dive of the glider continues to increase, the buoyancy of the glider has an upward trend. At the same time, due to the pressure continues to increase and the volume of the pressure cabin continues to decrease, which makes the buoyancy of the glider have a downward trend. The combined effect of the two determines the passive buoyancy change of the underwater glider during the ascent and descending process. By quantitatively analyzing the compression deformation of the pressure chamber and referring to the density change curve of seawater, the net buoyancy change of the glider can be obtained, which provides for the determination of the buoyancy adjustment of underwater gliding and the analysis of the motion state during the ascent and descending process.

5.4.1 Weight analysis

From table 1, section 5.1 and figure 58 gets answers for all parameters about density, total weight, and freight-glider structure parameter. Table 1 shows the concept design parameter max length 50 meters, Cargo tank with 5 meters in diameter, dead weight 1533 tons and structural weight 470 tons, Cargo weight 785 tons. We know oil density is $0,8 \text{ kg/m}^3$. In section 5.1 have calculate inner diameter to Cargo tank is 4,7-meter, vessels length is 50 meters, so we know at max volume to Cargo tank to oil is:

$$V = \pi r^2 L = \pi \left(\frac{4,7}{2} \right)^2 50 = 867,5 \text{ m}^3 = 867500L = 7275 \text{ Barrel oil}$$

$$W = V * \rho = \frac{0,8kg}{m^3} * 867,5m^3 = 694 \text{ kg}$$

Design subsea freight glider with 2 buoyancy tanks, start with the same wall thickness of 0.3 meters and outer diameter of 2.2 meters (Table 1), then we have:

$$V_{Bu0} = 2\pi r^2 L = 2\pi \left(\frac{2,2 - 0,3}{2} \right)^2 * 50 = 283,53m^3$$

Sea waters density changes with depth, from table 1 have we dive depth with 200 meters, from Tabell 7 use thesis density with 1029 kg/m³. So total buoyancy force capacity is:

$$F_{Bu0} = V * \rho * g = 283,53m^3 * 1029kg/m^3 \\ = 291751 \text{ kg} * g = 2862077N$$

Concept design parameter in table 1 show the dead weight is 1533 ton equals 15038730 N.

Archimedes' principle:

Any object, totally or partially immersed in a fluid or liquid, is buoyed up by a force equal to the weight of the fluid displaced by the object[13].

Weight of displaced fluid = weight of object in vacuum – weight of object in fluid

$$F_a = \rho g V$$

Density changes with depth (seawater 35 parts per thousand and 0 °C)		
depth (m)	pressure (decibars)	density (g/cm ³)
0	0	1.02813
1,000	1,000	1.03285
2,000	2,000	1.03747
4,000	4,000	1.04640
6,000	6,000	1.05495
8,000	8,000	1.06315
10,000	10,000	1.07104

Table 7

Above result results in dead weight greater than max buoyancy force, and concept design will not be achieved in practice. To achieve the concept design parameter with dead weight 1533 tons plus transport oil weight 694 kg, buoyancy force must equal 1533694kg.

$$D_{Buoy} = 2 * \sqrt{\frac{1533694kg}{2 * \pi * L * \rho}} = 4,36 m$$

Equation shows that according to the concept design, the buoyancy tank must have a minimum diameter of 4,36 meters (2 buoyancy tank) to achieve the Archimedes principle.

Figure 59 show the Carbon fiber density with 1800 kg/m³. Base on structure from figure 36 and parameter from table 1, if subsea freight-glider use Carbon fiber which is the new material, dead weight of freight-glider should be:

$$\frac{1800 \text{ kg/m}^3}{7850 \text{ kg/m}^3} = \frac{W}{1533 \text{ ton}}$$

$$W = 351,516 \text{ tons}$$

Consider fluid boundary and stability for float and dive, changes stiffener to an integrity solid, as show in figure 70 below:

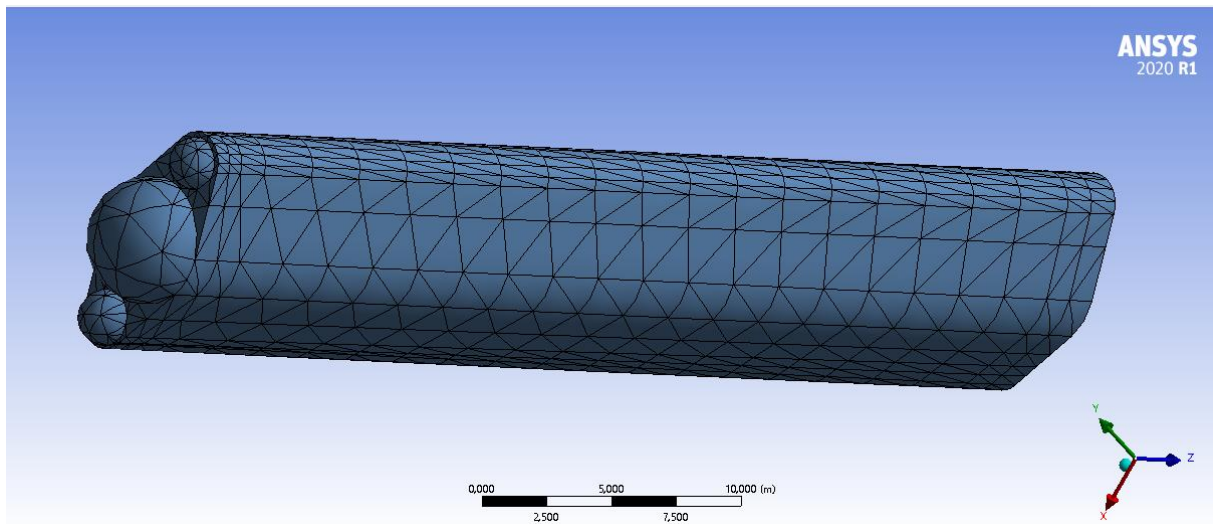


Figure 70

Result from ANSYS show the total volume is $649,56 \text{ m}^3$, and total weight is 1169,208 tons. Result show the total weight greater than buoyancy force from buoyancy dimension parameter in table 1. For achieve requirement for Archimedes 'principle, must have two larger diameter buoyancy tanks, such

$$D_{Buo} = 2 * \sqrt{\frac{1169902kg}{2 * \pi * L * \rho}} = 3,8 \text{ m}$$

Figure 71 below show the clear reduction of the weight and size of the buoyancy tank.

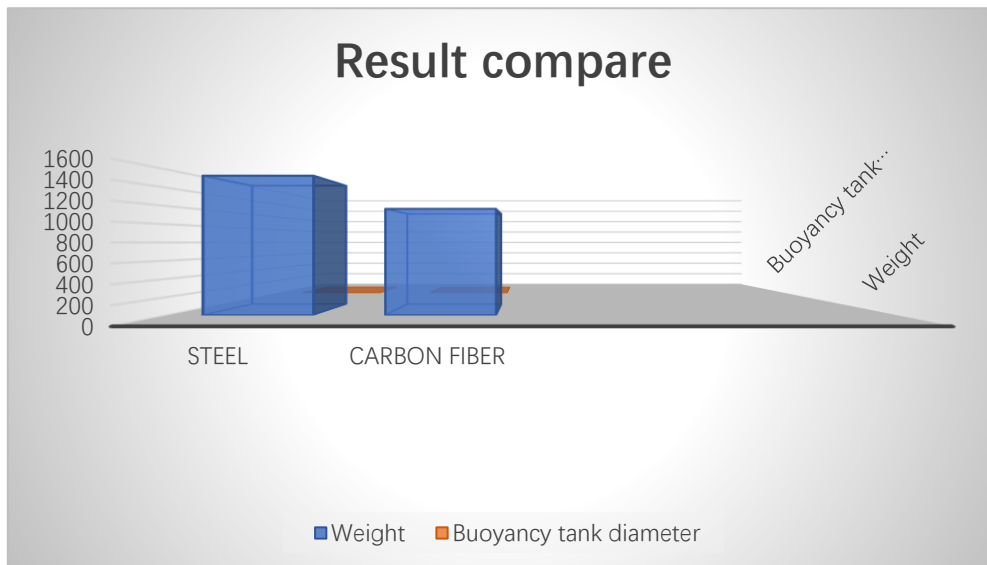


Figure 71

5.4.2 Integrity deformation analysis

In section 4 analysis hull building parts deformation for each individual parts. From ANSYS deformation analysis it shows that after assembling all parts together, integrity deformation will change, both the change formal and the deformation value. This may be since analysis changed in fixed support, reinforcement of parts apart, and integrity elastic ability changed. we also see that the deformation value changed after the replacement of new material such as carbon fiber instead of steel. in section 2, the thesis has the name of Carbon fiber characteristic, less density but greater elastic modulus and tensile strength. Figures 72 and 73 show integrity total deformation analysis. Figure 72 is for deformation analysis for steel and Figure 73 is deformation analysis for integrity hull design with Carbon fiber which are materials. Both analyses used same value with $1e+005$ Pa compare the pressure under sea

surface. The figures show a sharp reduction in deformation worthy. Figure 72 is the total analysis for steel with vessel length of about 10 meters total while figure 73 with vessel total length in 50 meters as concept design in table 1.

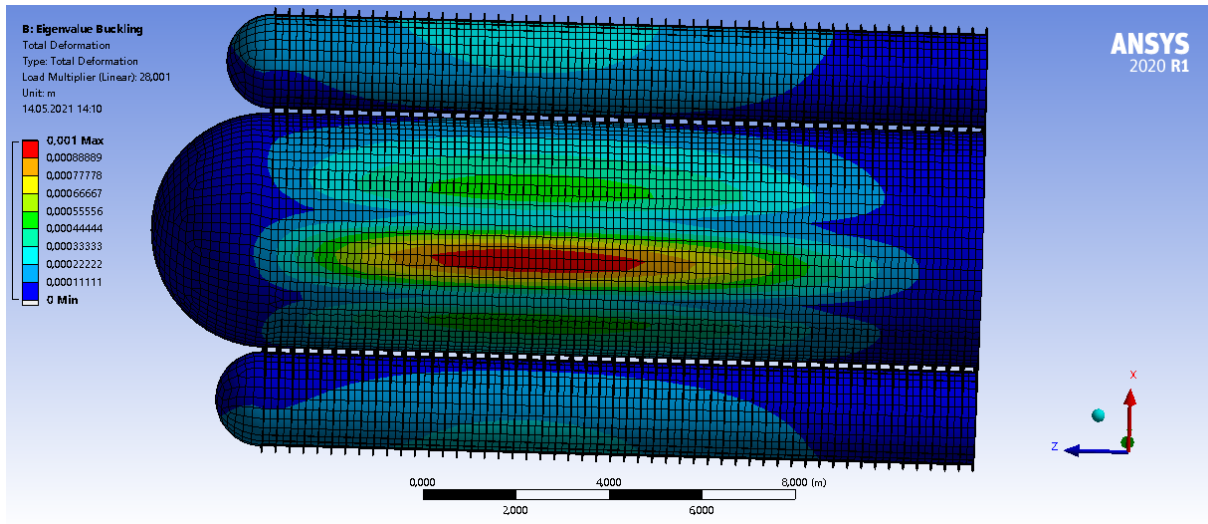


Figure 72

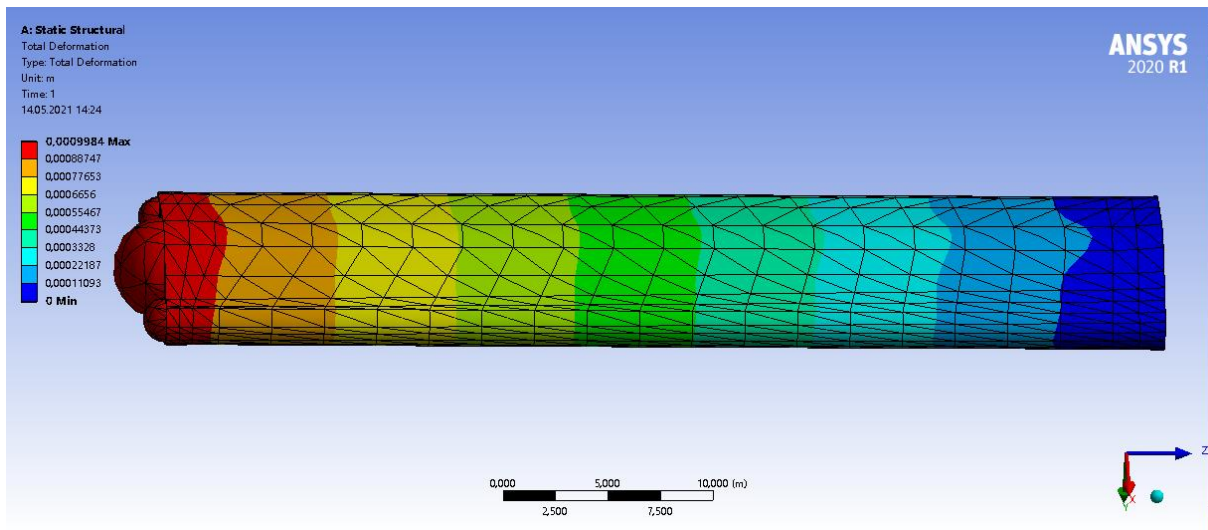


Figure 73

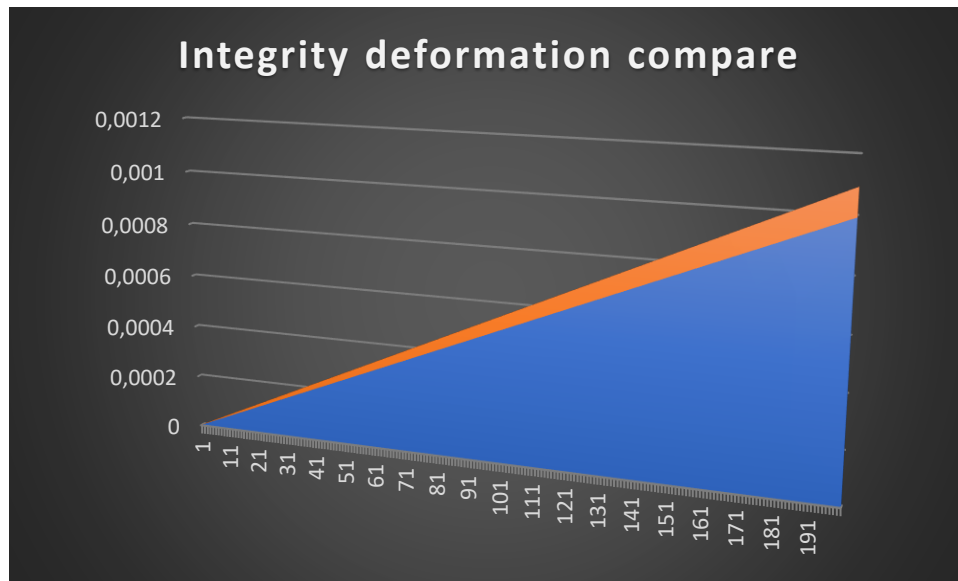


Figure 74

The subsea freight glider has the main function of floating up and diving into sea water. Hull total volume will be decreasing during the diving process due to increasing pressure and density in sea water. (section 5,4,1) According to data, China Jiaolong's deep-sea loading probe has reached a depth of 10,000 meters under the sea. The pressure-resistant chamber body is affected by external pressure, and the volume of the pressure-resistant chamber body is compressed to 1,29 liters. This subsea freight-glider by design diving depth only 200 meters under sea surface, in this master thesis will the hull volume compression of the pressure chamber is not considered. In section 3,5 figure 28 shows the manufacturing process of a layered orthogonally stiffened column of carbon fiber reinforced resin composite materials. The layered orthogonally braced column of carbon fiber reinforced resin composite materials has the function of reinforcing pressure chamber body such hull with external pressure will lead to less deformation. This argument

will be analyzed later in the thesis.

5.4.3 Integrity hull structure analysis

From previous figure 1 and figure 72 can see that Stiffener between Cargo tank and Buoyancy tank is too divided into many small parts, in table 2 see X is equal to 375 mm, vessel has a total length of 50 meters. That means in the whole vessel will build about 130 pieces of Stiffener. The goal of many small Stiffener is to reduce the total weight of the freight glider. The figure 75 below shows how stiffeners between the tanks are built in Freight-glider concept design.

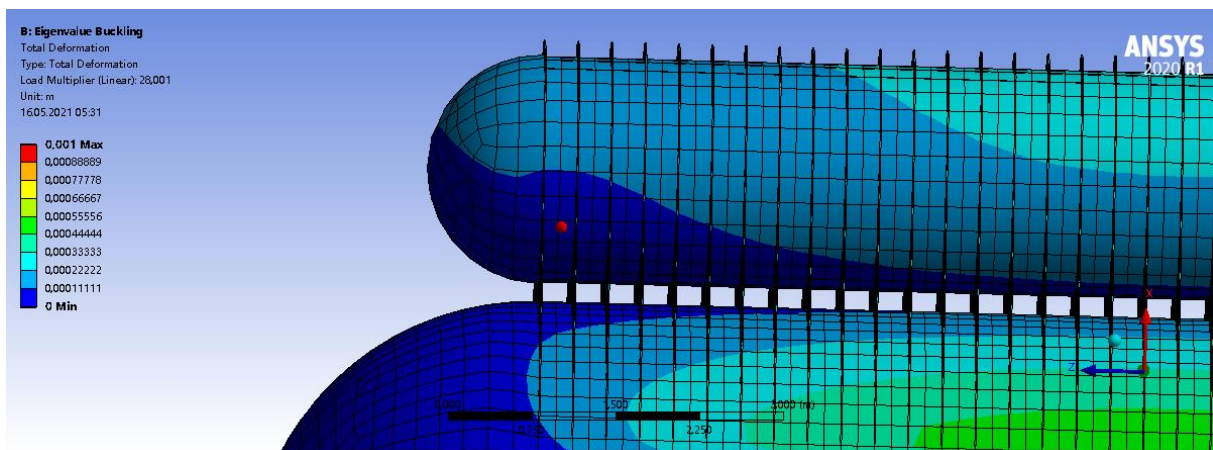


Figure 75

Section 2 has described how Freight glider works. Freight glider transports gas and oil from the seabed up to the sea surface and down again with an empty Cargo tank with a max Glider path angle of 38 degrees (see table 1). It will occur seawater will pass spaces between stiffeners when either the vessel floats up or sinks from the sea surface. Viscosity on the stiffener surface will occur and then will form shear force downward as the vessel

moves up and shear force upward as the vessel float downward. The entire process of seawater flowing in and out between stiffeners will show in Figure 76 and Figure 77 below.

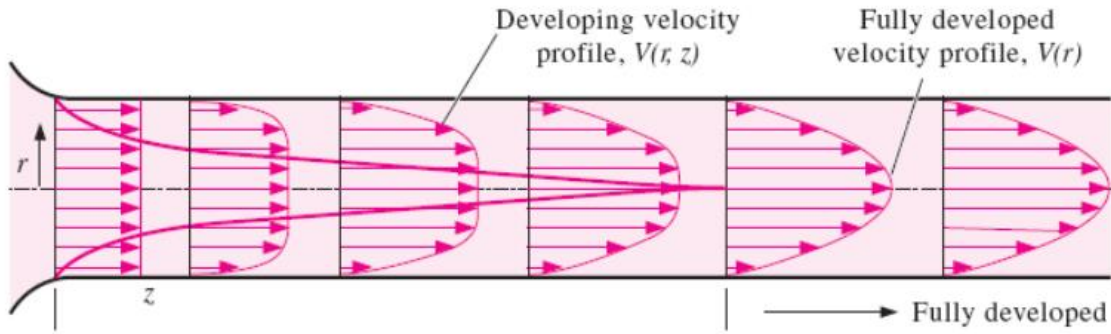


Figure 76

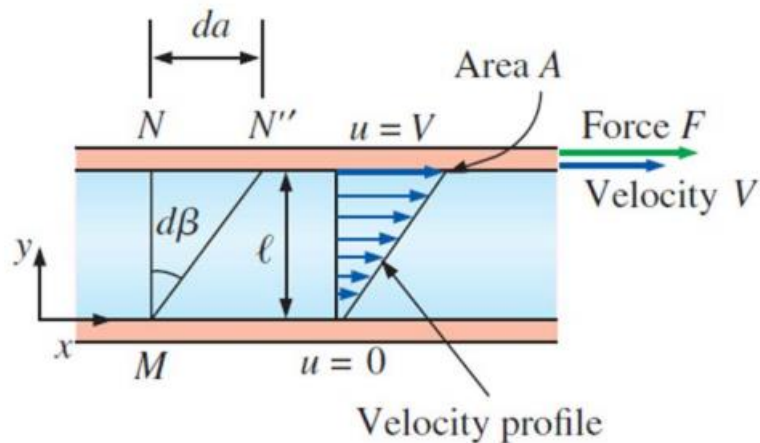


Figure 77

Newtonian fluids: fluids for which the rate of deformation is proportional to the shear stress [14].

$$\tau = \frac{F}{A} \quad u(y) = \frac{y}{l}v \quad \text{and} \quad \frac{du}{dy} = \frac{v}{l}$$

$$d\beta \approx \tan d\beta = \frac{da}{l} = \frac{vdt}{l} = \frac{du}{dy} dt \quad \frac{d\beta}{dt} = \frac{du}{dy}$$

$$\tau \propto \frac{d\beta}{dt} \quad \text{or} \quad \tau \propto \frac{du}{dy}$$

$$\text{Shear stress: } \tau = \mu \frac{du}{dy} \quad \left(\frac{N}{m^2} \right)$$

$$\text{Shear force: } F = \tau A = \mu A \frac{du}{dy} \quad (N)$$

Where μ is coefficient of viscosity Dynamic (absolute) viscosity $kg/m \cdot s$ or $N \cdot s/m^2$ or $Pa \cdot s$ 1 poise = 0,1 Pa·s

Simultaneously on the surface of the Cargo tank and buoyancy tank will occur another fluid flow situation as shown in Figure 78.

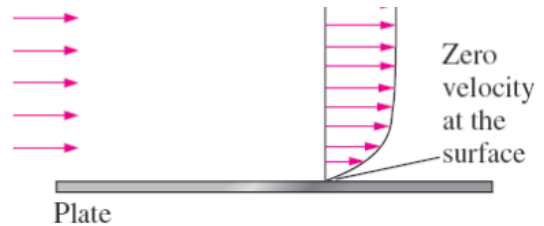


Figure 78

And then some seawater moves in between stiffeners and some seawater flows over surfaces around the tanks shown in figure 79. Viscosity of liquid will change by temperature changes. Usually liquids viscosity decreases by

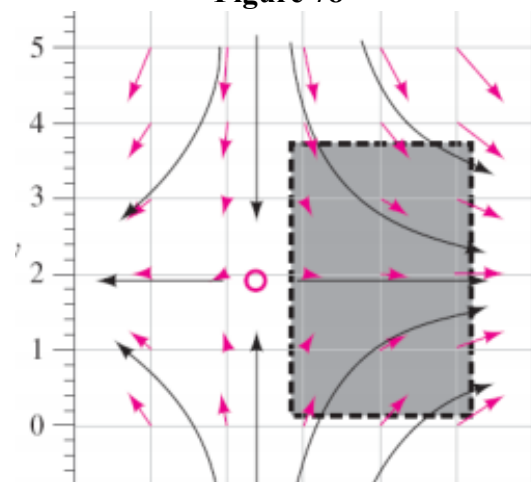


Figure 79

increases temperature. Streaklines on the vessel front change to streamlines and streamtubes when seawater passes the entire vessel and through spaces between stiffeners. All these flow turbulences cause vessel vibration and affect stabilization when the freight glider moves up and down. As in figure 73, design shows changing structure shape, instead of building 130 pieces of stiffener between cargo tank and buoyancy tank, a whole structure is built to avoid many small spaces. the idea is to increase the whole glider stabilization, improvement structure is based on material with Carbon fiber

due to material density changes from 7850kg/m^3 to 1800kg/m^3 . After removing all the small stiffeners and building an entire cover over the vessel as in Figure 73, one will not need to consider flow change, the only factor affecting moving speed and stabilization is the Boundary layer shown in Figure 80. In this master thesis will not come deeper into the Boundary layer. In section 3.5, the thesis has been described about ring ribbed reinforce cylinder. and in figure 72 one can see

most deformation change in the cargo tank occurred at the top of the tank. when freight-glider installed ring ribbed inside, then will create support from the inside, at the same time with stiffener support

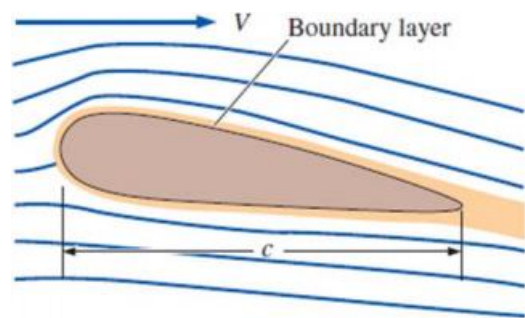


Figure 80

from the outside of the tank, the tank has been supported firmly, deformation tolerance will increase. Deformation analysis in figure 73 has fixed support on the back of the entire vessel. if built a ring ribbed within the tank, will in a way understood fixed support throughout the inside of the tank (both Cargo tank and Buoyancy tank). Deformation effect on the whole vessel will change from structure to materials. In ANSYS analysis' task, Carbon fiber chooses 35 MPa as the analysis material, from table 3 we see that for 200 meters under sea surface, it has a pressure of 2.01 MPa and 300 meters under sea surface has a pressure of 3.016 MPa. With ring ribbed reinforce cylinder built into the tanks, the concept design as described in table 1 will then be

achieved.

5.4.4 Design of experiment for measuring compression deformation

To verify the correctness of the compression deformation analysis of the pressure chamber, it is necessary to design corresponding experiments for verification. The principle of the experiment is shown in Figure 81. Fill the carbon fiber pressure cabin with clean water and connect it to a cavity container through a one-way valve. When the carbon fiber pressure cabin is under external pressure, the volume of the internal cavity decreases. Currently, the water in the carbon fiber cabin passes through the one-way valve. Flow into the cavity container on the left.

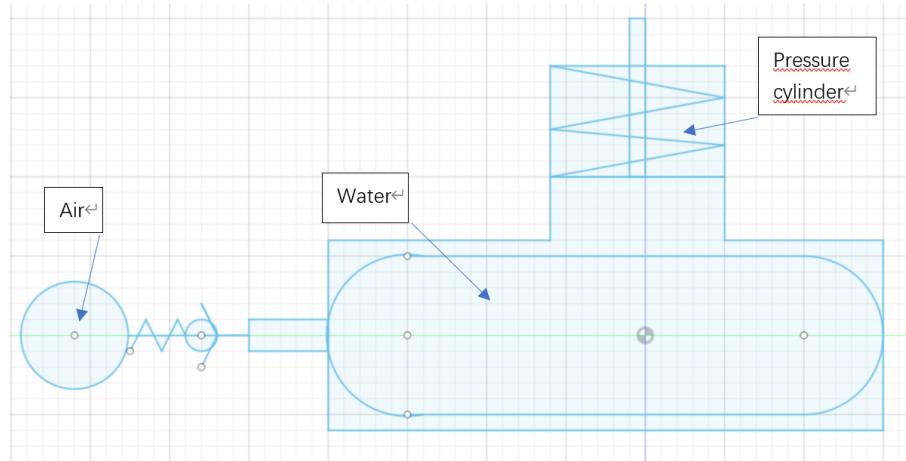


Figure 81

The internal volume and external volume of the carbon fiber pressure chamber before compression and deformation are: V_{in0} and V_{out0} , The internal volume and external volume of the cavity after compression deformation are respectively: V_{in} and V_{out} , Then the physical volume of the

carbon fiber cabin is:

$$V_{ph} = V_{out0} - V_{in0}$$

We know that physical volume is difficult to be compressed, can be considered an entity with the volume of the front cabin pressure after the pressure constant, you can get:

$$V_{out} - V_{in} = V_{out0} - V_{in0}$$

So, we know:

$$\Delta V = V_{in0} - V_{in} = V_{out0} - V_{out}$$

ΔV is the amount of compressive deformation. It can be known that the volume change in the cavity of the carbon fiber cabin is the volume change outside the cabin. After measuring the pressure experiment, the volume of water in the cavity container is the volume compression change of the carbon fiber cabin. The measurement experiment of the amount of compression deformation has not been carried out temporarily due to the time relationship.

6.0 Summary and outlook

With the continuous deepening of human exploration of the ocean, the use of traditional metal materials to make deep-sea underwater tanks can no longer meet the harsh conditions of the deep-sea environment. Carbon fiber composite materials have the advantages of high specific strength, high specific rigidity, and strong corrosion resistance. The use of carbon fiber composite materials for pressure resistance in deep sea water can help reduce their own weight and improve the load performance of underwater hulls. However, the use of carbon fiber composite materials for marine engineering structures is far less mature than metal materials. The anisotropy of carbon fiber composite materials and its complex failure models make its use and design more complicated than traditional metals. Therefore, the use of carbon fiber composite materials in deep sea gliders faces many challenges. Therefore, it is of great significance to carry out research on composite pressure cabins.

The important research work of this paper is summarized as follows:

- According available subsea freight glider concept design to work with optimization analysis.
- Theoretical description of strength and mechanical of Carbon fiber, pressure increase in seawater below sea surface, deformation analysis and dynamic of movements.

- Due to the complexity of carbon fiber composite materials, it is difficult to accurately analyze the cylindrical shells of carbon fiber composite materials under external pressure. In this paper, a simplified mechanical analysis model is established by the sub-laminate method to calculate the axial direction of each layer. For stress and hoop stress, the maximum strength theory, Tsai-Wu theory, and Tsai-Hill theory are used to verify the strength of the carbon fiber cylindrical shell.
- The ANSYS finite element method was used to further analyze the hull deformation in detail. Based on the analysis results, the hull was optimized and designed to effectively reduce the total vessel weight and deformation value. Finally, the seawater fluid penetrates the stiffener process during the dive and float of the glider. In this paper, the compression deformation of the pressure cabin and the stability of the hull during the diving and floating motions are analyzed, and solutions are proposed.
- This paper also proposes theoretical experimental methods for the deformation of the hull caused by external pressure and the change of the internal volume of the hull.
- This article highlights the optimization analysis and conclusions of materials and hull structure. In the process of hull structure optimization analysis, the importance of wing to hull stability during the ascent and descending of the hull was not considered. Based on the evaluation of

the overall hull stability, this article believes that the 20 square meter wing mentioned in table 1 is very necessary. As shown in Figure 82:

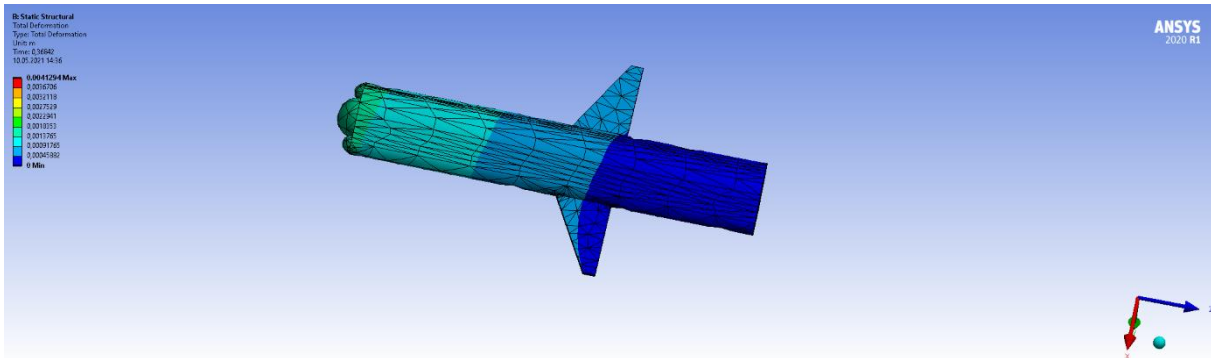


Figure 782

Based on this master thesis, the following aspects need to be further studied:

- ✚ In the preparation process of composite materials, due to various reasons, such as environmental magazines, imperfect technology and other factors, different types of defects in composite products, such as pores, fiber curling, fat-rich or poor fat, delamination, layering and Errors in fiber direction, missing layers, etc. In addition, the composite material pressure cabin will experience damage and performance degradation in the harsh marine environment, which will affect the performance of the composite material. How to use advanced non-destructive testing and advanced repair methods to maintain the deep-water composite pressure cabin is also a problem worthy of in-depth study.
- ✚ The subsequent compression deformation test should be carried out to verify the correctness of the theoretical analysis. Provide experimental support for the determination of buoyancy adjustment.

- ✚ Conduct ultimate destructive tests on the trial-produced pressure cabin model to provide reasonable experimental support for subsequent carbon fiber weight optimization.

Reference

- [1] Vervoort J (2009) Modeling and control of an unmanned underwater vehicle.
- [2] Lind E, Meijer M (2014) Simulation and control of submarines.
- [3] Ridley P, Fontan J, Corke P (2003) Submarine dynamic modelling. In: proceedings of the 2003 Australasian conference on robotics & automation. Australian Robotics & Automation Association
- [4] Proceedings of the ASME 2021 40th International Conference on Ocean, Offshore and Arctic Engineering OMAE2021 June 21-30, 2021, Virtual, Online
- [5] Johnson W. the structure of PAN based carbon fibers and relationship to physical propensities. Handbook of composites, volume 1, strong fibers. Amsterdam, Elsevier science publishers B V; 1988
- [6] Research progress on mechanical properties of deep-sea fiber reinforced resin composite cylindrical pressure shells. Wang Xiaoxu, Zhang Diantang, Qian Kun, Wang Yingying, Liu Tao, China ship Scientific Research Center, wuxi 214082 China
- [7] LI B, Pang Y J, Cheng Y X, et al. Collaborative optimization for ring-stiffened composite pressure hull of underwater vehicle based on lamination parameter. International journal of Naval Architecture and Ocean Engineering, 2016, 9(4):373-381
- [8] Wu H, Lai C, Sun F, et al, Carbon fiber reinforced hierarchical orthogrid stiffened cylinder: Fabrication and testing J. Acta Astronautica, 2018, 145.
- [9] https://en.wikipedia.org/wiki/Tsai%E2%80%93Wu_failure_criterion

- [10] Hyer M W. hydrostatic response of thick laminated composite cylinders. Journal of reinforced plastics and composites, 1988,
- [11] Composite material mechanics and a composite structural mechanics. Zhen M Wang (J) 1991.
- [12] <https://ahidao.baidu.com/que/569137777.html>
- [13] https://en.wikipedia.org/wiki/Archimedes%27_principle
- [14] Based on PowerPoints supplied for Fluid Mechanics: Fundamentals and Applications, 2nd Edition Yunus A. Cengel, John M. Cimbala, McGraw-Hill, 2010